POTENTIAL GENETIC CONTRIBUTIONS TO A PNEUMOPATHOGENIC MHV-1 VIRUS: ANALYSIS BY TARGETED RECOMBINATION AND WHOLE GENOME SEQUENCING IN THE MHV-1 MODEL OF SARS-COV LUNG DISEASE

A Dissertation

by

BRENNA MARIECHEN MCGRUDER

Submitted to the Office of Graduate and Professional Studies of
Texas A&M University
in partial fulfillment of the requirements for the degree of

DOCTOR OF PHILOSOPHY

Chair of Committee,	Julian Leibowitz
Committee Members,	Vernon Tesh
	Susan Payne
	Jane Welsh
Head of Department,	Jim Samuels

May 2014

Major Subject: Medical Sciences

ABSTRACT

A targeted recombination system was developed for MHV-1 by generation of a Donor plasmid that consisted of sequences consisting of the first 448 nucleotides of the MHV-1 genome fused to sequences from codon 28 in the HE gene through the 3'UTR to the poly(A) tail. The Donor plasmid was transcribed *in vitro* and transfected into FCWF cells that had been infected with a felinized MHV-1 recombinant virus. Recombinant viruses were selected by overlaying infected/transfected FCWF cells onto murine DBT cells and monitoring for syncytia formation and cell death. Recombinant viruses were plaque purified and expanded in murine cells. Several recombinant viruses that were not significantly different from MHV-1 in tissue culture were isolated, but none were pneumopathogenic in the A/J mouse. During the generation of multiple wild type MHV-1 stocks for mouse studies we discovered that MHV-1 rapidly lost pnuemopathogenicity during passage in DBT cells. This finding demonstrated that targeted recombination may not be a viable method of genetic manipulation of MHV-1 because the multiple passages in cell culture required to generate viruses by targeted recombination may cause loss of virulence. Using Next-Generation sequencing technology a virulent and non-virulent MHV-1 passage were sequenced, and two potential mutations that are present in the subpopulation of virulent viruses were identified that may contribute to pneumopathogenicity: nsp13 C17015A and ns4 G28454A.

We are developing an infectious cDNA clone using *in vitro* assembly of MHV-1 cDNA fragments. The fragments are flanked by type II restriction enzymes which, when digested liberate cDNA fragments that only contain MHV-1 genetic sequence and can be ligated together. By housing portions of the MHV-1 genome in low-copy plasmids we were able to create a system that is easily maintained in bacteria and easily manipulated by restriction digestion or site-directed mutagenesis. This infectious clone will be used to determine if the mutations that were discovered during the sequencing of the MHV-1 pneumovirulent virus are sufficient and able to generate a pnueumopathogenic virus. The infectious clone will also be used to determine the role, if any, of ns2 in an MHV-1 infection of lungs.

DEDICATION

I dedicate this work to my parents, Merle and Mariechen, who supported all my academic pursuits with love and patience. I promise, no more school.

I dedicate this work to my husband, Andrew, who has supported me with love and encouragement since the day we met.

And finally I dedicate this work to my firstborn, who will arrive shortly after I graduate. You didn't make finishing easy, but you definitely made it worth it.

ACKNOWLEDGEMENTS

I would like to thank my mentor and committee-chair, Dr. Julian Leibowitz, for supporting myself and my work during my time as a graduate student. I would like to thank Dr. Tesh for his kind words of support. I would like to thank Dr. Payne for her advice and encouragement during my research as well as my classes. I would also like to thank Dr. Welsh for her ideas and encouragement. Thank you all for working together as my committee to help me during my graduate school career. You will never be forgotten.

I want to thank Krystal Yakshe for being with me from the beginning, for being a challenging study buddy, an excellent sounding board, and a wonderful friend.

I want to thank my parents for supporting me emotionally, and financially when needed, while I spent many years pursuing my academic goals. I know it must have been difficult being supportive when you were not really sure exactly what I was doing. I promise, no more school.

I want to thank my husband, Andy, who was willing to date someone while they were taking qualifying exams, who was willing to stay with me while I cried about my research, and who was willing to marry someone who had no clue how much longer she would be in school. You are my rock, and I love you.

NOMENCLATURE

SARS-CoV	Severe Acute Respiratory Syndrome Coronavirus
MHV-1	Murine Hepatitis Virus Strain 1
MHV	Murine Hepatitis Virus
fMHV-1	recombinant MHV-1 virus expressing the Feline Infectious Peritonitis Virus spike
S	Spike
E	Envelope
HE	Hemagglutinin Esterase
M	Membrane
N	Nucleocapsid
P	Passage
LD50	Lethal dose, 50%
pfu	plaque forming units
BL	Biosaftey Level
DBT	Delayed brain tumor, cell line, mouse
FCWF	*Felis catus* whole fetus, cell line, cat
L2	Lung, cell line, rat

TABLE OF CONTENTS

Page

LIST OF FIGURES

Page

Page

LIST OF TABLES

Page

CHAPTER I

INTRODUCTION AND LITERATURE REVIEW

INTRODUCTION

Severe acute respiratory syndrome coronavirus (SARS-CoV) is a novel human coronavirus that caused the first major pandemic of the new millennium in 2002-2003(6, 31, 56, 189). Bats have been a source of a number of emerging zoonotic diseases, including Nipha and Hindra (51, 159). The animal source of the novel human SARS-CoV is thought to be Chinese horseshoe bats (80, 159). It is believed that a bat coronavirus had adapted to infect civet cats and from civet cats was able to adapt to infect humans (80, 85, 159). The receptor utilized by these SARS-like coronaviruses was shown to be angiotensin converting enzyme 2 (ACE2) (87). Until the 2003 SARS-CoV pandemic there was little urgency to study coronavirus-related human disease, because the disease in humans was usually a self-limiting upper respiratory infection (1, 76, 98). The SARS-CoV pandemic spurred a search for additional human coronaviruses and several new human respiratory coronaviruses, HKU1 and NL63 were discovered (1, 88, 118, 187). These viruses, as well as previously known human coronaviruses (HCoV) OC43 and HCoV-229E were found to cause significant human respiratory disease in the elderly and in infants (1, 15, 19, 98, 118, 187). A study done in Beijing, published in 2013, showed that infection with four different human coronaviruses takes place during childhood (187).

Originally coronaviruses were thought to be limited to individual species and a narrow organ tropism in a given species (75, 85, 178). The spike protein binds to its cognate receptor and initiates viral entry into a host cell. Spike is a very strong determinant of tissue and species tropism. There are also viral accessory genes that are thought to aid in viral replication in target species and tissues. The spike protein and specific accessory genes were both thought to contribute to the limited the host-range of coronaviruses. Since the SARS-CoV outbreak, and the resulting population studies, it has been postulated that these cross-species events occur more often than originally hypothesized (121). The adaptation of SARS-CoV from bat to civet to human only required four amino acid mutation changes that resulted in a drastically increased binding affinity of the receptor binding domain from a human isolate for human ACE2, up 1000-fold from the original binding affinity of the receptor binding domain from a civet isolate of SARS-CoV (86). So while spike and accessory genes can be host limiting, they are also capable of rapidly developing mutations that allow the virus to thrive in a different host.

The more recent 2012 emergence of the Middle East respiratory syndrome coronavirus show a continuing need for animal models of severe coronavirus disease (5, 97). There are two overarching approaches to model penumopathogenesis: the direct contributions of the virus and the response of the host immune system. It is the current opinion that the severity of the acute respiratory disease (ARD) in some SARS-CoV patients is, in large part, due to the immune response of the individual patient more than any predominant contribution of the virus (40, 110). Herein is a review the genetic

methods that are available to study viral contributions to disease, the animal models that can be used in SARS-CoV infection, the ability of the animal model to mimic human disease, and the viruses that are used in studying SARS-CoV biology and disease pathogenesis.

REVIEW OF CORONAVIRUS BIOLOGY

Coronaviruses are a member of the family *Coronaviridae* in the order Nidovirales. The *Coronaviridae* are further subdivided into the *Torovirinae* and *Coronavirinae* subfamilies. The *Coronavirinae* in turn are split into four genera (alpha, beta, gamma, and delta coronaviruses) based on phylogenetic classification (72). SARS-CoV has been phylogenetically classified as a betacoronavirus (72, 155). Other related betacoronaviruses include mouse hepatitis virus strain-1 (MHV-1), mouse hepatitis virus strain A59 (MHV-A59), and mouse hepatitis virus strain JHM (MHV-JHM). Human coronaviruses CoV-HKU1 and HCoV–OC43 are also classified as betacoronaviruses.

Coronaviruses are enveloped RNA viruses with genomes that range in size from 28 to 31 kb in length. The genomes have a 5' cap and a 3' polyadenosine tail and contain untranslated regions at the 5' and 3' ends of the genome which have been shown to contain secondary structures that are important for virus replication and growth in cell culture (47, 67, 140, 168). The 5' two-thirds of the genome encodes two open reading frames (ORF): ORF1a and ORF1b. These have a relatively short region of overlap which contains a ribosomal frame shift signal that results in the translation of two large polyproteins called ORF1a and ORF1a/b. ORF1a is encoded in the first third of the genome and ORF1a/b is encoded by the first two-thirds of the genome. Once translated

these polyproteins are cleaved into 15-16 nonstructural proteins (nsps1-nsp16) (19). These ORF1a/b derived proteins are responsible for RNA replication and transcription. However, while the cleavage sites and number of proteins are consistent among coronaviruses, and the proteins are generally well conserved, especially in ORF1b, the actual genes in this region also contain unique regions that are not conserved. Because of their limited coding capacity, viruses, even large viruses like coronaviruses, encode proteins that have more than one functional domain, though only some of the functional domains are conserved between viral groups (43, 56, 68, 104). In general coronaviruses have, after the ORF1a/b region, a series of virus species-specific genes dispersed amongst genes that code for structural proteins. All coronaviruses encode the spike protein (S), envelope protein (E), membrane protein (M), and nucleocapsid protein (N) in that order going from the 5' to 3' direction of the genome, and this is followed by an untranslated region that is functionally important (48, 90, 161). Many betacoronaviruses, including two pathogenic human coronaviruses, CoV-HKU1 and HCoV-OC43, contain a hemagglutinin esterase gene (HE) but SARS-CoV and other SARS-like-CoV do not. Encoded with the S-E-M-N are strain-specific genes, also referred to as accessory genes, which greatly vary between coronaviruses.

It is generally accepted that the SARS-CoV of 2002-03 pandemic was the result of host switching from bat to civet cat to human due to mutations in the spike protein. The actual genetic history of SARS-CoV is less clear on the events that lead to the pandemic because genomic analysis demonstrates that SARS-CoV have a unique evolution consisting of both mutation and recombination events (141). Early genomic

analysis showed that SARS-associated coronaviruses might have possessed a recombinant RNA dependent RNA polymerase that was derived from an avian coronavirus (121). However, later studies seem to point towards bats as the likely source because bats have a high diversity of coronaviruses present in the population, and it is more likely that SARS-CoV was generated from the bat coronavirus lineage (7, 80, 122, 159). There is also indication that the SARS-associated coronaviruses have been evolutionary independent for a period of time prior to the outbreak (64, 121). Also, while SARS-CoV is considered as a single entity, there are several studies that indicate that SARS-associated coronaviruses also maintain a quasispecies, which may indicate that the events leading up to and during the pandemic were not solely due to the host range changes that can be attributed to the spike protein, but rather to a complex interplay of different virus subspecies that allowed for the selection of a new human pathogen (64, 141). During the epidemic different quasispecies strains were being generated and had potential effects on patient health and survival (144). Studies have demonstrated the presence of multiple quasispecies of SARS-CoV in a individual patient (142, 166). The role of quasispecies in SARS-CoV is unclear, though intriguing. Coronaviruses do have a mechanism to recognize and correct mutations that arise during genome replication, the nsp14 exonuclease. The presence of this exonuclease lead to reasoning that assumed that coronaviruses did not utilize the mechanisms of quasispecies diversity to the extent that other RNA viruses did (32). However, with the new data that supports quasispecies in SARS-CoV this idea may need to be reevaluated. To date there have been no studies reporting the clinical severity and outcome related to SARS-CoV quasispecies.

After a coronavirus enters the cell through receptor mediated endocytosis and fusion with the endosomal membrane or direct fusion of the viral envelope with the plasma membrane (33, 44, 88, 149, 158), the positive-stranded genome is translated into the ORF1a and ORF1a/b polyproteins (44). These polyproteins are cleaved into individual nsps 1-16 by virally encoded protease activities: papain-like-protease domain(s) (PLP) and a 3C-like protease (3CLpro), with the PLP domain(s) mediating the nsp1-nsp3 cleavages, with remaining proteolysis steps being mediated by the 3CLpro (20, 48, 96, 112). Once the viral polymerase and other non-structural proteins required for viral RNA synthesis are translated and subsequently cleaved from the polyprotein, transcription of the genome and of the subgenomic fragments begins. Viruses of the order Nidovirales have a distinct replication strategy in that ORFs 3' to ORFs1a/b representing the 3' one-third of the genome are expressed via multiple subgenomic viral mRNAs. These subgenomic mRNAs make up a 3'coterminal nested set. Coronaviruses have a unique transcription regulatory sequence (TRS) that is present in the 5' region of the genome, called the leader TRS, and at other locations throughout the genome, usually directly upstream of a coding region outside the ORF genes and these are called body TRS (34, 188). It is believed that during negative strand synthesis the leader TRS is brought around to the 3' end of the genome and forms a 5'-3'complex with the RNA dependent RNA polymerase. As the polymerase generates the negative strand the polymerase passes a body TRS, which can now base-pair with the leader TRS and can allow for the polymerase to switch templates. The polymerase moving from the TRS to the 5' end is what generates the coterminal ends of the subgenomic negative RNA. The

negative RNA is then transcribed into a positive strand to be used for protein synthesis. The number of mRNAs (including the genome RNA) synthesized varies from virus to virus and ranges from 7-9. The transcription of each subgenomic mRNA is not equal, with the molar ratios of the mRNAs generally decreasing as their size increases (115). All proteins encoded 3' to ORF1a/b are under a unique transcription regulatory sequence (TRS) that is just upstream of the coding sequence of the protein. The TRS is critical to the generation of the subgenonic mRNAs and TRS sequences are unique to different coronavirus species (132, 188). The relative amount of mRNA affects the amount of translated protein. The proteins are translated and the virus is assembled in the endoplasmic reticulum-Golgi intermediate compartment and a complete viral particle buds from the endoplasmic reticulum into the trans-Golgi network (94, 169). Virus particles, or in some cases virus-like particles that are have structural proteins but no genomic RNA, are transported to the cell membrane and released. Because coronaviruses bud through the ER and trans-Golgi, some of the S protein is able to be transported to the plasma membrane independently, and if the S protein has the ability to fuse at neutral pH (not all coronavirus S proteins have this property) some coronaviruses are capable of forming syncytia, or large multinucleated cells. The size and amount of syncytium formation varies by virus strain and syncytium formation and size is considered to be a part of the viral life cycle and to contribute to viral spread and pathogenesis (169).

Coronaviruses overwhelm an infected cell by promoting the degradation of the host cell's mRNA (66). When most of the host cell's mRNA is degraded the only

mRNA available to translation is viral, so viral proteins will be primarily produced. Coronavirus nsp1 is able to reduce host mRNA expression without effecting the 28 and 16S ribosomal RNA levels. Studies have shown a difference in the modification of cell cycle genes between young and aged animals (6, 138). Viruses control the cell cycle so that they can utilize the cellular machinery and products that are usually present in the synthesis phase of the cell cycle which contributes to pathogenesis and can create difference in disease out come in different ages of hosts (6, 124, 128, 137, 138). This is possibly due to the idea that in older individuals more cells have reached a senescence phase and do not have large numbers of cells actively undergoing mitosis.

SARS-CoV HUMAN DISEASE AND PATHOGENESIS

Early cases of SARS-CoV are believed to have originated in southern China where, in November of 2002, there was an unusual epidemic of a severe pnueumonia in Foshan, Guangdog (55, 180). The Foshan index case infected his wife and three other relatives, but not his children or any hospital staff. The early phase of the SARS-CoV outbreak began with the Heyuan index case, a chef working in the city of Shenzhen, began to have fever and flu-like symptoms on December 10th of 2002 and was hospitalized in Heyuan on December 15th (180). During his stay he infected seven hospical staff members and one patient, which was the first recognized case of SARS-related hospital infection. This disease was, at the time, of an unknown aetiology and would prove to have a high rate of transmission to healthcare workers in China (55). In February of 2003 a 64 year old nephrologist from southern China visiting Hong Kong and he is believed to have been the index case of Hong Kong and source of infection that

lead to subsequent SARS-CoV outbreaks in Hong Kong, Vietnam, Singapore, and Canada, which started the pandemic middle phase of the outbreak (30, 55, 79). During his stay at least 16 hotel guests and visitors were infected and within weeks the atypical pneumonia had spread an affected more than 8000 people in 25 countries and regions across five continents.

In 2003 the epidemiologically linked patients from Hong Kong that presented with a fever, rigor, dry cough, dyspnea, malaise, headache, hypoxia, and crackles and percussion dullness in physical exams of the chest (150). Serial chest radiographs showed a progressive air-space disease. Two patients died of progressive respiratory failure that was a result of diffuse alveolar damage. This disease was named Severe Acute Respiratory Syndrome (SARS) and appeared to be of infectious origin. This disease had already been reported to the World Health Organization in Guangdong Province, China in late 2002 (14, 180, 189). Later in 2003 the infectious agent was shown, through electron-microscopy and RT-PCR sequence analysis, to be a novel coronavirus (31, 109).

Clinical Features and Histology

Though SARS-like viruses are capable of infecting individuals of all ages, mortality due to disease is highest in the elderly. Patients present with a fever and rigor with a nonproductive cough, malaise and headache (37, 150). Chest crackles and dullness on percussion were also detected in most patients upon physical examination of the chest. Most patients have abnormal chest radiographs on presentation with the primary abnormality in the initial radiograph showing air-space shadowing that included

ground glass opacities, focal consolidation, or patchy consolidation. Opacities were predominant in the lower lung zones in most patients, though some patients did show opacities in the upper zones. In general, air-space opacities increased in size, extent, and severity within the first 10 days. The predominant abnormalities that were found on CT scans of patients were subpleural focal consolidation with air bronchograms and ground glass opacities that occurred mostly, but not exclusively, in the posterior aspects of the lower lobes. While the mortality rate for SARS-CoV infection is, overall, only around 10%, that rate rises to 50% for those patiens over 60 years of age (14, 124, 150)

Severe clinical worsening with the development of dyspnea occurs about 5 days after the onset of illness, coincident with the development of an antibody response to infection and a decrease in viral titer and replication (105). In cases of severe disease of short duration, 10 days or less, the histopathologic changes in the lung include acute-phase diffuse alveolar damage, edema, fibrin deposition, hyaline-membrane formation, and pnuemocyte proliferation (31, 36, 109). Lungs of patients that succumbed to their disease after 10 days of illness displayed histopathologic lesions of organizing-phase diffuse-alveolar damage, type II pneumocyte hyperplasia, squamous metaplasia, multinucleated cells, and acute bronchopnuemonia. In all cases analyzed the diffuse-alveolar damage was the primary pathology. A three stage process in the lungs has been described with an initial inflammatory or exudative phase, a proliferative phase, and a final fibrotic phase (91). Macrophage proliferation occurs in consolidated areas of the lung (106). Haemophagocytosis in the lung and white-pulp atrophy in the spleen, has

been attributed to cytokine dysregulation that is reminiscent of fatal influenza subtypes H5N1 disease from 1997 (39, 161).

SARS-CoV primarily targets the pneumocytes and macrophages, where pneumocytes are the initial site of infection and the macrophages take up the virus and disseminate virus throughout the lungs (42). Once the pneumocytes are infected, macrophages will take up the virus and disseminate it throughout the lungs and, potentially, other organs. A Toronto study analyzed fatal cases of SARS-CoV and found that there was often virus dissemination to other organs (36). SARS-CoV was found in all patients' lung tissue, in 73% of bowel samples, 69% of lymph node samples, 41% of liver samples, 40% of cardiac samples, 38% of kidney samples, and 12% of skeletal muscle samples. The bowel had a high viral load, but had minimal histopathological changes. There was a 100% correlation of patients having SARS-CoV in the liver and abnormal liver function tests antemortem. Only 40% of patients with abnormal liver function had no SARS-CoV in the liver. Patients secreted virus in nasopharyngeal aspirate and from feces for up to 21 days after disease onset (182). The Toronto study found high viral loads in the gut and liver and moderate loads in the kidney, which is consistent with viral shedding patterns (36). The length of time of post-infection viral shedding, up to 21 days, indicates a difficulty in clearing the virus, which is a common feature of murine coronavirus infection in mice (6, 45).

Studying the innate immune response that is initiated in SARS-CoV infection is difficult because the human lung is a heterogenous mixture of cell types, each of which will respond differently to infection (135, 172). Only some of those cell types express

the ACE2 receptor and are susceptible to infection by SARS-CoV. A major effector in the pathogenesis of SARS-CoV is the role of ACE2 in lung injury. In addition to its role as the receptor which allows SARS-CoV to infect its target cells, ACE 2 is thought to have a pneumoprotective role in lung injury. Intratracheal installation of recombinant Spike-Fc protein in mice resulted in decreased ACE2 expression and a worsening of acid induced lung injury (61). It is thought that the down regulation of ACE2 receptor by Spike-Fc protein reduces the ability of the lungs to negatively regulate AngII signaling. In recombinant Spike-Fc protein treated lungs there is a significant increase in the amount of AngII present after an acid wash. If the mice are treated with an AngII receptor blocker the increased severity of lung injury observed in mice after Spike-Fc treatment in the acid injury model is significantly decreased, but is not returned to control levels. The pharmacological blockade of Ang II receptor AT_1 also decreased the amount of pulmonary edema in the injured lung. This study demonstrates that down-regulation of the ACE2 receptor for SARS-CoV is capable of causing a worsening of lung injury independently of viral infection.

SARS-CoV Cytokine/Chemokine Response

IL-6 and IL-8 are highly expressed in SARS-CoV infected patients (150, 179) and also in patients with ARDS induced by other causes (128) (Table 1). In this latter group of patients TNF-α, and IL-1β are also strongly induced (128). SARS-CoV infected patients also have elevated levels of circulating IP-10, with high IP-10 being correlated with poor patient outcome (41). There has been little to no detection of

Table 1. List of Cytokines/Chemokines elicited during a SARS-CoV infection of humans, cells, and animals[1]

Cytokine/ Chemokine	Function[2]	Increase or Decrease		
		Human	Cell line	Animal Model
IFN-β	Antiviral properties	No change	No change	↑early
TNF-α	mainly secreted by macrophages, involved in the regulation of a wide spectrum of biological processes including cell proliferation, differentiation, apoptosis, lipid metabolism, and coagulation	↑		↑
TGF-β	Multifunctional protein that controls proliferation, differentiation and other functions in many cell types	↓		
IFN-γ	produced by lymphocytes, potent activator of macrophages		↑	
IL-18/ IGIF	cytokine that augments natural killer cell activity in spleen cells, and stimulates interferon gamma production in T-helper type I cells		↑	
IL-6	functions in inflammation and the maturation of B cells, primarily produced at sites of inflammation	↑end		↑
IL-8	chemotactic factor that attracts neutrophils, basophils, and T-cells, but not monocytes; involved in neutrophil activation	↓ ↑progressive and end		↑
NF-κB	transcription regulator activated by various stimuli such as cytokines, oxidant-free radicals, ultraviolet irradiation, and bacterial or viral products	↑late		
STAT	signal transducer and transcription activator that mediates cellular responses to interferons, cytokines, and growth factors	↑activation ↓nuclear transport	↑activation	↑activation
Elk-1	functions as a transcription activator in MAPK signal transduction			
CCL-20	chemotactic factor that attracts lymphocytes and neutrophils, but not monocytes; involved in mucosal lymphoid tissues by attracting lymphocytes and dendritic cells towards epithelial cells.	↑early		
IL-1α	produced by monocytes and macrophages and released in response to cell injury, and thus induces apoptosis	No change		
CXCL-10/ IP-10	stimulation of monocytes, natural killer and T-cell migration, and modulation of adhesion molecule expression	↑		
CCL-2/	chemotactic activity for monocytes and	↑		

Table 1. continued

Cytokine/ Chemokine	Function[2]	Increase or Decrease	Cytokine/ Chemokine	Cytokine/ Chemokine
MCP-1	basophils but not for neutrophils or eosinophils. It has been implicated in the pathogenesis of diseases characterized by monocytic infiltrates.	↑		↑
CCL-5/ RANTES	functions as a chemoattractant for blood monocytes, memory T helper cells and eosinophils; causes the release of histamine from basophils and activates eosinophils.	↑		↑
CXCL9/ MIG	thought to be involved in T cell trafficking as a chemoattractant	↑		
CCL-3	involved in the recruitment and activation of polymorphonuclear leukocytes	↑		
IL-10	produced primarily by monocytes and to a lesser extent by lymphocytes; down-regulates the expression of Th1cytokines, MHC class II Ags, and costimulatory molecules on macrophages; enhances B cell survival, proliferation, and antibody production.	↑convalescent		-
IL-17	proinflammatory cytokine produced by activated T cells; regulates the activities of NF-κB and mitogen-activated protein kinases; can stimulate the expression of IL6 and cyclooxygenase-2 (PTGS2/COX-2), as well as enhance the production of nitric oxide (NO)			-
IL-12	Acts as a growth factor for activated T and NK cells, enhance the lytic activity of NK/lymphokine-activated Killer cells, and stimulate the production of IFN-gamma by resting PBMC			↑

[1]References Used: (22, 41, 42, 48, 65, 81, 128, 138, 172, 179, 182, 186)
[2]Functions are adapted from entries in Gene Cards (http://www.genecards.org/)

interferon early in SARS-CoV infection in patients (13, 148). Coronaviruses are in general poor inducers of interferon relative to most other RNA viruses, and this has been attributed to the sequestering replication complexes containing dsRNA in double membrane vesicles to avoid detection by the host and activation of the interferon response (21, 183, 185). For SARS-CoV a large number of proteins including ORF 3b, ORF6, ORF7, N, nsp1, and M proteins antagonize the IRF-3-STAT axis of the interferon pathway (48, 66, 143). These proteins promote the degradation of cellular RNA and inhibit the formation of the TRAF3TANKTBLI/IKKKε complex (172). SARS-CoV ORF6 protein also prevents STAT1 from being imported into the nucleus, but only in infected cells (39, 42). Neighboring uninfected cells are still able to phosphorylate STAT1 and transport it into the nucleus, which leads to the eventual expression and accumulation of significant levels of interferon in some patients.

In the Calu3 lung cell line NF-κB, STAT, and Elk-1 were persistently expressed starting 12 hours post infection (172). CCL-20, IL-1A, IL-6, and IL-8 are the first group of cytokines activated in Calu3, but are not activated until 24 hours post infection. The activation of IRF-7, which is a critical mediator of the antiviral effects of type 1 interferons, was not observed until 48 hours post infection. The consequence of this delayed activation of IRF-7 is that significant antiviral effect from type 1 interferon would not occur until 2-3 days post infection.

Immune Response to SARS-CoV Infection

Cells that are infected with SARS-CoV do not express IFN-β, creating an initial failure of the innate immune system to be able to respond to infection. SARS-CoV

infection is known to, *in vitro*, result in inefficient activation of macrophages and dentritic cells (DC) (42). In the MA15 infected BALB/c mouse model of SARS-CoV infection alveolar cells have been shown to have a poor ability to activate T cells, which are needed for the adaptive immune response in coronavirus infection (181, 182). In BALB/c mice the majority of virus specific T-cells did not produce IL-10 or IL-17 (181). When BALB/c mice were immunized to SARS-CoV by injection of DC that had been pre-coated with an immunogenic portion of the SARS-CoV spike protein then mice were able to generate specific, protective T-cells in the lungs and spleen. However, during normal infection of mice, DC are not activated properly, so DC are unable to generate specific, protective T-cells that can protect in a primary SARS-CoV infection.

Alveolar cells have been shown to suppress the ability of macrophages and DC to present antigens to induce adaptive immune responses (182). Consistent with the increased severity of SARS with increasing age in human patients depletion of alveolar macrophages in young mice had no effect on disease, but depletion of alveolar macrophages in aged mice protected these mice from otherwise lethal disease, suggesting that a dysregulation of macrophage responses to infection with aging contribute to severe disease (182).

GENETIC APPROACHES TO STUDY CORONAVIRUS PATHOGENESIS

Coronaviruses have been studied for over 60 years. Throughout the years the methods of evaluating viruses have changed, and scientists are continually developing methods that allow us to rapidly evaluate viruses. Some of the methods that are

available to evaluate the role of SARS-CoV in infection and disease are discussed below.

Transgenic Animals

The use of transgenic mice in studying coronaviruses is twofold: elimination of the need for host adapted viruses and abrogating elements of the host immune response to study changes in the pathology induced by infection and the role of these elements in pathogenesis. Several labs have generated transgenic mice that express the human ACE2 receptor so that SARS-CoV could be studied without the requirement of virus adaptation to a murine host. McCray et al generated a transgenic C57Bl/6 mouse that expresses the human ACE2 receptor (hACE2) under the control of the human cytokeratin 18 promoter which confers transgene expression in airway epithelial cells (but not in alveolar epithelia), as well as in epithelia of other internal organs (3). The transgenic mice expressed similar levels of mouse ACE2 as the non-transgenic counterparts in the lung, but in addition hACE2 was expressed in multiple organs, where the ACE2 receptor is not normally found, though this did not guarantee SARS-CoV infection as the virus was not detected in the liver, kidney, or ileum at either 2 or 4 days post infection. Furthermore, the level of hACE2 in the brain was increased as well as in other tissues that normally express ACE2. These mice suffered a lethal disease, with 100% mortality by day 7 in both strains when infected with $2.3x10^4$ PFU. Tseng et al (151) generated two lines of transgenic mice, AC70 and AC63, which both expressed hACE2 ubiquitously, but AC70 expressed hACE2 at a higher level. Because of this AC70 mice developed clinical illness regardless of the route of inoculation (intranasal or

intraperitoneal) and died uniformly within 8 days if infection; whereas AC63 mice developed clinical symptoms but eventually recovered from the infection. These mice also had extensive infection of the CNS during infection. However, researchers noted that not all hACE2 expressing cells in the CNS were susceptible to SARS-CoV infection, finding that they were unable to detect SARS-CoV antigen in endothelial cells of the brain despite their abundant expression of ACE2. While both models may seem extreme in the over-expressing of hACE2 throughout the mouse it is important to realize that SARS-CoV has been found in multiple organ sites in human patients, and that multiorgan involvement is associated with fatal cases of SARS-CoV infection (36, 50). The transgenic hACE2 mice that have been developed to date result in lethal disease when infected with wild type SARS-CoV but in addition to pulmonary infection, a severe encephalitis which is not a feature of SARS in humans likely limits their usefulness to studies of antiviral agents and vaccines on SARS-CoV infection.

Knock-out mice have been successfully used in evaluating the roles of the interferon system in controlling coronavirus infection (40, 119, 135, 162). $IFNAR^{-/-}$ mice, mice that have the IFN receptor knocked out, have been used to demonstrate that IFN signaling is important in control of virus replication and dissemination as well as protection of pulmonary disease (119, 120). These mice also demonstrate that there are secondary mechanisms by which the cell can signal genes that are predominantly regulated by IFN, though these mechanisms were not discussed. Experiments with mice that have had the ACE2 receptor knocked out have confirmed that ACE2 is important in the infection of SARS-CoV, as animals not expressing ACE2 had a 105 fold lower titer

in the lungs than wild type animals (60). STAT1-/- mice are resistant to the antiviral effects of IFN and show worsening of pulmonary disease and an increase of viral replication in the lungs (54). These animals also have a systemic spread of virus to the liver and spleen.

Reverse Genetic Systems For Studying Coronaviruses

Adaptation mutations are useful in identifying genes that are species unique, but do not test the effect of other genes that may be able to effect pathogenesis regardless of species. To investigate a gene's individual contribution a method to make predetermined and targeted changes in select genes is required. There are two options for manipulating coronavirus genomes: targeted recombination and a complete reverse genetic system.

Targeted recombination

Targeted recombination takes advantage of the high natural recombination rate of coronaviruses (89). During normal coronavirus replication the coronavirus RNA dependent RNA polymerase (RdRp) employs a mechanism akin to template switching during minus strand RNA synthesis to accomplish leader-body joining and generate templates for subgenomic mRNA synthesis (115, 132, 188), and this property of the RdRp is thought to contribute to the high recombination rate through template switching (34). Targeted recombination takes advantage of this natural event, in vitro transcribed RNA is electroporated into an infected cell and recombinant virus is generated (38, 53, 84, 93). Recombinant viruses need to be selected from non-recombinants and the selection methods employed have limited this method to manipulating only the 3' most

third of the genome. It is possible for there to be multiple template switching events, so the distance from the original template switch site is important to consider when using this method. The first targeted recombination system used a temperature sensitive trait to select and screen for template switching between the original temperature sensitive virus containing a mutation in the N gene and the new recombinant virus that had lost the temperature sensitive phenotype due to recombination (73). A later experiment optimized the targeted recombination method by substituting the spike protein of MHV-A59 with the spike protein from Feline Infectious Peritonitis virus on the donor RNA (75). This allowed recombination events to be selected based on the host range of the spike protein: mouse or feline, and selected for template switching events that were 5' to the S gene rather than recombination events that were 3' to the temperature sensitive mutation in N. The host range selection was much more stringent: a recombinant MHV that expressed the FIPV spike would only grow on feline cells, the non-recombinant MHV would not. The resulting recombinant felinized virus expressing FIPV S was then used as an acceptor using transcripts of donor RNAs containing the original MHV spike and any additional mutations engineered into the S gene or sequences 3' of the S gene. Any viruses that underwent template switching to the donor RNA would now have the MHV spike and can be selected by their ability grow on mouse cells, whereas the felinized MHV acceptor virus could not. This efficient selection based on host range facilitates the identification and culturing of recombinant viruses.

Complete reverse genetic systems

In order to evaluate the remaining genes in the coronavirus genome complete reverse genetic systems were developed. There are three different systems that can be used for coronaviruses: a systematic assembly of 7 plasmids (134, 175), an infectious cDNA clone that houses the genome in a bacterial artificial chromosome (BAC) (4, 114), and a recombinant vaccinia vector (146). Both the BAC and vaccinia vector are able to house the entire coronavirus genome as a single piece. Because the viral genome is housed as a single piece unique restriction sites may need to be introduced into the genome in order to facilitate assembly of the clone as well as to facilitate later manipulations of the genome, though this is not always necessary (4, 114). BACs can be stably maintained for over 200 passages (4). Vaccinia vectors are classically known for their stability (77). One advantage of these systems is a consistently higher amount of whole genomic cDNA that can be prepared for *in vitro* transcription since there is no stepwise ligation of cDNA fragments, and loss during this process, to generate the genomic cDNA. The BAC system also can be designed with a CMV promoter and thus the BAC can be transfected into cells and generate recombinant virus without *in vitro* transcription. The vaccinia model has been able to successfully generate a reverse genetic system where the 7 plasmid system failed (146). A drawback to these systems is that having the entire genome housed in one vector makes generating mutant viruses more challenging than when the genome is subdivided into multiple plasmids because the number of unique restriction sites is reduced.

The most widely used system is the 7 plasmid in vitro cDNA ligation system (19, 23–26, Weiss lab personal comminuation). The complete reverse genetic system is comprised of 7 plasmids that each contain a cDNA fragment corresponding to a portion of the genome (173–176). The plasmids that contain the genomic fragment are digested with type IIS restriction enzymes that have been engineered to flank the genomic cDNA insert. Enzyme digestion can then liberate the cDNA genome fragment without altering the viral genome sequence. These cDNA fragments are ligated together and *in vitro* transcribed to form a viral genome RNA that can now be transfected into cells with the N gene, either independently expressed or as transcribed RNA) and a recombinant virus can be generated. This system requires more *in vitro* manipulation to generate a full length cDNA that can be used for transcription. However, the maintenance of the genome in multiple fragments facilitates the manipulation of the genome.

SARS-COV MODELS OF DISEASE

A recent paper comparing transcriptional profiling in human systemic inflammatory diseases and the corresponding mouse models reported that transcriptional responses in murine models were a poor mimic of the responses in human disease (136). This study compared the transcriptional responses between humans and mice in large part because of the poor success rate of drug trials moving from mouse to human. They found that responses are similar between humans and mice at, 6-12 hours. However, the overall recovery time for genes to return to base line was drastically different between humans and mice. Specifically, in the case of ARDS, mouse models show R^2 correlations between 0 and 0.8 with 47-61% of the genes shifting in the same direction.

Random chance is 50%, so the correlation between mouse studies approximates that of random occurrence. The investigators also noted that despite all the potential causes for inconsistency in human responses (ie. age, different treatments, disease /trauma severity) the human case studies are highly consistent with each other. In cases of ARDS human responses the R^2 value of the correlation is .55, with 84% of the genes changing in the same direction. Thus caution needs to be exercised in extrapolating results from mouse (and likely other rodent models as well) to human disease.

In the following sections we will examine the validity of the animal model's response to SARS-CoV infection. Animal models fall into three types: animal models using SARS-CoV isolates, animal models using rodent adapted SARS-CoV, and animal models using related coronaviruses.

Animal Models of SARS Employing SARS-CoV

Knowing the zoonotic origins of SARS-CoV it would seem that finding a good animal model for SARS would be straight forward. However, this was not the case for SARS-CoV. For some zoonotic diseases the natural host is unknown because these animals show no signs or symptoms of illness, while in others disease in the natural host is mild and transient, related to differences between the immune responses of the natural host and that of humans (164). In the case of SARS-CoV the natural animal reservoirs show limited disease (bats and civit cats), whereas the human infection is more severe. Because of the limit disease in bats and civit cats other animals were examined for fitness to serve as a model for SARS-CoV infection and pathogenesis.

There are many factors that go into choosing an animal model. The ability of the animal model to actually mimic the disease in humans is required, but one must also consider the cost of experimentation and the ease of working with the animals. Different species of animals have differing responses to coronavirus infection, and so the models must be evaluated in terms of fitness compared to human SARS-CoV infection and disease. In this section we will review the models that have been used in studying SARS-CoV disease.

Primate models

While primates are more closely related to humans than other animals, they are still unique in their responses to infection. Primates are also very expensive to purchase and to house. There is a demarcation between Old World Primates (ie macaques) and New World Primates (ie marmosets) and their responses to disease. Both Old and New World primates are susceptible to infection by SARS-CoV (49, 138). However, neither primate group are susceptible to a lethal SARS-CoV disease (99).

Marmosets that were experimentally infected with SARS-CoV developed a multifocal mononuclear cell interstitial pneumonitis (49). They also develop a more severe hepatic inflammation than human patients and the course of disease began at 2 days and begin to resolve 7 days post-infection. This is a shortened disease course compared to the course of human SARS which typically took 4 to 16 days to resolve.

Macaque models have had mixed results as a viable animal model in the study of SARS-CoV infection. One study reports the effects of SARS-CoV infection in rhesus and cynomolgus macaques (131). Both rhesus and cynomolgus macaques had a limited

disease 2 or 3 days post infection, and all disease quickly resolved. No animals demonstrated signs of respiratory distress, body temperatures remained normal during the study, blood chemistries and hemotologic parameters were, largely, unchanged. A second study with cynomolgus macaques demonstrated that infection with SARS-CoV did not reproduce a severe illness, but did have results similar to the milder SARS-CoV infections seen in younger children (82). A study that used an aged cynomolgus macaque model did show a disease that was similar to the severe SARS-CoV illness seen in elderly patients (138). Using an aged macaque model researchers demonstrated that there is a difference between innate immune response in young animals and aged animals that are infected with SARS-CoV (138). There were only 14 genes differentially regulated, of 518 examined, between the two age groups. After infection of aged macaques there is a more robust induction of NF-κB regulated genes such as IL-6, which has been implicated in SARS-CoV pathogenesis, than in young animals. STAT1 was differentially expressed between the two age groups, with its up-regulation being blocked in younger animals but not older animals. Another study used cynomolgus macaques to evaluate pegylated interferon-α treatment of SARS-CoV infection (52). The researchers do not state the age of animals used in the study, but report infection of type 1 pneumocytes by day 4 post infection, and extensive hyperplasia of type 2 pneumocytes by day 6. The lungs showed multifocal, acute defuse alveolar damage with edema fluid mixed with neutrophils and extensive loss of alveolar and bronchiolar epithelium. Animals that were pre-treated with pegylated interferon-α showed decreased viral titer in the lungs and the severity of the difuse alveolar damage

was reduced by 80%. Animals that were treated with pegylated interferon-α after SARS-CoV infection also had reduced virus titer in the lungs. The other study parameters showed a minor reduction in pathogenesis. Macaques as a model for SARS-CoV are limited in that the lethal disease is only seen in older animals, and it is difficult to obtain an appropriate number of older animals for study.

Medium-sized mammals

Other mammals that can be infected with SARS-CoV include civets, ferrets, and domestic cats (9, 92, 99). These models are intriguing because these animals are less expensive and easier to handle than primates. Cats or ferrets are also able to transmit virus to uninfected animals that are housed with them (9, 92) making them useful for epidemiological and transmission studies. Cats do not show any lethargy or difficulty breathing, but they do show multifocal pulmonary consolidation in the lungs. Cats also develop histological lesions in Peyer's patches (9). Although SARS-CoV replicates in the human GI track, lesions in the intestinal tract are not common in human cases of SARS. Ferrets become lethargic from day 2 post-infection and also show multifocal pulmonary consolidation in the lungs but fail to develop lethal disease (165). The ferret model has only used animals in a single age range and, to date, there have been no published reports of an aged ferret model. There are histological lesions in infected ferret lung, liver, spleen, and tracheo-bronchial lymphnodes. Civet cats, which were the intermediary host when SARS-CoV moved from bats, are capable of being infected with human and civet isolated SARS-coronavirus (80, 85, 99, 152). They become lethargic, develop fever, leucopenia and an interstitial pneumonitis (165). Civet cats do not die

from the infection, and recover about 13 days post infection. There are some histological differences in the pulmonary histopathology from human SARS and the lesions found in civet cats lungs in that multi-nucleated syncytia are absent in civet cats. The lung pathology shows alveolar septa enlargement with macrophage and lymphocyte infiltration, with lesions similar to infected macaques.

Golden Syrian hamsters

Syrian hamsters have also been proposed as a model for SARS-CoV infection (127). Syrian hamsters, 5 week old females, support efficient viral replication that continues to 5 days post infection. At day 2 post infection there is bronchial swelling and mild mononuclear inflammatory cell infiltrates in the bronchioles. By day 3 post infection there are increasing mononuclear and polymorphomuclear cell infiltrates. Lung consolidation was the most extensive at day 7 post infection and affected up to 30-40% of the cut surface of the lungs in some animals. The disease resolved in 14 days with no mortality reported. In hamsters low titers of virus were present in the liver and spleen at days 2 and 3 post infection, but not thereafter. The animals developed a robust protective neutralizing antibody response by day 7, one that the researchers report was more robust than the antibody response in mice.

Two other studies used the golden Syrian hamster model to evaluate monoclonal antibody therapy (126) and the immunogenicity of a live attenuated SARS-CoV infection (78). When treated with monoclonal antibodies after infection 5 week old female hamsters showed a reduced viral burden (126). Hamsters also showed reduced lung pathology by virtue of decreased interstitial pneumonitis and decrease lung

consolidation by day 7 post infection. Neither response was dose dependent, though researchers did show that 4 mg/kg of antibody was not sufficient to protect from infection because not all hamsters had measurable levels of circulating antibodies in their serum. The study evaluating the use of a live attenuated vaccine used 7 week old male hamsters vaccinated with a recombinant SARS-CoV Urbani strain or a recombinant SARS-CoV lacking the E gene (78). After 4 weeks the hamsters were challenged with either SARS-CoV Urbani or a recombinant SARS-CoV with the spike protein of the GD03 strain of SARS-CoV. All vaccinated hamsters had no detectable virus in the nasal turbinates by day 5 post infection or the lungs at any time post infection.

While these studies are promising, the use of the Golden Syrian hamster is limited. These animals do not suffer any type of obvious clinical disease and they completely resolve their lung lesions (127). These animals also do not appear to develop the same clinical disease as in humans. The damage to the lungs does not appear to be immune mediated, so the use of healthy hamsters to study disease pathogenesis is limited. To date there is no evaluation of aged hamsters, so it is possible that, like some mouse strains, there is a lung disease that develops in older animals. There is an immunosuppressed Golden Syrian model that uses cyclophosphamide treatment of hamsters that leads to significant weight loss, expanded tissue tropism of SARS-CoV infection, and increases the viral pathology in the lung, heart, kidney, and nasal turbinate tissues (133). This model is useful because the hamsters have a longer duration of illness, mortality being at 20-35 days post infection, depending on cyclophosphamide

treatment, and have a slower progression of SARS-CoV like disease. However, because cyclophosphamide does cause lymphopenia, suppress B-cell activity and activation, and supresses regulatory T cell function this model is limited only to the study of viral replication and pathogenesis in the host and cannot be used to evaluate the effectiveness of vaccination or antiviral treatment in SARS-CoV infection.

Rodents

Rats and mice are commonly used laboratory animals in disease study. Both are capable of being infected by a human SARS-CoV strain (17). The virus will replicate in different inbred lab strains of mice. However, non-transgenic or non-knock out strains of mice will not develop a human SARS-CoV pathology with a human SARS-CoV. In order to generate a disease with a pathogenesis that is similar to SARS-CoV infection of humans the viruses must be passaged and adapted to mice or rats (22, 99).
Mice make ideal animals to work with because of their low cost and the ability to genetically manipulate these animals. As mentioned before, transgenic mice make for ideal tools to study infection and immune responses in coronavirus infection.

Host-adapted viruses, viruses that have been passaged in an animal until there is a desired result, are useful in dissecting host-function specific genes. These multiple passages in animals result in mutations that allow the virus to thrive in a specific environment (85, 178). Adapted viruses are sequenced and then compared with the parent genome to find mutations that occurred and to attempt to correlate them to the adaptation. Then animals can be infected with the parent or adapted virus and the animal's immune response, ability to grow in target organs, and pathology can be

compared. Adapted viruses have multiple components to their evaluation. Because of the adaptation mutations the virus may not utilize the same set of pathogenic mechanisms as the parent virus does in humans. These viruses are also useful in conjunction with transgenic animals. Both mice and rats have adapted viruses that can be used to mimic a SARS-CoV like disease (22, 100, 101, 114, 123).

Rats have been used in ARDS and ACE2 studies, and so seem like a viable option for an animal model of SARS-CoV infection and disease (12, 16, 27). Researchers developed a rat adapted SARS-CoV by serially passaging the SARS-CoV Frankfurt 1 strain, a mixture of the original virus without an ORF7a deletion and a variant virus that did have the ORF7a deletion, ten times through young F334 rats (101). They found that adult rats (7 to 8 month old males) showed more severe acute lung injury with higher level of cytokines expressed than in the young (4 week old females) rats. Young rats showed limited clinical symptoms and had pathology that was limited to the bronchi, bronchioles, and the alveoli with only mild edema around the blood vessels. Adult rats became lethargic, had ruffled fur and abdominal breathing. Pathology showed congestion, edema, and consolidation of the lungs at days 3 and 5 post infection. They also had fibrin deposition and hyaline membrane formation in the alveolar ducts and alveoli. There was no mortality in either young or old animals.

The limitation of this study is that there is no clear study endpoint. The disease appears to resolve, though researchers do not state when clinical symptoms stop, and there is still virus reported in the lungs of young and old rats by day 21 despite the presence of neutralizing antibodies. Neither of these makes for a compelling argument

for rats as a model for human disease. This study also fails to address the potential differences between older male and young female rats, since they did not maintain gender in the age groups. This study also does not report if the adapted rat virus contains the ORF7a deletion as a majority or minority of the virus population. They also do not address what other mutations, other than the spike Y442S, were required to adapt the Frankfurt1 strain to rats.

A mouse-adapted SARS-CoV that caused disease and mortality in previously resistant young BALB/c mice was first developed in 2007 (123). SARS-CoV Urbani was passaged 15 times through BALB/c mice to generate MA15. In 2009 Day et al reported the development of a new mouse adapted strain of SARS-CoV that could be used as a lethal model for SARS-CoV infection in BALB/c mice. Strain V2163 was adapted to mice from SARS-Urbani after 25 serial passages. This strain caused severe illness in 5-6 week old mice. When MA15 and V2163 were compared it was found the V2163 was more lethal and produced higher virus titers in the lungs of infected animals. However MA15 was found to cause more weight loss and had a later mean date of death in older animals. When compared genetically both strains contained a conserved mutation in the spike protein (Y436H), and both contained mutations in the membrane proteins, in nsp9, and in nsp13 that were not identical between the two strains. Both of the strains elicit expression of IL-12, IL-6, MIP-1α, MCP-1, and RANTES. They also stimulate low levels of IFN-γ, which is not seen in mice that are infected with SARS-CoV Urbani. MA15 stimulates significantly more MIP-1α and RANTES and V2163 stimulates more MCP-1 compared to an infection with the Urbani strain. V2163

stimulates 6-fold more IL-6 than MA15, which researchers believe demonstrate a correlation between IL-6 and mortality.

Later studies used MA15 to study T cell responses that are required for protection for clinical disease (181, 182). In one study, researchers found that the elimination of alveolar macrophages protected mice that were lethally challenged with MA15, but only in older mice, as depletion of alveolar macrophages in young mice had no effects on disease (182). Mice that were depleted showed an earlier and more robust virus-specific T cell response, however it is possible that the use of clodronate to deplete the alveolar macrophages has an effect on T-cell responses independent of SARS-CoV infection, as animals that were treated with clodronate show higher pro-inflammatory cytokines pre-infection. Weight loss was similar in infected and uninfected treated mice by day 2 post infection, but it is possible that the priming response may be affecting overall mortality. Further studies with MA15 infected mice found that SARS-CoV specific CD8 T cells were more protective than SARS-CoV specific CD4 T cells purified from lethally infected mice, and that the protection is dose dependent in animals in which activated CD4 and CD8 T cells were transferred individually or together (181). Both enhance survival in BALB/c mice that are lethally challenged with MA15. They also found that immunization with dendritic cells that were coated with a specific spike peptide were almost 100% protective in BALB/c by induction of a specific T cell response in the lung and spleen.

Another study developed a strain of mouse adapted SARS-CoV, F-musX, from the SARS-CoV Frankfurt strain (100). Researchers found that disease was caused only

in aged animals by day 2 post infection, with a mortality rate of 30-50%. Lungs from aged mouse had significantly higher IL-4 and lower IL-10 and IL-13 levels before infection than young mice, whereas lungs from young mice lungs produced not only proinflammatory cytokines but also IL-2, interferon-γ, IL-10, and IL-13.

The major drawback to the use of the MA15 or other mouse adapted SARS-CoVs is the requirement of older mice for the development of lethal disease. Aged animals are more difficult to acquire in large numbers and they are more expensive than younger mice.

Other Betacoronaviruses as Models

By comparing the members of the betacoronavirus group we can identify mechanisms of lung injury that occur during betacoronavirus infection. Virus-unique contributions and mechanisms of pathogenesis, like contributions of the virus receptor to disease, can also be identified. By virtue of being in the same betacoronavirus genus as SARS-CoV, MHV qualifies as a closely related virus that is capable of being used as a model. However, the specific organ tropism of infection for many MHV strains makes them unsuitable as a model. MHV-JHM and –A59 do not primarily infect the lung with MHV-JHM being neurotropic and MHV-A59 being both neurotropic and hepatotropic. The brain is considered an immune-privileged site, and so the cytokine/chemokine signaling and the cellular response will not be the same as in a less privileged organ, like the lung.

Other betacoronaviruses have already been used to dissect the function of SARS-CoV genes *in vitro* and *in vivo* both by the study of homologous genes and by placing

SARS-CoV proteins into an MHV virus that does not express a homologue to the SARS-CoV gene (57, 76, 113, 145). One example is the study of nsp3, which contains multiple functional domains, one of which is called the X domain (76). The X domain is not consistently conserved in coronaviruses. The X domain is a functional monophosphatase, called ADP-ribose-1"-pase. ADP-ribose-1"-pases are important and ubiquitous cellular processing enzyme involved in the tRNA splicing pathway, catalyzing the conversion of ADP-ribose-1 monophosphate (Appr-1-p) to ADP-ribose and are conserved in coronaviruses and in members of the "alpha-like supergroup" of phylogenetically related positive-strand RNA viruses that includes viruses of medical importance, such as rubella virus and hepatitis E virus (35). Researchers have demonstrated that the X domain is nonessential for replication in cell culture in human coronavirus 229E (76), but the ADP-ribose-1"-pase has been shown to be important in the liver pathology in MHV-A59 infection (35). Another protein conserved amongst lineage one betacoronaviruses, but not SARS-CoV, is the ns2 protein. The Weiss lab demonstrated that the MHV-A59 ns2 is a cyclic phosphodiesterase, similar to those functioning in tRNA metabolism, but its physiologic role is the hydrolyis of 2-5oligo(A), thus functioning to block the induction of RNaseL during MHV-A59 infection (130). Ns2 was found to be non-essential in cell culture (129), but was determined to be critical in liver infection (130, 184). Ns2 activity is not important in all cell types. It has been found to be important in bone marrow derived macrophages (183), but ns2 does not play a significant role in the infection of the brain (130). Thus it is possible that ns2, which is present in other MHV strains, is important to the ability of the virus to replicate in

specific tissues. In another study the SARS-CoV ORF6 protein was placed into a MHV-JHM variant and it was discovered that ORF6 had a role in replication that was previously unable to be identified in SARS-CoV (57, 113, 145). However, the MHV-JHM strain does not produce pulmonary disease, but rather has the CNS as the primary target of infection. Although these studies were helpful in understanding the role of SARS-CoV ORF6, they could not assess the role of ORF6 in the lung because JHM does not traffic to that organ. When comparing the individual contribution of viral genes to pathogenesis it can become difficult to ascertain the role of individual genes. While the nsp1 of SARS-CoV has been shown to play a role in cytokine dysregulation (81), it is important to note that the nsp1 of SARS-CoV is different, by sequence, and is shorter than the nsp1 of MHV. It is possible that the differences in size are in nonfunctional regions or that the differences are purely host-related. However, it is also possible that these sequence differences reflect important functional differences regarding the role of nsp1 in pathogenesis.

In 2006 a study was published that examined that ability of multiple MHV strains to cause a SARS-CoV like disease in various inbred mouse strains after intranasal challenge (3). This study showed that MHV-1 infection of 5-6 week old A/J mice induced a lethal pneumonitis that was similar to human SARS-CoV infection in terms of histopathologic changes and levels of type I interferon and cytokine responses. A/J mice displayed multiple features observed in SARS-CoV infected patients including interstitial pulmonary infiltrates, hyaline membrane formation, multinucleated syncytia, congestion, hemorrhage in the lung, pulmonary edema and the presence of virus in the

liver. Mice develop disease, demonstrated by weight loss, by 2 days post infection and usually die by 7-10 days post infection. The disease is shorter in duration than human SARS, but it is lethal.

A/J mice have a high incidence of spontaneous lung adenomas and tumors readily develop in A/J mouse lungs in response to exposure to carcinogens. They also have a mutation in the IL-3 receptor α chain which is believed to play a role in the abnormal leukopoesis that is seen in these animals compared to C57BL/6 (59). These mice are also susceptible to *Legionella* infection due to a polymorphism in *Naip5*, NLR family apoptosis inhibitory protein 5 (28). A/J mice have an abnormal neutrophil physiology which is demonstrated as a decreased neutrophil infiltration in response to LPS compared to C57BL/6 mice (107). A/J mice are also studied for their Th2 skewed T cell response to allergens as well as autoimmune diseases (2, 157, 163). It is likely that one of these alterations to host immune system of the A/J mouse strain plays a major role in the immunopathogenic response to MHV-1 infection.

In a series of experiments Khanolkar et al compared the T-cell CD4 and CD8 responses in susceptible C3H/HeJ mice with the responses in non-susceptible B6 mice to MHV-1 infection (71). They found that in susceptible C3H/HeJ mice there was a stronger CD4 T-cell response that mapped primarily to epitopes contained in 2 regions in S protein, 2 regions in N protein, and 1 region in M protein. In resistant B6 mice there was a stronger CD8 T-cell response that mapped mostly to S, and none of the CD4 or CD8 responses mapped to the N protein. The CD8 T-cell response in B6 mice was ~11 fold greater than the response in C3H/H3J mice, but the CD 4 response was ~4 fold

higher in C3H/HeJ. From this they concluded that MHV-1 infection induces a more robust and broader CD4 T-cell response in susceptible mice, whereas resistant mice mount a more "broad and vigorous" CD8 T-cell response. This may be due to the genetic background of the mice, as B6 mice lack the I-E^b allele and so they are I-A^b restricted; because of this restriction B6 are unable to bind certain peptide sequences. Similar to SARS-CoV infected patients there is a marked elevation of IL-6 and IP-10 during MHV-1 infection (2, 27). It has also been reported that in MHV-1 susceptible mice that the IFNγ-TNF-α coproduction by CD8 T-cells is reduced in the lung, but not in the spleen or lymph tissues. Also CD4 coproduction of IFNγ-TNF-α is increased in all tissues compared to B6 resistant mice (70). C3H/HeJ mice also had a higher fraction of IFNγ-IL-2 coproduction in the spleen and draining lymph, but not in the lung. This was the opposite in B6 resistant mice which had more IL-2 production in the lung. The reduced expression of TNF-α is similar to SARS-CoV infected patients, but IFN-γ usually remains unchanged in humans.

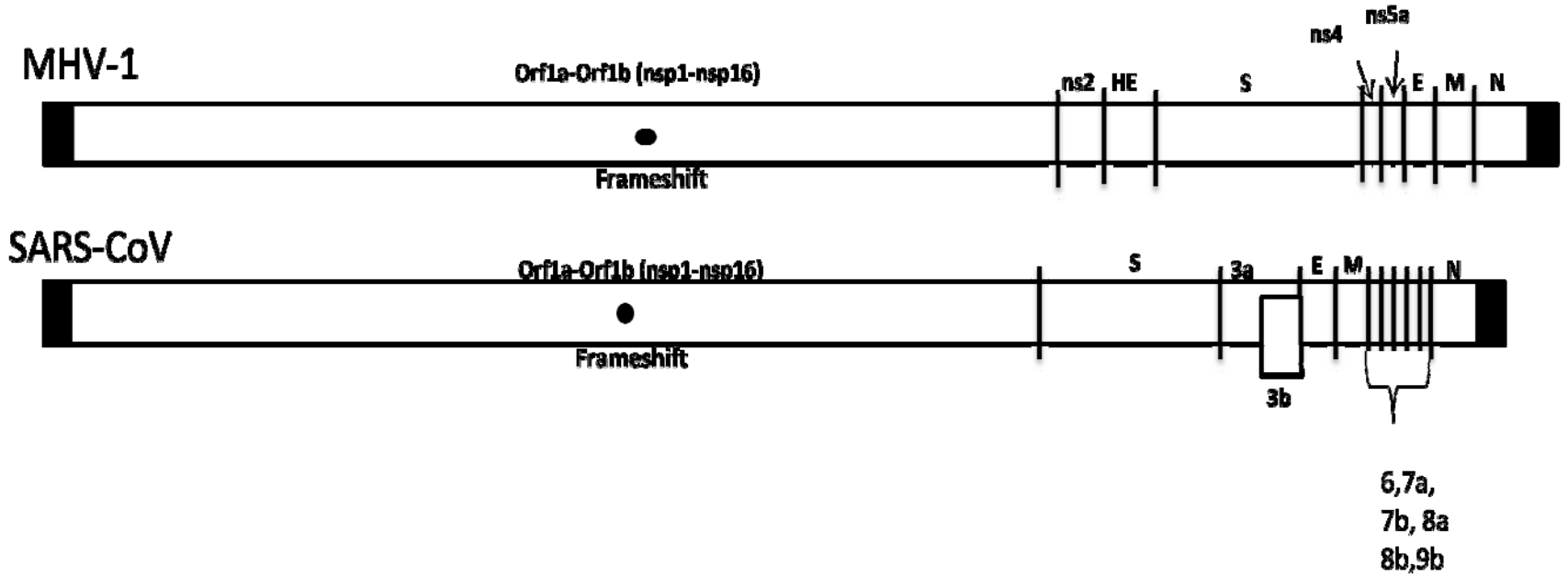

Figure 1. Schematic drawing of the genomes of murine hepatitis virus strain 1 (MHV-1) and severe acute respiratory syndrome coronavirus (SARS-CoV). Both genomes are similar in ORF1a/b, but have different 3' ends with different accessory proteins

Table 2. Comparison of gene size (nucleotide length) between severe acute respiratory coronavirus (SARS-CoV) and murine hepatitis virus strain 1 (MHV-1)

Virus Fragment	Fragment Length, nucleotides	
	SARS-CoV	MHV-1
Genome Size	29751	31386
5' UTR	246	191
ORF1a	13133	13376
ORF1a/b	21220	21499
Spike	3767	4091
Envelope	230	266
Membrane	665	686
Nucleocapsid	1268	1367
Accessory Proteins (size nt)	3a (824) 3b (464) 6 (352) 7a (368) 7b (134) 8a (119) 8b (254) 9b (296)	2 (797) HE (1268) 4 (419) 5a (323) I (405)
3'UTR	362	280

MHV-1 seems like an ideal model of pathogenesis. MHV-1 requires no BSL3 facilities, is a lower risk pathogen than SARS- or SARS-associated CoV, it naturally infects the lungs of mice, and creates a lethal SARS-CoV like disease in a specific mouse strain (A/J) while still causing non-lethal lung disease in other strains. Because it produces a non-lethal pulmonary infection in most strains, various mouse strains can be used to evaluate gain of function or effect of genes in mutated or recombinant MHV-1 viruses and to interrogate the role of specific host genes. However, the MHV-1 model also has admitted limitations. The absence of exact copies of SARS-CoV specific genes makes it difficult to evaluate those genes' role in pathogenesis (Table 2, Figure 1). To date no complete reverse genetic system is available for MHV-1, however there is a targeted recombination system that could be used to introduce some of the specific SARS-CoV genes into MHV-1and study their effect on pathogenesis in this model (83). Another considered issue is that because SARS-CoV utilizes ACE2 the virus is regulating a major signaling cascade that is not mimicked in other betacoronavirus models that use a different receptor.

SUMMARY AND CONCLUSIONS

Animal models will likely not be able to completely recapitulate disease and pathology that occurs during infection of humans with SARS-CoV. Models should be able to accurately represent what occurs in human and should be able to do so in a manner that is safe for researchers and that is not overly expensive. While primate models of disease are, generally, considered to accurately mimic human disease they are expensive and difficult to handle. Smaller mammals are safer and less expensive to

work with and house, and but usually require host-adapted viruses to recapitulate human disease. This still puts the researcher at risk by handling a virus closely related to the human infectious agent. Related coronaviruses that are non-infectious to humans that naturally infect a small mammal are ideal in terms of cost and safety. However, differences between humans and mice can make understanding the pathogenesis of SARS-CoV difficult. In fact, a recent publication has called into question the relevance of much of the mouse data regarding human inflammatory diseases (136). However, in this review we have demonstrated that the models of SARS-CoV do, in part, mimic the disease course that is seen in humans not only in terms of cytokine/chemokine response, but also in histology and cellular pathology.

CHAPTER II

MATERIALS AND METHODS

VIRUSES AND CELL CULTURE

Delayed brain tumor (DBT) cells were maintained at 37°C and 5% CO_2 in Dulbecco's modified Eagle's medium (DMEM) supplemented with 10% calf serum (HyClone), 2% 0.2M glutamine (Sigma-Aldrich), and 1% penicillin-streptomycin (5,000 IU/mL and 5 mg/mL respectively, MP Biomedical). *Felis catus* whole fetus (FCWF) cells were grown in DMEM supplemented with 10% fetal bovine serum (HyClone), 2% 0.2M glutamine, and 1% penicillin-streptomycin at 37°C and 5% CO_2. L2 cells were maintained at 37°C and 3% CO_2 in DMEM supplemented with 10% calf serum 2% 0.2M glutamine, and 1% penicillin-streptomycin.

The origin and growth of Murine Hepatitis virus strain 1 (MHV-1) (3) has been described. MHV-1 was originally acquired from the ATCC® as isolate/strain VR-261™, plaque purified and then passaged it in DBT cells to expand.

MHV-1 and recombinant MHV-1 viruses were propagated in DBT cells. The recombinant feline MHV-1 (fMHV-1), in which the sequences encoding the spike protein ectodomain are replaced by the corresponding region of the feline infectious peritonitis virus (FIPV) spike protein ectodomain, was created for us in the Weiss lab. This virus was propagated in FCWF cells.

PLAQUE ASSAYS AND PLAQUE CLONING OF VIRUS

Virus was prepared in 10-fold serial dilutions in DEM2. Six-well cluster dishes were seeded with $0.8x10^6$ L2 cells 2 days prior to the assay. 200µL of each dilution was placed into two wells of a cluster plate and incubated at room temperature for 1 hour on a rocking platform. At the end of the incubation period wells were overlayed with 0.8% agarose containing DMEM supplemented with 2% calf serum, 2% 0.2M glutamine, and 1% penicillin-streptomycin and incubated at 37°C and 3% CO_2. 2.5mL of DME2/0.8% agarose mixture, warmed to 50°C was carefully pipetted into each well. Clusters were maintained at 37°C, 5% CO_2 for two days. On the second day, if plaques were visible, the DME2/agarose layer was removed and the wells were stained with crystal violet. Excess stain was removed by gently flooding the wells with water until the water was clear. Cluster plates were allowed to dry for at least 24 hours prior to counting or characterizing plaques.

If plaques were to be picked the monolayer was not fixed and stained, rather on the second day of incubation plaques were identified by circling plaques with a marker. Plaques were picked using a pasture pipette into a small volume of DME2. The agarose plug and any cells and debris in the plaque was pipetted up into the pasture pipette and was placed into a 1.5mL tube with 0.5-1ml DME2 and vortexed. The plaque was stored at -80°C until passaged. To propagate the virus contained in a plaque the DME2 containing the plaque was inoculated into DBTs in a T25 flask that was at about 80% confluency. The DBTs were incubated at 37°C in a 5% CO_2 atmosphere and monitored daily for cytopathic effect.

GROWTH KINETICS ASSAY

One day prior to the experiment six 96-well plates were seeded with $5x10^4$ DBT cells per well (three wells per virus to be used in the study and additional control/surplus wells), fed with DME10, and incubated overnight at 37°C. For each virus used in the study three wells of DBTcells (making three replicates per virus) were infected at an MOI of 3 by incubating them with viral inocula at room temperature for one hour while rocking. After one hour one plate was stored at -80°C as the time zero time point, and the remaining plates were washed with DME0, cells were fed with DME2, and remaining plates were then incubated at 37°C until 4, 8, 12, 16, and 24 hours post infection where one plate was moved to -80°C for each time point. Once all the time points had been collected the virus was titered by plaque assay, as described above.

RNA PREPARATION

For routine sequencing of virus 80% confluent DBTs were infected at an MOI ≥1 and incubated for 8-10 hours. When approximately 80% of the cells were either lysed or fused into syncytia, the cells were lysed with RLT+ βME, as described in the RNeasy Mini Kit (Qiagen) instructions. Lysate was stored at -80°C until RNA was purified as described in the manufacturer's protocol.

TARGETED RECOMBINATION

The original MHV-1 Donor plasmid was generated from MHV-1 infected cell RNA. DBT cells were infected with MHV-1 at a multiplicity of 0.3 and total RNA extracted at 7 hours post infection using an RNEasy Mini Kit. The freshly prepared RNA was used as template for cDNA synthesis (Superscript II, Invitrogen) with primers

specific to regions containing the structural genes. For the region encompassing the HE gene from codon 28 extending into the E gene, cDNA was primed with an oligonucleotide designated E60-40rev with the sequence GACTATAAAAATAATCTGCC. The resulting cDNA was PCR amplified with the forward primer HE28-BsmBI-FW-new (sequence GTACGTCTCAACCTCTCAACATCGTTTCAC), containing a BsmBI site at its 5'end to facilitate later recombinant addition of the MHV 467 nucleotides from the 5' end of the genome with a T7 promoter, and the reverse primer E60-40Rev using a mixture of Vent and rTth DNA polymerases as described previously (28). The resulting amplicon designated HE-S was TA cloned into pGEM-T Easy (Promega). Similarly, a cDNA that would encompass the 3' end of the genome was synthesized by RT-PCR using primer N-RV-SfiI (GGCCATTTAGGCCTTAATTAA$(T)_{15}$GTGATTCTTCAATTGGCC) for the cDNA synthesis reaction and amplified with S45-FW5 (GCGATTGGTGCTATACAGG, nts 4109-4128 in GenBank Accesssion EF682498) and N-RV-SfiI primers for the PCR step. The amplified DNA fragment extending from nucleotide 4109 to the 3' poly (A) tail in Genbank Accession EF682498 was subsequently TA cloned into pGEM-T Easy and two clones designated SN#4 and SN#13 were obtained. A cDNA extending from position 1379 - 5477 and containing the S gene from codon 9 was similarly RT-PCR amplified with a forward primer, CCTAATACCCTCTTGCCTAGGGTATATTGGTGACTT, and a reverse primer, CTGTCCTTCCACCTGCAGGTGTACATCTAGTCAATCCTCG. To allow subsequent recombinant DNA manipulations, the forward primer contained two coding silent

mutations in codons 13 and 14 of the spike gene (T1394C and T1395C relative to GenBank Accesssion EF682498) to introduce an AvrII site (underlined in the primer sequence). The reverse primer introduced mutations G5458C, C5460T, T5461G, T5463A, C5464G, and C5465G (all mutations are in the positive sense) to introduce the SbfI site (underlined in the primer sequence) 3' to the spike gene termination codon and prior to the gene 4 transcriptional regulatory sequence. The resultant cDNA fragment was TA cloned into PCR 2.1 Topo and designated clone 4B. All clones were sequenced in their entirety. The first 467 nucleotides of MHV-1 containing the entire 5'UTR and a portion of ORF1a was amplified with a forward primer containing a T7 promoter followed by MHV-1 sequences 1-21 and a reverse primer that contained a BsmBI site. The 5' UTR with a T7 promoter was fused to the remainder of pDonor utilizing the BsmBI site at the 5' end of the HE sequence contained in this plasmid.

A recombinant MHV-1, designated fMHV-1 was generated for us in the Weiss lab using targeted recombination. Briefly, a restriction fragment containing the Feline Infectious Peritonitis Virus (FIPV) spike protein ectodomain fused to the highly conserved MHV-A59 transmembrane and cytoplasmic domains was excised from pfMHV (75) by digestion with AvrII and SbfI and exchanged with the corresponding MHV-1 sequences in pDonor to produce the plasmid pDonor-S_{Fe}. fMHV-1 was generated by targeted recombination by electroporating in vitro synthesized T7 transcripts from pDonor-S_{Fe} into L2 cells that had been infected with MHV-1 and overlaid on FCWF cells to select viruses that had acquired the ability to enter and replicate in feline cells. One recombinant virus, designated fMHV-1, was then plaque

cloned and expanded in FCWF cells. This virus was then used in later targeted recombination experiments as the acceptor virus.

Recombinant MHV-1 viruses were generated by targeted recombination essentially as described in Kuo et al. (75) with the exception that fMHV-1 was used as the acceptor virus and transcripts from pDonor and mutant versions of pDonor were used as donor RNAs, rather than transcripts from the MHV-A59 based plasmid, pMH54. pDonor plasmids were digested with PacI to linearize the plasmid. pDonor RNA was transcribed using mMessage mMachine® T7 Transcription kit (Ambion) as previously described (75). FCWF cells, at approximately 80% confluence, were washed in DMEM and infected with fMHV-1 at an MOI of 0.5 to 1.0 for one hour. After infection with fMHV-1 cells were fed with supplemented growth media and incubated at 37°C, 5% CO_2 for 6-8 hours prior to transfection. RNA was transcribed the day of infection and was transfected into infected FCWF with the Nucleofector using Kit V, protocol T-21 according to manufacturer's instructions (Lonza Corp.). Infected/transfected cells were then overlayed onto subconfluent, ~40%, DBT cells and incubated as described for 3 days (75, 83). Cells were visually monitored and on day 3 were blind passaged onto fresh DBT cells to further enrich for recombinant viruses that had regained the ability to infect murine cells. If syncytia and plaques were visible in the blind passage then virus was plaque purified on L2 cells. If no signs of infection were present in the first blind passage, a second passage was done prior to plaque cloning. Recombinant plaque purified virus that was recovered was expanded in DBT cells and viral RNA was collected from infected cells. RNA was purified using the Qiagen Kit according to

manufacturer's instruction and reverse transcribed as described and the cDNA was sequenced to confirm the presence of the desired genetic markers (for primer list see Table 4).

CONSTRUCTION OF CDNA CLONES

DBT cells at a confluence of 80% were infected with MHV-1 at a MOI of 0.5-1.0 and the infection was allowed to proceed until 80% of the cells were dead or or in syncytia. Cell supernant was removed and centrifuged at 2,000 rpm to clarify and remove cellular debris. Virus in clarified supernant was partially purified by pelleting through a 30% (w/w) sucrose pad at 4°C, 25,000rpm, for 3 hours using the Sorvall SW28 rotor (Sorvall Ultracentrifuge, Thermo Electron Corp). Pelleted virus was resuspended in Tris-buffered saline containing 20U of RNase (RNase cocktail, Invitrogen) and 40U of DNAse (Turbo DNase, Invitrogen) and digested at 37°C for 60 minutes. Viral RNA was extracted with either the RNA-Easy kit (Qiagen) or the RNA Mini kit (Bioline). RNA was converted to cDNA using Super Script III (Invitrogen) and a MHV-1 specific primer (Table 3). cDNA fragments ranging 2 to 5 kb were then amplified using long, accurate PCR using a mixture of Vent (New England Biolabs) and rTth (Invitrogen) DNA polymerases as described previously (83) with the MHV-1 specific primers listed in Table 3. Fragments were also amplified using the Kapa HiFi Master Mix (Kapa Biosystems,) according to the manufacturer's instructions. Fragment

Table 3. Primers used to generate the MHV-1 Complete Reverse Genetic System fragments.

MHV-1 genome position	Purpose	Primers (lower case red letters indicate planned mutations, bold underlined indicate addition of restriction sites)
1-21bp	A start Fw'	GTACCCTCTCAACTCTAAAA
4838-4868	A/B junction Rv'	**GCTCTTC**TTTgTAACAAGACGCCAGTCTGTGGGCAG
908-914	Δ BsQI internal mut	GGCGTATGCaCTcCTTAAGGGCTATCGC
4863-4887	A/B junction Fw'	**GCTCTTC**AcAAATTTGATAGTGTTGATGGTG
9500-9518	B end Rv'	CCACTGAACTTGCCGTTAA
8877-8897	C start Fw'	GGTATGAGTCTACATTTGGTC
11438-11461	C/D junction Rv'	**GCTCTTC**TGgTTTATGCTGCGCATGGTGAC
11455-11479	C/D junction Fw'	**GCTCTTC**AAAcCACGACGTCTTCTCTATTATG
13006-12986	D/E junction Rv'	**GCTCTTC**TAAGTATAGCATACACAATCCTGCCC
13006-13031	D/E junction Fw'	**GCTCTTC**TACTTAGTGACTGTGACGGTCTCAAG
15704-15683	E/F junction Rv'	**GCTCTTC**ATgACATTAGGTATAGGCGC
15699-15721	E/F junction Fw'	**GCTCTTC**TGTcTACCGCGCGGACCATGTTG
19108-19090	F mid Rv	TAGGGTTGCCAATGTCATA
18920-18940	F SbfI Fw	ATGCTATCATGACTCGATGCT
21513-21497	F SphI Rv	AGCCCCTCCATTCCACA
18942-18961	Fmid Fw	AGCTGTCCATGATTGCTTTT
22666-22688	F/G junction Rv'	**CGGACCG**ACTGTCACCAAATAGA
22689-22700	F/G junction Fw'	**CGGTCCG**ACTGTAACTATG

sizes are as follows: A, 4868 nt; B, 4655nt; C, 2584nt; D, 1531nt; and E, 2677nt. The F fragment (6999nt) was PCR amplified in three parts where native SbfI and SphI sites between 22662 and the start of G were used to ligate the fragments together. cDNA was cloned into the LC-Kan vector (Lucigen) per manufacturer's protocol. Clones were picked and sequenced to confirm the presence of the desired insert as well at to confirm if the sequence matched the NCBI MHV-1 genome (Accession FJ647223.1). The G fragment was generated by using a forward primer that contained an RsrII site and PCR amplifying the region between the HE gene and the AvrII site introduced into S with pDonor as the template. The PCR fragment was cloned into a pGEM T-Easy (Promega) vector and the RsrII fragment was introduced into the G fragment by restriction fragment exchange. Deviations from the MHV-1 genome that we wished to correct were corrected by restriction digestion and fragment swapping or site-directed mutagenesis. Site directed mutagenesis was done using the QuikChange II XL Site Directed Mutagenesis kit (Stratagene) per manufacturer's instructions.

COMPLETE REVERSE GENETIC SYSTEM

Primer boundaries and fragment sizes were selected based on previously designed MHV Complete Reverse Genetic Systems (Figure 2) (176, 177). We elected to use BspQI, a Type IIS restriction enzyme rather than BsmBI employed in for the MHV-A59 (176) and MHV-JHM (personal communication, Weiss lab) reverse genetic systems, because the number of native BspQI sites that would need to be eliminated during construction were fewer in the MHV-1 genome than if we had used BsmBI. There is a native BspQI site located in the "A" fragment. Because of this a mutagenesis primer

was designed to make non-coding mutations to remove the native BspQI (Table 3). A second BspQI site is located in a highly conserved region of coronavirus genomes, called the "octomer"(46). We elected to introduce a RsrII site, to avoid altering this highly conserved region, to join the "F" and "G" fragments, a strategy that has been previously employed for constructing a targeted recombination plasmid and shown to have no effect on replication of the resultant virus (75). Primers used to introduce point mutations or restriction digestion sites into the fragments are listed in Table 3.

PLASMID CONSTRUCTION

Amplified cDNAs were cloned into the pSMART LC-KAN vector (Lucigen Corp.) according to the manufacturer's instructions. Plasmids were sequenced to confirm sequence identity to the reference MHV-1 sequence posted in GenBank, accession FJ647223.1, which is missing the first 25 nucleotides. To generate the entire MHV-1 genome sequence we combined FJ647223.1 with Murine hepatitis virus strain 1 leader plus the most 5' part of ORF1ab, GenBank accession EF682499.1. Mutations found in the clones were corrected either by restriction fragment exchange with clones not containing a particular mutation or by site directed mutagenesis. Site directed mutagenesis was performed with the QuikChange XL kit (Agilent Technologies) according to manufacturer's instructions.

CDNA FOR WHOLE GENOME SEQUENCING

Approximately 20 T175 flasks of 75% confluent DBT cells were infected with MHV-1 P2 or P3 stocks at a MOI=.01-.05 and cultures incubated for 24-48 hours until CPE completely involved the monolayers and cells were beginning to detach. The

infected cell supernatants were collected and clarified by centrifugation at 20,000 rpm (rotor 42) for 30 minutes at 4°C in a refrigerated Sorvall RC6 plus centrifuge. Virus was pelleted through a 30% sucrose (w/w) in MSE buffer (10mM MOPS, pH 6.8; 150mM NaCl; 1mM EDTA) pad at 25,000rpm for 2.5 hours in an SW28 rotor in a Sorvall Ultracentrifuge. The supernates were decanted and the pellets were resuspended in MSE buffer (total volume <1 ml) and then placed on a continuous 20-60% sucrose gradient and centrifuged overnight at 25,000rpm. The opalescent virus-containing band was collected by puncture and aspiration with a needle and syringe, diluted to a total volume of 11.5 ml with MSE, and virus was pelleted by centrifugation in an SW41 rotor at 35000rpm for one hour. The virus-containing pellet was resuspended in 200μL MSE buffer per pellet, multiple pellet volumes were combined and incubated with 20U RNase and 20U DNase for 1 hour at room temperature in order to remove any pelleted nucleic acids from co-sedimenting material. Viral RNA was extracted with the Qaigen RNeasy Mini kit per the manufacturer's instruction. Viral RNA was converted to cDNA using both MHV-1 specific primers, random primers, and a polyT-containing primer specific for the MHV 3' end. For first strand synthesis, purified viral RNA and 2μg of random hexamer primer (Takara, catalogue no. 3801), 1μg of (dT)15 GTGA (a primer specific for the 3'UTR of MHV), and 83ng of MHV-1 specific primers listed in Table 4 were reverse transcribed with Superscript III (Invitrogen). Primers were annealed by incubating at 65°C for 5 minutes and placing on ice for 2 minutes. cDNA synthesis was initiated by the addition of 4μL of 5x First-Strand Buffer, 2μL of 0.1M DTT, 1μL of 10mM dNTPs, and 0.5μL of RNase inhibitor (Ambion or New England Biolabs),

incubating at 25°C for 2 minutes and adding 1μL of Superscript III Reverse Transcriptase. The reaction was continued at 25°C for 10 minutes, 42°C for 60 minutes, and 70°C for 15 minutes. For second-strand synthesis 20μL of the first-strand reaction was mixed with 59.5μL of water, 10μL of NEBuffer2, 1.5μL of 1M $(NH_4)_2SO_4$, and 3μL of 10mM dNTPs and incubated on ice for 5 minutes. RNase H (NEB M0297) was added at 1μL and DNA polymerase I (*E. coli*, NEB M0209) was added at 5μL and the reaction was incubated at 16°C for 3 hours. The double-stranded cDNA was purified with the PCR purification kit from Bioline (BIO-52057) and the concentration was determined with a NanoDrop spectrophometer. The cDNA was taken to the Borlaug Institute (Texas A&M University) where it was purified, and a library for Illumina sequencing was constructed by the staff.

COMPLETE GENOME SEQUENCING AND ANALYSIS

Sequence was obtained with the Illumina HiSeq 2500 and was analyzed using CLC Genomics Workbench 6 software (CLC Bio). A Qualitative Variant analysis was run at 10%, 5%, and 2% on sequence aligned to a whole MHV-1 genome that is a combination of the MHV-1 genome (FJ647223.1) and the MHV-1 5' UTR leader (EF682499.1), which added 25 nucleotides to the 5' end of the MHV-1 genome submission in GenBank. We set the Neighborhood radius at 5, the Maximum gap and Mismatch count at 2, the Minimum Neighborhood quality at 10, we ignored non-specific matches, and the minimum coverage was set at 10. Because of our primer selection we did not require the presence of the mismatch in both forward and reverse reads.

SUBCLONING AND SEQUENCING OF NSP13 AND NS4

MHV-1 P2.2 was inoculated onto subconfluent DBT cells (~80%, T175) at an MOI of 0.1 by removal of the media from the cells, washing with DME0, addition of the supernant, rocking at room temperature for one hour, removal of the media, and feeding the cells with DME10. Cells were incubated at 37°C, 5% CO_2 for 20 hours. After 20 hours the supernant was removed and clarified and 1mL was passed onto a new T175 flask of subconfluent DBT's (~80%) and was inoculated as described above.

The cells from the T175 were lysed with lysis buffer RLT with 10% β-mercaptoethanol (Quaigen, RNAeasy). Manufacture's instructions were followed to extract RNA. SuperScript II (Invitrogen) was used to reverse transcribe cDNA for the nsp13 region (primers: F822 (GTGAGGACCATAAGCCACAG), MHV-1_17145-22RV (CTGTACAGTACAATAGCGCTTCAT)) and ns4 (S45 FW7 (AATTGTTGTGATGAGTATGG), EfixC-TRV(GGGGACAGCAACAAAGTA)) in separate reactions. This was done for P3.2 and P4.2.

A ten percent lung homogenate was prepared from a mouse infected with MHV-1 (P2.2) and euthanized on post infection day 3 and clarified by low speed centrifugation. The clarified homogenate was then pelleted through a 30% (w/w) sucrose in MSE pad for one hour at 40,000rpm using a TLS55 rotor in the Optima TLX Ultracentrifudge (Beckman Coulter). The pellet was resuspended in 200µL of lysis buffer RLT with 10% β-mercaptoethanol and RNA was extracted per manufacturer's instructions. Superscript II was used to reverse transcribe cDNA as described above.

cDNA was PCR amplified using the 5'Master Mix (5'Prime, 2200100) and the resulting product was cloned into the pGEM T Easy vector, per manufacturer's instructions (Promega). Colonies from P3.2, P4.2, and lung nsp13 and ns4 ligations were picked and sequenced to verify the presence of the variant nucleotide found during whole genome sequencing.

CARE AND INFECTION OF ANIMALS

Female A/J mice between 5 to 8 weeks of age (Charles River Laboratories or Jackson Laboratories) were maintained in microisolator cages and fed standard lab chow diet and water ad libitum. Mice were held for varying lengths of time, no less than 2 days and no more than one week, and allowed to acclimate before being infected. Mice were anesthetized by exposure to isoflurane for infection with MHV-1. Once anesthetized 50μL of virus diluted in ice-cold DMEM supplemented with 2% serum, 2% glutamine, and 1% Penicillin-Streptomycin was instilled onto the nares, and mice were observed until the virus was inhaled. Mice were weighed daily, and percent oxygen saturation determined with a MouseOx® pulse oximeter, and monitored for symptoms of disease including ruffled fur and visible difficulty breathing. Mice were euthanized if they lost more than 20% of their start weight or if they had oxygen saturation levels equal to or less than 80%. At various times postinfection, mice were sacrificed by lethal CO_2 exposure. Lungs, livers, and brains were collected and analyzed for viral titers and histology as previously described (83). Processing of organs for histology is described below. Samples for viral titration were weighed and 10% homogenates (w/w) were prepared with supplemented DME2. The organs were homogenized manually in

Dounce homogenizers and then the homogenized sample was clarified by low speed centrifugation and virus titers determined by plaque assay. All protocols were approved by Animal Welfare Committees and complied with NIH guidelines.

MEASURING OXYGEN SATURATION

Oxygen saturation levels were measured and recorded in mice using the MouseOx® pulse oximeter (Starr Life Sciences Corp.)(154). All measurements were taken while the mice were awake, using the small size collar clip from Starr Life Sciences. Oxygen saturation, pulse, and breathing rate was measured and recorded for at least 30 seconds. Data was reviewed to make sure there were no error messages. Any measurements with error messages relating to oxygen saturation or lost signal (error code 4, 6, or 7) were deleted from the data set.

HISTOLOGY

Organs that were collected from mice were placed into a 4% paraformaldehyde solution for at least 24 hours, organs were sectioned and sent to the Texas A&M Veterinary Integrative Biosciences Histology laboratory where samples were embedded in paraffin, sectioned, and stained with hematoxylin and eosin per the histology laboratory's protocol. Sections of the lung from all groups and controls were examined by light microscopy. Assessment of the degree of lung pathology was scored from 1 to 4 as follows: Extent, alveolar thickening and inflammation, edema, desquamated cells, and presence of hyaline membranes.

Table 4. List of MHV-1 primers for sequencing confirmation

Genome Start	Primer
23779	GTGTCTTATTGGGTATAGC
24487	CATTTTTACCAACAGGG
28135	CAATAAATAACTAGGCC
25301	ATGGCGATACTSTGGCTGG
25551	AATGTGGTGGAAGCAACG
25601	AGAAAATGTGGCAGCG
26467	GGAACTTAGCGTGACACC
26722	CATAAAAGTGCTGCCTCC

Table 5. List of Primers used for the MHV-1 whole genome sequencing

Primer name	Primer Sequence 5’ to 3’
5’FW	GAGTGATTGGCGTCCGT
5’ RV	CTTACGAAGAAGGATGG
A406	TCAGTCCGCCATAATCCG
A1356	ATTGCTGTGGTGACGC
A2973	GAGGCGATGAAGTGATTG
A3400	ACTTAATGCGCCAGCGGAC
B514	ATGGCAGGAGGCTTGGAA
B1773RV	AAACCACATATCTACACCC
B1510	TGCCAATGAGTTCTGAT
B2826	ATGGCTAACGGCGGC
B3907	ATGGTGTGCTAAGGGAT
B4291	ATGCCTCTCTGTA
D1215	TTCAAGATGCTGATGGCG
E469	TTGGCGAGATGGTAGC
E1293	TACTTATAGGGAGTTCGACC
C723	GCTGTGGTTGGATGATA
C1068	CTGCGGTTCTGTAGGAT
F365	AGCGTTCTCTTGATAGAGCG
F1826	CCTCGTGTGCTACTGAATAAGG
F2771	GGAATGTTTGCCGAGAGAG
F3023	TGTAGTGTCTGCAACAAGCG
F4607	AATGAAGCTCTAGCACGTGG
F5563	TCGTGACAAGTTGGCTCTG
F6386	GATCCCACACTGCACAGTG
MHV3’UTR	CCTGGGAAGAGCTCACAT
C1451	GATTCCAGGGTAAACAAA
HE308FW	CAATTATACGGGTGAGGGAGAC
HE35208	AATGAGAGCTACATCAACCTC
S45 2957FW	CATAAAAGTGCTGCCTCC
S45 FW8	AAACCTCATCTTAATTCTGG
S45 FW3	AATGTGGTGGAAGCAACG
E1to22	ATGTTTAATTTATTCCTTACG
N 643-663	CCAAATAATCGCGCTAGAAG

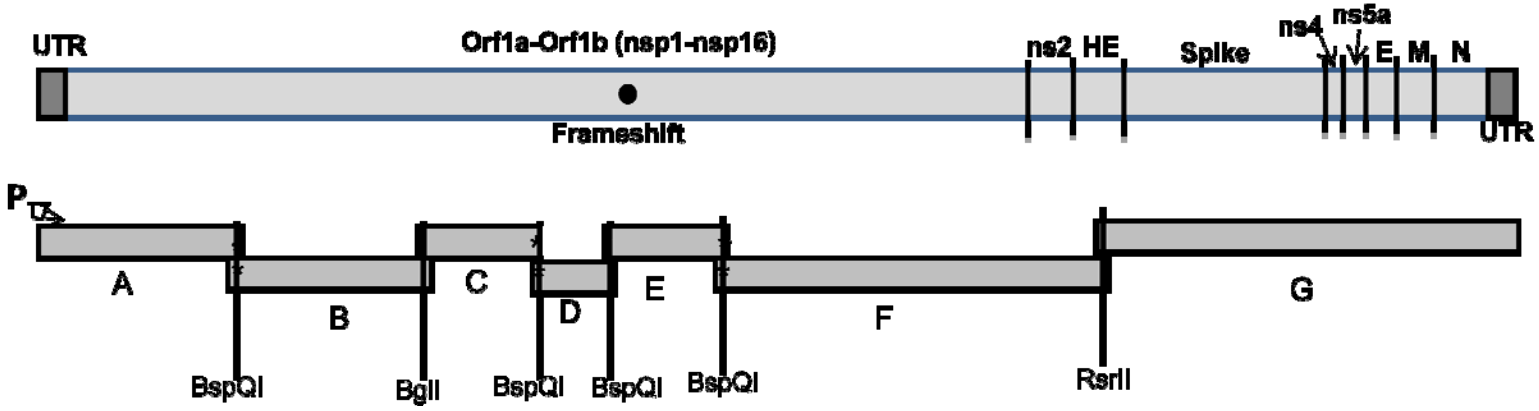

Figure 2. Schematic of MHV-1 genome and schematic to assemble a complete infectious cDNA clone. The component clones junctions are shown relative to their position in the MHV-1 genome. The A fragment has a T7 promoter cloned in front of the 5' untranslated region (UTR). Clones A-F encompass Open reading frame (ORF) 1a and 1a/b which are proteolytically cleaved to form nonstructural proteins 1-16 (ns1-16). Clone F also includes nonstructural gene 2 (ns2) and a portion of the hemagglutinin esterase (HE) gene. The G clone includes the 3' portion of the HE gene and the remaining structural genes and strain specific non-structural genes: spike, nonstructural gene 4 (ns4) and 5a (ns5a), envelope (E), membrane (M), nucleocapsid (N). G also includes the 3' UTR. Native BspQI sites are not shown in this figure (see Chapter 5).

CHAPTER III

GENETIC MANIPULATION BY TARGETED RECOMBINATION PRODUCES RECOMBINANT VIRUSES THAT HAVE AN *IN VITRO* PHENOTYPE IDENTICAL TO NON-RECOMBINANT VIRUS BUT ARE NOT PNEUMOPATHOGENIC AND MHV-1 RAPIDLY ATTENUATES IN CELL CULTURE

INTRODUCTION

In November of 2002 a Severe Acute Respiratory Syndrome (SARS) disease began in China and spread to Hong Kong, Singapore, Vietnam, Taiwan, and Canada (14, 106, 150). It was discovered to be a new coronavirus that was named SARS-CoV (31, 109). SARS-CoV infection has not been seen outside laboratory source infections since 2003 (14). The new SARS-CoV was found to be a relation to the group 2 coronaviruses, with viruses like Mouse hepatitis virus (MHV) (72). Coronaviruses are known to cause a variety of diseases in animals, and was only thought to cause limited upper respiratory infections in humans (98, 110, 187). However, SARS-CoV causes severe pulmonary disease characterized pathologically by acute alveolar damage and virus has been found systemically in infected patients (105, 116, 147, 166).

Coronaviruses have a 5' untranslated region (UTR) that has important RNA structural features that contribute to replication (67, 168). Following the UTR are two large open reading frame (ORF) that generates a large polyprotein via a -1 frameshift (10, 25). In general coronaviruses have, after the ORF1ab region, a series of virus-species specific genes (so-called accessory genes) dispersed amongst genes that code for

structural proteins. Two other pathogenic human betacoronaviruses, CoV-HKU1 and HCoV-OC43 contain a hemagglutinin esterase gene (HE), as do many strains of MHV but SARS-CoV and other SARS-like-CoV do not. MHV-1 also does not contain a functioning HE gene (170). All coronaviruses encode the spike protein (S), envelope protein (E), membrane protein (M), and nucleocapsid protein (N), in that order, in the 3' third of the genome and this is followed by an untranslated region that is functionally important (72, 160). Encoded with the S-E-M-N are strain specific accessory genes that greatly vary between coronaviruses (40, 53, 160).

The more recent 2012 emergence of the Middle East respiratory syndrome coronavirus show a continuing need for animal models of severe coronavirus disease (5, 26, 62, 97). There have been several animal models proposed for SARS-CoV disease including mouse-adapted SARS-CoV, ferrets, cats, Syrian hamsters, and non-human primates (9, 22, 23, 125, 127). All of these models use SARS-CoV or a host- adapted SARS-CoV to study disease in the animal. In 2006 De Albuquerque demonstrated that MHV-1 infection of 6 week old A/J mice produced a disease that was clinically similar to SARS-CoV in humans (3). In infected A/J mice the mononuclear cellular infiltrates, fibrin deposition, hyaline membrane formation, and the cytokine response was similar to activity and responses seen in SARS-CoV patients. This MHV-1 model is more convenient and less expensive than any of the models using SARS-CoV or its derivatives because MHV-1 can be used in a BL2 setting and reduces the potential hazards to human scientists.

In order to study the genetic contributions of viral genes to pneumopathogenicity a method to introduce mutations into viral genes is required. Targeted recombination has been used in other MHV strains, such as –A59 and -JHM, to manipulate the 3' most genes to study their functions and effects on viral replication and pathogenesis. Targeted recombination takes advantage of the naturally occurring RNA recombination events that can occur during coronavirus replication (69, 89). Originally the system was developed using temperature sensitive mutants but in 2000 Kuo et al developed the spike protein as a selector for positive recombination events (75). By generating a mutant MHV virus that expressed a spike with a unique tissue tropism, recombination events upstream of S could be screened for by using mixed cell cultures and then passing progeny virus onto cell cultures that would select for the desired recombination events. This method has been successfully used in generating recombinant MHV-A59 and MHV-JHM viruses, as well as A59 or JHM recombinants that express the MHV-1 spike in isolation or the MHV-1 genes from the spike to the 3' UTR (8, 58, 83, 102, 103).

Our lab had begun developing the targeted recombination system for MHV-1 (83) and to date have been working on generating an isogenic control virus to use for the MHV-1 targeted recombination system. In 2010 Leibowitz et al demonstrated that expression of the MHV-1 S gene within the MHV-A59 background (rA59/S_{MHV-1}) increased the pneumovirulence of MHV-A59 (83). Mice that were infected with rA59/S_{MHV-1} recombinant virus developed pulmonary lesions that were similar to those observed with MHV-1, although it was significantly less virulent than either MHV-1 or MHV-A59.

RESULTS

Recombinant MHV-1/S

Our lab generated the donor plasmid (pDonor) for a MHV-1 targeted recombination system (83) (Figure 3). The plasmid was used to generate an isogenic control plasmid where the MHV-1 spike (pDonor-1) was swapped back in to generate isogenic control virus (MHV-1/S_{MHV-1}). Our plasmid contained known mutations that were required to generate a donor plasmid that could be used with other established MHV targeted recombination systems, as well as additional mutations that were acquired during the cloning process. An AvrII site was introduced at the 5' end of the spike region, two BsmBI sites were eliminated in the spike, and a SbfI site was introduced in the short non-coding sequence 3' of the spike protein coding sequence. All sites were non-coding mutations and were made to ensure that codon usage would not be negatively affected. During the generation of the portions of the pDonor plasmid a coding mutation was introduced into the 5a gene and a non-coding mutation was introduced into the E gene. Also a G was deleted from the 3' side of the SbfI site. These mutations were left in the plasmid because the only coding mutation was in the 5a gene, which, at the time, had no function assigned and had never been demonstrated to produce detectable levels of a protein product.

Two independent isogenic recombinant viruses were generated and plaque purified and four recombinant viruses were compared to MHV-1 (P3) in plaque size analysis (Figure 4). None of the recombinants were significantly different from non-recombinant MHV-1 in plaque size.

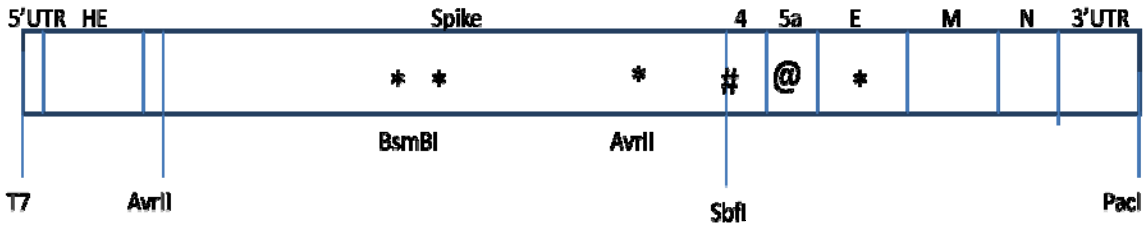

Figure 3. pDonor plasmid map. The pDonor plasmid consists of a T7 promoter joined to the first 467 bases of the MHV-1 5'UTR and adjacent ORF1ab sequences and were joined to a plasmid that housed the HE-3'UTR of MHV-1. The plasmid was engineered to have an AvrII, SbfI, and a PacI site. Two BsmBI sites and an AvrII site were eliminated by point mutations (*). In the process of generating the SbfI site a G nucleotide was deleted (#). In the process of generating the plasmid a coding mutation was introduced into gene 5a (@) and a non-coding mutation was introduced in the E (*).

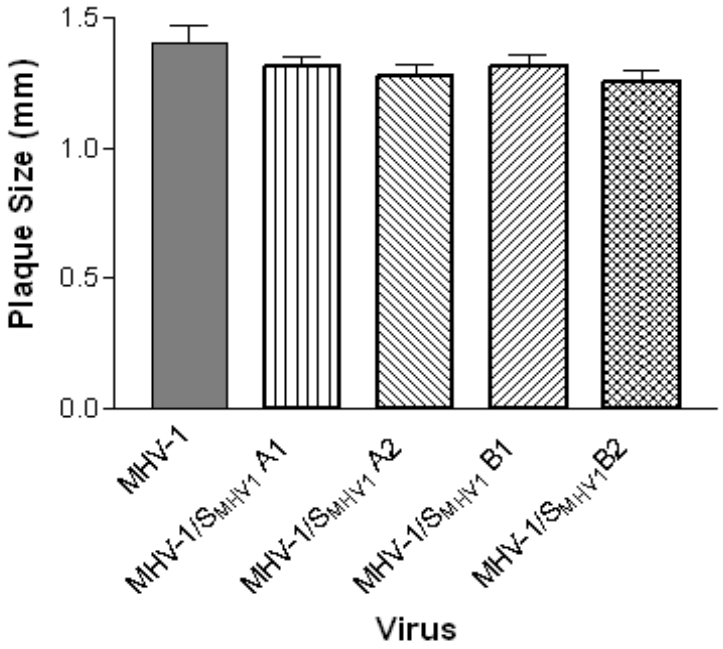

Figure 4. Plaque size comparison of MHV-1 and MHV-1/S_{MHV-1} recombinants generated by targeted recombination. Two independent targeted recombination reactions were used to generate a MHV-1/S_{MHV-1} virus. Isolates were plaque purified and plaques were selected and expanded. Plaque size was compared to MHV-1 to verify a homogeneous pheynotype in cell culture.

While we established that the MHV-1/S_{MHV-1} virus was not significantly different from MHV-1 in its plaque phenotype in cell culture we also generated spike recombinant viruses. The pDonor plasmid described above was used for targeted recombination to generate recombinant MHV-1 strains containing the MHV-A59 and -JHM spike (MHV-1/S_{A59} and MHV-1/S_{JHM}, respectively). Isolates were plaque purified, and expanded. Figure 5 shows the plaque size comparisons between MHV-1, MHV-A59, MHV-JHM, and the recombinant viruses. MHV-1/S_{JHM} produced plaques similar in size to those produced by MHV-1, and thus larger than plaques produced by MHV-JHM. Plaques formed by MHV-1/S_{A59} recombinants were larger than MHV-1 plaques, with one isolate forming plaques similar to MHV-A59 and the other forming plaques intermediary in size to MHV-1 and MHV-A59. We also performed a 24 hour growth curve comparison of the recombinants and the MHV spike donors (Figure 6). We found that the recombinant viruses grew similarly to MHV-1 in cell culture assays.

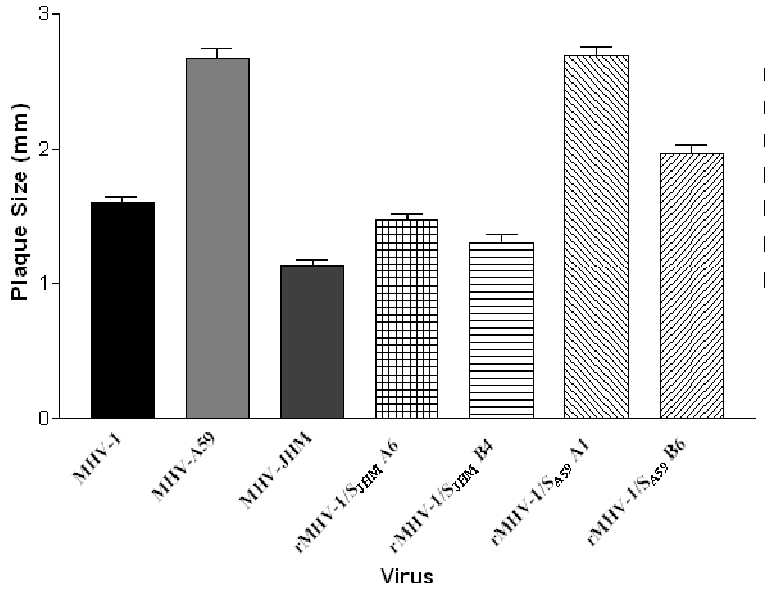

Figure 5. Plaque size comparisons of MHV-1, MHV-59, MHV-JHM, MHV-1/$S_{MHV-A59}$, and MHV-1/$S_{MHV-JHM}$. Targeted recombination reactions were used to generate MHV-1/$S_{MHV-A59}$ and MHV-1/$S_{MHV-JHM}$ recombinants. Isolates were plaque purified and plaques were selected and expanded. Plague size was compared to the background MHV-1 and the spike MHV-A59 and MHV-JHM donors to verify phenotype in cell culture.

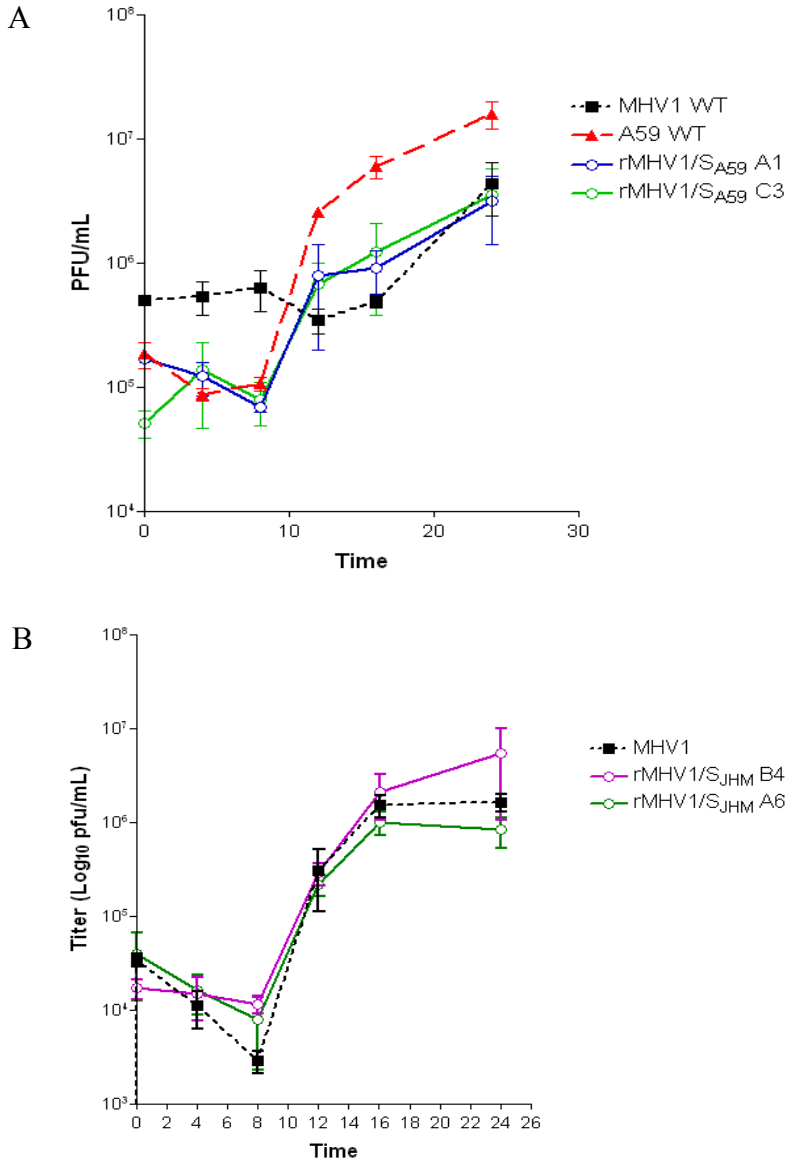

Figure 6. 24 hour growth curves of MHV-1 and MHV-1/S recombinants. A. rMHV-1/S$_{A59}$ viruses grew to a similar end point titer and with similar kinetics to MHV-1. MHV-A59 had a higher end point titer than the recombinants. B. rMHV-1/S$_{JHM}$ viruses grew to a similar endpoint titer and with similar kinetics to MHV-1.

To determine the effect of the spike protein on respiratory pathogenesis mice were infected with MHV-1 (P3) and MHV-1/S recombinant viruses. Mouse weight and oxygen saturation was recorded daily. Oxygen saturation was measured using the MouseOx pulse oximeter. Clinical scores were also taken for each mouse based on movement, appearance, and if breathing appeared labored. Mice that were infected with MHV-1 had both weight loss of 20% or greater and had oxygen saturation decrease to 80%, and so were euthanized. The mice infected with MHV-1 had a modified LD50 of approximatley 15,000pfu. Weight loss in mice infected with the MHV-1/S recombinant viruses was limited, no more that 5% in any group, and quickly resolved by day 4. No deaths were observed in any of the mice infected with recombinant virus (data not shown). Mice infected with recombinant viruses also did not suffer any decrease in oxygen saturation (data not shown).

MHV-1 5a*

Because none of the mice that were infected with any recombinant virus suffered anything more than transient weight loss we decided to focus on the MHV-1/S_{MHV-1} virus. We considered the possibility that the coding mutation in 5a might be affecting pathogenesis and be responsible for the attenuated phenotype. A recent publication demonstrated that the 5a gene might have an important role in pathogenesis by functioning as an interferon antagonist (74).

We generated a recombinant MHV-1 5a*, which had the 5a coding mutation corrected to the native (Genbank Accession FJ647223.1) sequence, reasoning that the coding mutation might have eliminated or impaired the function of the 5a protein.

Plaque size data showed that most of the recombinants had essentially identical plaque phenotypes as MHV-1 (Figure 7A). The MHV-1 5a* B2 isolate produced smaller plaques in this assay, but not in a later plaque size comparison. A comparison of the viruses' growth kinetics showed that MHV-1 5a*A2 reached titers that were not significantly different than that of MHV-1 (Figure 7B). We considered that these changes in in vitro phenotype might have an effect on pathogenesis in mice and moved on to mouse infection studies.

We decided to test the MHV-1 5a* mutant in mouse challenge experiments because of the recent publication that demonstrated the importance of a functioning 5a in interferon antagonism (74). However, infection with MHV-15a* resulted in no mortality in 6 week old A/J mice, where infection of MHV-1 (P3) at the same doses resulted in mortality of at 75% at 10,000pfu and 100% mortality at 25,000pfu (Figure 8). Despite the minor difference in growth kinetics for A2 and the difference in plaque size for isolate B5 there were no differences in morbidity or mortality in the infected mice.

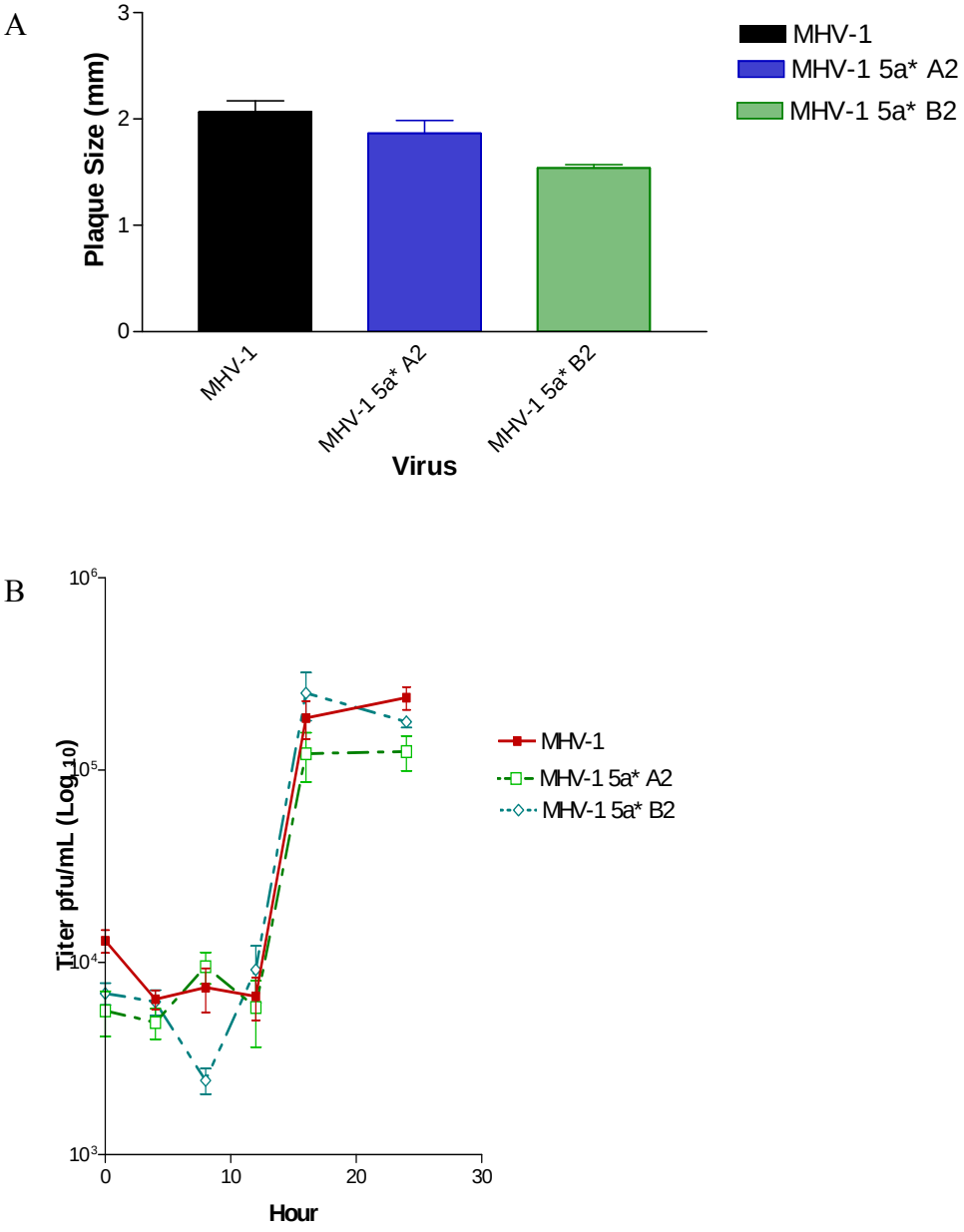

Figure 7. Plaque size comparison and 25 hour growth curve comparison of MHV-1 and MHV-1 5a* and NC recombinant viruses. A. Plaque size comparison of MHV-1 and the 5a mutation fix and recombinants only containing the AvrII insert and elimination mutations, BsmBI elimination mutations, SbfI insert mutation, and the G-base deletion. Only one isolate of the 5a* is significantly smaller than MHV-1. B. 24 hour growth kinetic comparison of MHV-1 and the recombinant viruses. MHV-1 Silent A6 and MHV-1 5a* B2 both have end point titers that are significantly less than MHV-1.

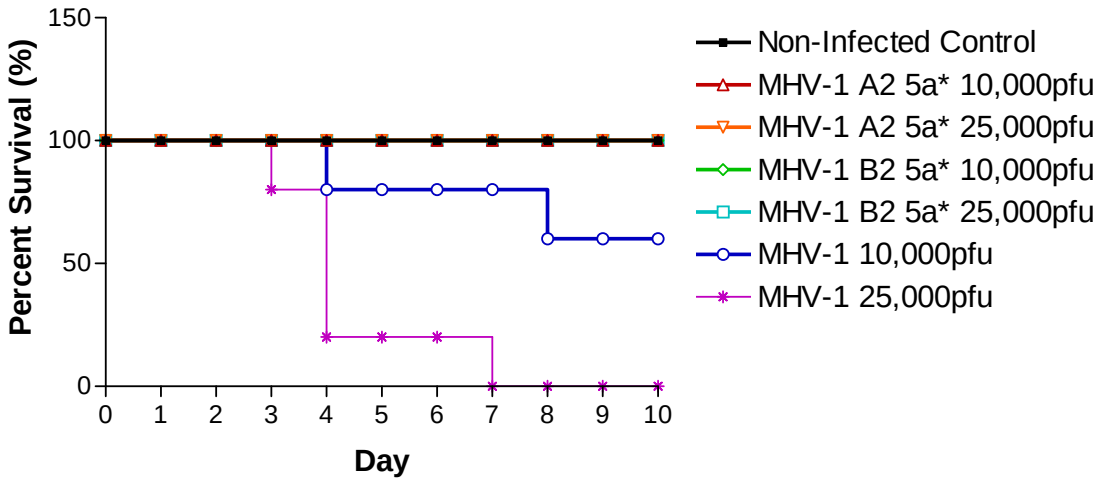

Figure 8. Survival plot of 6 week old female A/J mice infected with MHV-1 or MHV-1 5a* recombinants. Mice infected with the MHV-15a* recombinant show no mortality compared to the MHV-1 infected mice.

MHV-1/S$_{\text{MHV-1 Non-coding Mut}}$

Because the return of the 5a coding mutation to native sequence did not result in an increase, or any, mortality in mice this led us to question if the non-coding mutations were causing a loss of pathogenicity. However it is unclear which mechanism a non-coding mutation that utilized a codon with equivalent usage statistics in the mouse would affect pathogenesis if there were no major differences in plaque size or growth kinetics in at least one of the isolates. We decided examine the plaque isolates that contained only silent mutations introduced to generate an isogenic control virus for the targeted recombination system. These mutations were an AvrII site introduction mutation (TT23911-12CC,), an AvrII site elimination mutation (AAGA27253-56TAGG,), two BsmBI site elimination mutations (T24901A; G25069A), a SbfI site introduction mutation (CTCCT27981-85GCACC), and a G deletion (27977) that occurred during the introduction of the SbfI site because they allow us to manipulate the plasmid and exchange the spike region by restriction digestion (All positions relative to NCBI FJ647223.1).

We used the MHV-1$_{NC}$ virus. Figure 9 shows that MHV-1$_{NC}$ is not significantly different from MHV-1 in its in vitro growth properties. The 24 hour growth curve comparison showed that the kinetics of growth were generally similar with one of the recombinants having a statistically significant lower titer than non-recombinant MHV-1 at the 24 hour time point due to a drop in titer between 16 and 24 hours post infection (Figure 9B).

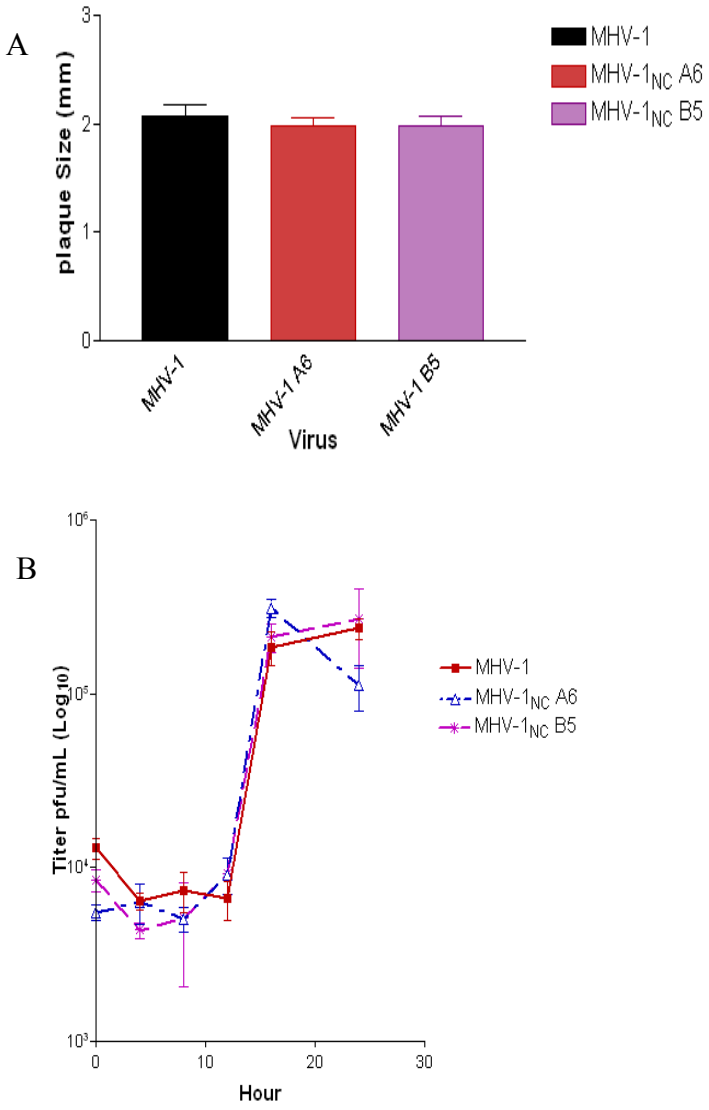

Figure 9. Plaque size 24 hour growth curve comparison of MHV-1 and MHV-1_{NC} recombinants. A. Plaque size comparisons of MHV-1 and MHV-1_{NC} show no significant difference between the isolates and the wild type virus. B. 24 hour growth curve shows that the growth kinetics are not significantly different, but that A6 has a statistically significantly a lower end point titer than MHV-1.

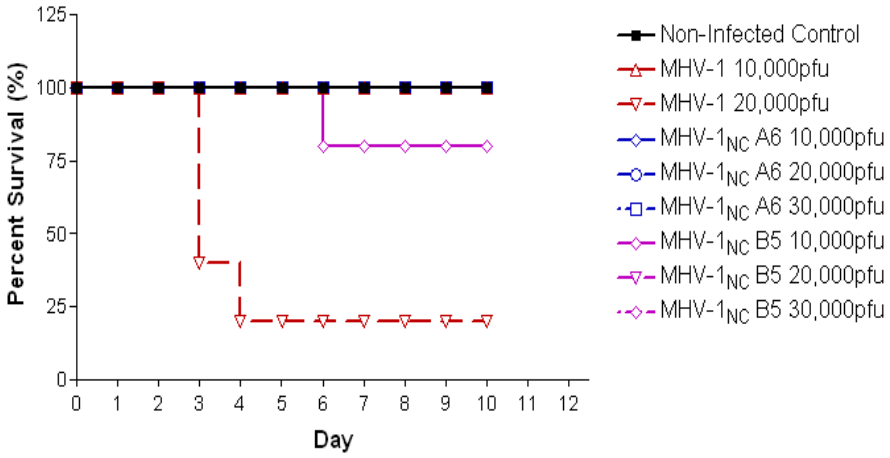

Figure 10. Survival plot of 6 week old female A/J mice infected with MHV-1 or MHV-1/S recombinants. None of the mouse groups infected with recombinant virus suffered any mortality.

Mice were infected at 6 weeks old with 10, 20, and 30,000pfu of the MHV-1_{NC} isolates. We chose to challenge some mice with a higher dose of virus, 30,000 PFU because our previous experiments had shown no mortality and limited morbidity, with our recombinant MHV-1_{NC} virus. Again, groups of mice that were infected with the MHV-1_{NC} isolates had no mortalities and only limited weight loss of no more than 5% (Figure 10 and data not shown). They also had no loss in oxygen saturation (data not shown). This data is consistent with the idea that the non-coding mutations are having an effect on pathogenesis.

The non-coding mutations had been selected so that they would not use uncommon or infrequently used codons. Most mutations used a codon with a higher frequency of usage in the mouse. This left RNA secondary structure as a potential cause of loss of virulence. We decided to evaluate the non-coding mutations' effect on RNA folding, as our lab, and others, have established that RNA folding can have an important role in virus replication (67, 108, 160, 168). Table 6 shows the effects of the non-coding mutations on folding ΔG. We used multiple algorithms to generate the ΔG and calculated the average ΔG. We determined that it was unlikely that the AvrII site introduction mutation had any effects, as there we no change in folding energy. This is also supported by other MHV targeted recombination systems that introduced an AvrII site at the same location to facilitate spike swaps, with no effect on the virulence of otherwise isogenic recombinant viruses (58). It was noticed that the largest effect on ΔG

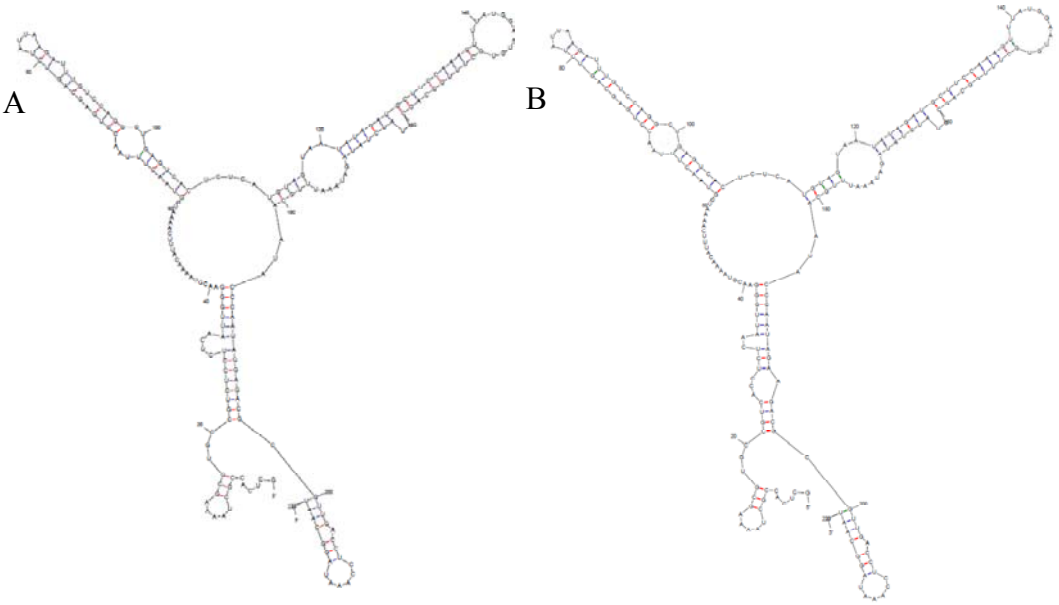

Figure 11. Mfold predictions of RNA secondary structures. A. MHV-1 structure prediction of the region of spike containing the two native BsmBI sites. B. Recombinant MHV-1_{NC} structure prediction of the region of spike containing the mutations used to eliminate the BsmBI sites. The mutations introduced to eliminate the BsmBI sites appear to destabilize a stem structure as well as alter a side loop on the left side of the stem.

Table 6.ΔG Calculations on the regions of the genome containing known mutations introduced by targeted recombination in the generation of MHV-1/S viruses.

	Difference in ΔG (Mut-WT)					
Mutations	MFE*	TE%	VC#	CF@	mFold&	Average Difference
AvrII Intro	0	0	0	0	0	0
BsmBI Elims	6.3	6.21	29.05	24.5	7.84	14.78
AvrII Elim	2	2.56	12.6	5.88	5.38	5.684
G deletion	0	2.52	-7.7	-2.5	0.89	-1.358
E nc mut	-1	-1.83	6.69	8.61	2.4	2.974

*MFE- Minimum Free Energy as calculated by RNAFold Web Server
%TE- Thermodynamic Ensemble as calculated by RNAFold Web Server
#VC- Centroid as calculated by RNAFold Web Server
@CF- Centroid Fold as calculated by ncRNA.org
&mFold- mFold as calculated by mFold

was the due to the elimination of the BsmBI sites within S and the Mfold generated predicted secondary structures for this region of the native MHV-1and recombinant MHV-1_{NC} RNA genomes are shown in Figure 11. The AvrII elimination mutation may also have an effect on RNA folding but it was relatively small, but that site had to remain in the isogenic control to permit subsequent use of the introduced AvrII sites in excision of the MHV-1 spike and the replacement of the MHV-1 spike with MHV-A59 or –JHM spikes, which was done above.

MHV-1/$S_{MHV\text{-}1\ AvrII}$

We reconsidered our strategy regarding the absolute requirements for an appropriate isogenic control virus. Because of the potential effects the BsmBI mutations had on RNA folding we decided to return those sites to the native sequence. We thus utilized targeted recombination to generate the MHV-1/$S_{MHV\text{-}1\ AvrII}$ virus. This left us with a virus that contained only the AvrII introduction mutation, the AvrII deletion mutation, and the SbfI introduction mutation. Those mutations were required to remain because they were vital for the restriction enzyme swaps that were necessary to insert in the spike genes from MHV-A59 and –JHM. Because previous plaque size comparisons and growth kinetic data revealed no differences from wild type for the MHV-1NC virus, we decided to move directly into mouse studies with the MHV-1/$S_{MHV\text{-}1\ AvrII}$ virus.

MHV-1 Loses Virulence during Passage in DBT

Our previous experiments had exhausted our supply of the wild type MHV-1 P3 virus, thus necessitating the growth of a new MHV-1 stock to use as a control virus in

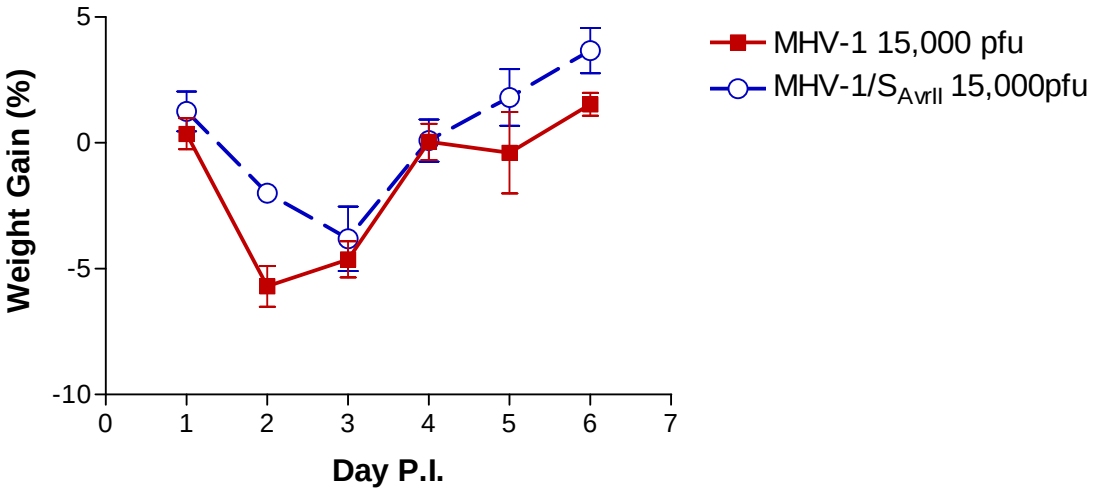

Figure 12. **Percent weight gain of 6 week old female A/J mice infected with the calculated LD50 of MHV-1P4 and an equal amount of MHV-1 AvrII virus. None of the mice suffered severe weight loss nor mortality. Most of the weight loss is not significantly different between the two viruses used.**

our experiments of MHV-1 AvrII. This new stock, a passage 4 virus generated from the P3 virus used in our previous experiments was used in a mouse challenge experiment (Figure 12). 15,000pfu was the LD50 established for MHV-1 P3 used in prior experiments. Mice were infected at 15,000pfu with MHV-1 or MHV-1AvrII. Surprisingly neither virus caused dramatic weight loss or any mortality.

With the attenuated phenotype of the new passage of MHV-1 we decided to increase the dose we used to infect mice, as well as generate a new P3 virus from the original seed stock of P2 virus in case this was a variance due to passage. We also increased the infecting dose to 25,000pfu, or 2x the LD50 of our original P3 stock used for prior experiments (Figure 13A). Both of these viruses failed to produce mortality at this challenge dose. We considered that the problem may be due to the mice. We considered that the acclimation time might be affecting the immune response to the MHV-1 infection, and since the pathogenesis is considered immune mediated then anything that might affect the immune response (ie travel stress or poor acclimation) would affect mortality. We held the mice for one week prior to infection, making them 7 weeks old at the time of infection, and used the 2x LD50 and the same virus as in the previous experiment (Figure 13B). This also failed to produce any mortalities so we considered that there may be something affecting the mice local to our supplier. While NCI labs did not report any positive tests for MHV during the period we obtained mice for our most recent experiments, we ordered mice from Jackson labs, and asked the Weiss lab to order NCI mice, since we established that the Weiss lab mice came from a different breeding location at NCI. The mice were held at our lab, and at the Weiss lab,

for 4 days and were infected with 2x LD50. The MHV-1 that was used was the same passage level, 3, but had been passaged, independently in the two labs. Both stocks were derived from the same vial of virus in the Leibowitz lab, where MHV-1 was obtained from the ATCC, was plaque purified and passaged to P2 at which time the P2 was sent to the Weiss lab and the Levy lab in approximately 2004. Figure 13C shows that our P3 stock inoculated into 6 week old A/J females from Jackson labs still failed to produce the expected mortality. The Weiss lab, with their independently passaged P3, also had no deaths in their experiment (data not shown). After this result we considered that we may need to increase the infecting dose as well as lower the age of the animals. Other studies have shown that age of the mice affects mortality rates and mice as young as 5 weeks have shown to be susceptible to MHV-1 infection (22, 71). We infected 5 week old A/J female mice, from NCI, with 30- and 90,000 pfu. There was no mortality and mice did not lose more than 8% of their starting weight (Figure 13).

Because of these experiments we decided to obtain a known virulent passage of MHV-1. We obtained a virulent MHV-1, P3, from the Levy lab. As stated earlier the Levy lab obtained their MHV-1 stocks from our lab many years ago. This P3 was generated independently in 17Cl-1 and had been used in previously published work (3). We noted that the LD50 reported by the Levy lab, 2.4 $x10^2$, was significantly lower than our experimentally determined LD50, $1.5x10^4$, for our original P3 virus. We did a plaque size comparison of this virus (MHV-1 GAL) to our recombinant MHV-1/S_{AvrII} and to our avirulent MHV-1 (Figure 14). Although the mean plaque diameter for MHV-

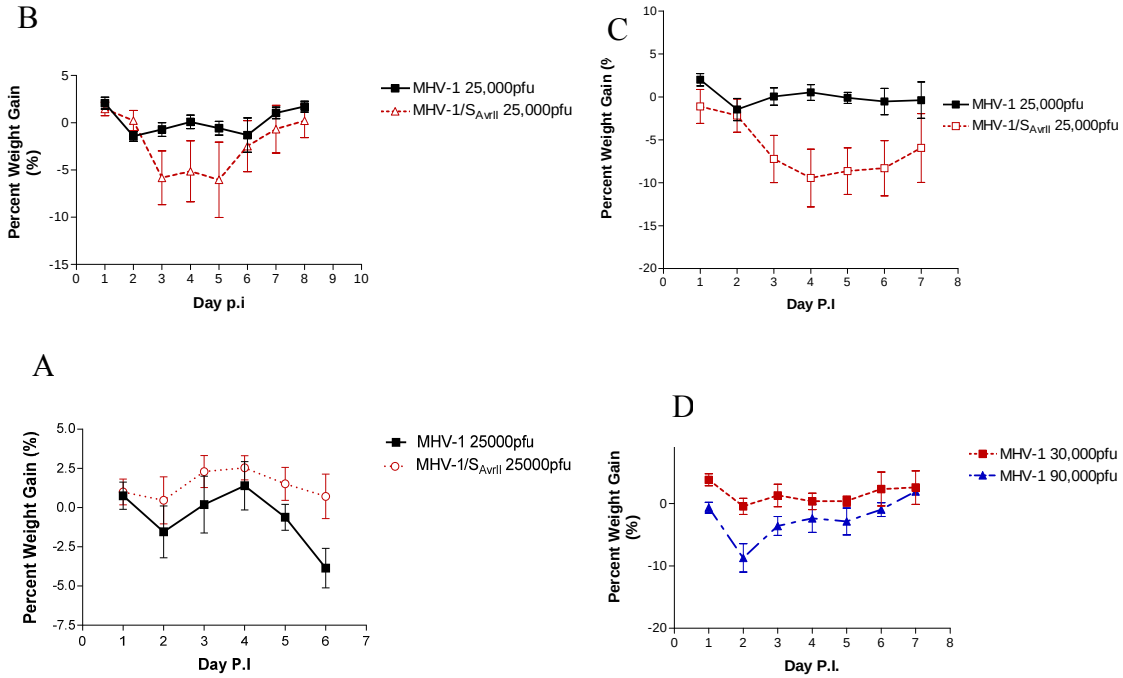

Figure 13. Percent weight gain of female A/J mice infected with P3.2 of MHV-1 using different acclamation times and different doses. A. Infection of mice a 2xLD50 that was originally calculated for MHV-1 using MHV-1 P3. B. 2xLD50 and mice were held for 1 week and were 7 weeks old at the time of infection with MHV-1 P3.2. C. Mice from different supplier, Jackson Laboratories, were infected with 2xLD50 with MHV-1 P3.2. D. 5 week old mice were infected with 30 and 90,000 pfu of MHV-1 P3.2 only.

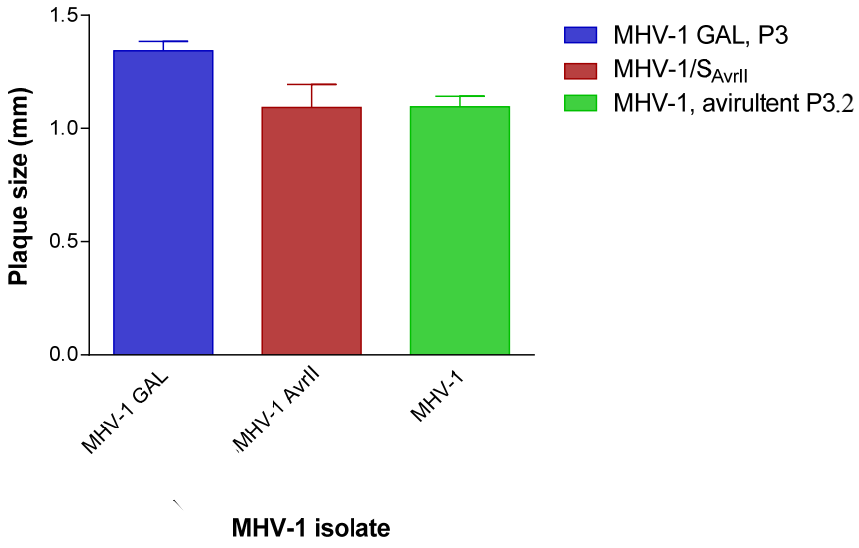

Figure 14. Plaque size comparison of a virulent virus, provided by the Levy Lab (P3), the Leibowitz lab MHV-1 (P3.2). MHV-1GAL produces larger plaques than MHV-1 or MHV-1 AvrII, but only MHV-1 plaque sizes are significantly different in size.

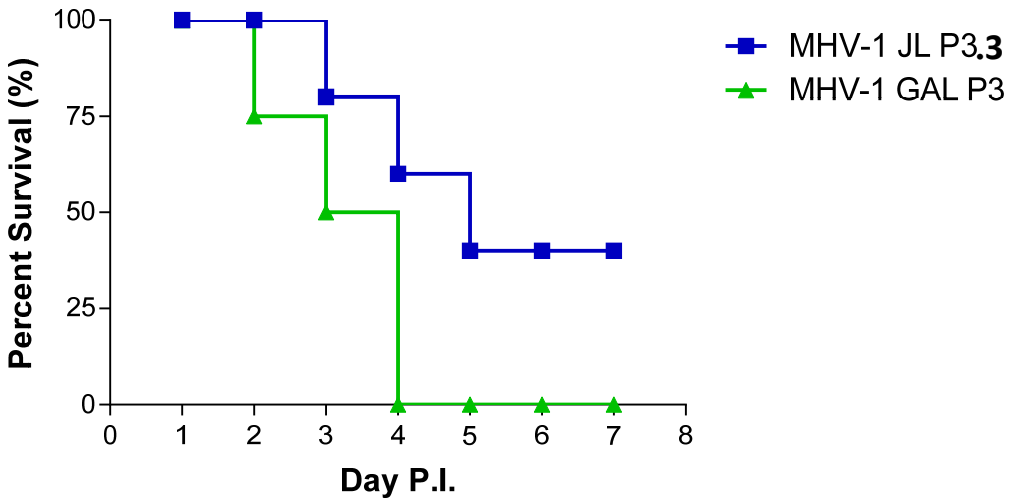

Figure 15. Mortality curve of mice infected with MHV-1 P3.3 (32500pfu) or MHV-1 GAL P3 (8300pfu). The MHV-1 GAL virus caused 100% mortality by day 4, while the MHV-1 virus had above 50% mortality at 32500pfu.

1 GAL is larger than that of our two viruses, this difference is not statistically significant for MHV-1 GAL and MHV-1AvrII. However there is a statistically significant difference between MHV-1GAL and our avirulent MHV-1 P3.2. The biological significance of this difference was not further investigated.

We then grew a new P3.3 virus stock and mice were infected with this new MHV-1 P3.3, at 32500pfu or MHV-1 GAL P3 at 8300pfu. The Levy virus was highly virulent producing 100% mortality by day 4 post infection. The new P3.3 stock that we had grown was also virulent and produced over 50% morality at 32,000pfu. We considered the difference in LD50 was likely due to natural variance between generated stocks. Our lab was able to generate a pneumovirulent P3 50% of the time, the Levy lab had a pneumovirulent P3, and the Weiss lab had an avirulent P3. This caused us to reconsider the use of MHV-1 at a 3rd passage for future experiments and we considered going back further into our stocks to generate lower passage virus stocks.

DISCUSSION

Our lab started with a plasmid with known mutations that was used to generate recombinant virus in the hopes of developing a targeted recombination system for MHV-1. Our initial isogenic control recombinant virus was severely attenuated and produced no mortality in contrast to our original P3 stock of MHV-1. We attempted to identify mutations to account for the attenuated phenotype that we were seeing in our recombinant isogenic control viruses. However, once we corrected the previously discounted coding mutation in ns5a and this did not affect the virulence of the recombinant virus, we had to resort to changing non-coding mutations that may have

effected RNA folding. We hypothesized that if RNA folding was dramatically effected that it might negatively impact the ability of the virus to utilize its' native interferon antagonsists and RNA masking methods. However, even upon return of the native sequences in regions that were most likely negatively effecting RNA folding we still did not recover recombinant viruses with a virulence similar to that of MHV-1.

These results, taken together, do pose a unique question: what is causing the loss of virulence in MHV-1? We have tested multiple 3rd passages of MHV-1, all independently generated, and had widely divergent LD50s, and in some cases none, for each. The MHV-1GAL virus had the lowest LD50, while P3 viruses (P3, P3.2, P3.3) generated in our laboratory varied from an LD50 of 15,000pfu to an LD50 which could not be determined, but was higher than 90,000pfu. The Weiss lab also generated a MHV-1 P3 that was not lethal at 25,000pfu. Based on published records we know that both the Leibowitz lab and the Weiss lab passage MHV-1 in DBT cells, whereas the Levy lab reports that they use 17Cl-1 cells for their MHV-1 propagation. While it is possible that the cell lines used for propagation may affect the viruses' maintenance of virulence genes it would be easier to look for possible genetic contributions of virulence.

Most importantly the loss of virulence in our MHV-1 over only 3 passages points to the fact that the targeted recombination system will not be viable for generating pneumopathogenic MHV-1 recombinant viruses. We can easily generate recombinant virus that is not significantly different from MHV-1 in tissue culture, however if the virus is going to be used in pathogenesis studies then targeted recombination may not be a viable method for genertating recombinant virus. Targeted recombination requires too

many passages in cell culture. The process of targeted recombination requires the use of a feline spike-MHV-1 that was generated by targeted recombination, was passaged, plaque purified, and expanded through multiple passages. This high-passage fMHV-1 is used to generate the desired recombinant MHV-1 which is, again, passaged multiple times, plaque purified, and then expanded into multiple passages.

Other strains of MHV have not shown significant attenuation when passaged multiple times in cell culture. We have utilized MHV-JHM P4 with no significant loss in neurovirulence, and MHV-A59 and MHV-3 P3 stocks with no significant loss in expected pathogenicity in the liver. We do not know for certain what the passage level of MHV-1 was used to generate the fMHV-1 virus. It is likely that the MHV-1 P3 or perhaps even a higher passage stock was used.If the P3 virus was used it was most probably done with the MHV-1 P3 from the Weiss lab which we have shown to be avirulent in the lung infection of A/J mice. The Weiss lab's MHV-1 P3 was also the virus that was used to generate the virus that was sequenced by the TIGR lab and the sequence was submitted to GenBank (FJ647223.1). We also cannot say for certain that targeted recombination can never be used to generate a pneumopathogenic virus, however our data show that it will be challenging to do so if pneumovirulence cannot be stably maintained over multiple passages.

CHAPTER IV

WHOLE GENOME SEQUENCING OF AN AVIRULENT AND VIRULENT PASSAGE OF MHV-1 SHOW DIFFERENCES IN VARIANT POPULATION

INTRODUCTION

Severe acute respiratory syndrome coronavirus (SARS-CoV) is a novel human coronavirus that caused the first major pandemic of the new millennium in 2002-2003 (150). The more recent 2012 emergence of the Middle East respiratory syndrome coronavirus show a continuing need for animal models of severe coronavirus disease (5, 62, 97). Animal models for SARS-CoV include civet cats, Syrian hamsters, non-human primates, rats, and mice (82, 85, 100, 101, 127). Another animal model involving MHV-1 in A/J mice has been shown to be a viable model of SARS-CoV disease (3). There are multiple advantages to the MHV-1 model of SARS-CoV infection: 1) MHV-1 can be safely worked with in BL-2 facilities, 2) there is no concern of human respiratory infection with MHV-1, 3) working with MHV-1 in mice at a BL2 facility is less expensive than working with SARS- or SARS-like- CoV in a BL3 lab.

MHV-1 infection of A/J mice produces pathologic changes in the lung which include progressive interstitial pneumonitis, including dense macrophage infiltrates, giant cells, and hyaline membranes (3), changes which are similar to the histopathology seen in human infections with the closely related SARS-coronavirus (106, 111). Infection of A/J mice with MHV-1 also results in death of animals, where other strains of mice developed less severe and transitory disease, which facilitates end points of

study (3). A/J mice also have similar cytokine and chemokine responses as those seen in SARS-CoV infected patients (65).

There is indication that the SARS-associated coronaviruses have been evolutionary independent for a period of time prior to the outbreak (64, 121). While SARS-CoV is considered as a single genomic entity, there are several studies that indicate that SARS and SARS-associated coronaviruses maintain a quasispecies (64, 141). During the epidemic, different strains were being identified and had potential effects on patient health and survival (144). Studies have demonstrated the presence of multiple quasispecies of SARS-CoV in an individual patient (142, 166). The exact role of quasispecies in SARS-CoV infection and pathogenesis is unclear. Coronaviruses do have a mechanism to recognize and correct mutations that arise during genome replication, nsp14 (32). The presence of this exonuclease lead to reasoning that assumed that coronaviruses did not utilize the mechanisms of quasispecies diversity to the extent that other RNA viruses did. The reports of quasispecies in patients and our findings in MHV-1 infection and pathogenesis support the hypothesis that quasispecies may play an important role in pathogensis.

Studies have evaluated the presence of quasispecies in patients, but none to date have evaluated if there is a correlation between quasispecies and clinical disease or outcome. One study evaluated the full-length spike glycoprotein of SARS-associated coronavirus from 19 hospitalized patients and found a total of 107 sequence variations with 9 recurrent variant sites in the S gene of the BJ01 strain (166). In 7 of the 19 subjects researchers found the coexistence of two variants, and one patient had three

variants. Researchers also found that the population variants would change over time, as samples collected from the same patient would show similar, but not identical, variant profiles. Another study found evidence of heterogeneous populations of subgenomic RNA 3 in patients with acute SARS-CoV infections (142). Looking at a T track repeat in SARS-CoV gene 3a they found different in T repeats between six and ten. In 6 of the 8 patients had viral populations with either 6 or 9T's, meaning a full length 3a, or with one additional amino acid, would be generated. Most patients only had two populations of T repeats: three with 6/7, one with 8/9, and one with 7/10. Two patients had homogeneous populations with 6 T's and one patient had three populations of T repeats, seven to 9 repeats. Vignuzzi et al show that quasispecies diversity is important in pathogenesis in a neuroinvasive polio virus model (156). They demonstrate that virus pathogenicity is decreased by a mutation in the polymerase, which causes enhanced fidelity and reduces virus sequence diversity. Viruses with the high fidelity polymerase show a reduction in total number of mutations per nucleotides sequenced and show a reduced number of mutations per genome. Viruses with enhanced fidelity are also less neuropathogenic and are less able to invade other tissues in a mouse infection. This paper supports the idea that quasispecies diversity is important in pathogenesis, though if this relates to coronavirus infection is not yet known.

RESULTS

Loss of Pneumovirulence in MHV-1 during Passage in Cell Culture

We investigated the reason that MHV-1 does not maintain pneumovirulence over serial passages in cell culture. Figure 16 shows the history of our MHV-1 viral stocks and the generation of our stocks used in this study. We used the same P2 stock to to generate both virulent P3.3 virus, an avirulent P3.2 virus, that was used in the previous chapter (Figure 14) in sufficient quantities to sequence. We retrived freezer stocks and used the P1 stock, a stock that is the parent to all of our MHV-1 stocks including the avirulent and P3 stocks described above, and we used this to generate a large P2.2 stock sufficient for sequencing. Both stocks were tested in mice to determine if they did or did not cause mortality or loss of lung function (Figure 17 and 18). We used avirulent P3.2 and a virulent P2.2 MHV-1 stock to attempt to identify any dominant mutations or any change in subspecies populations. No dominant population mutations were found, but there were subpopulation variances between the virulent virus and the avirulent virus. The dominant consensus sequence was identical to the sequences in Genbank, which include Genbank Accession FJ647223.1 which covers the entire genome, with the exception of the extreme 5' end of the MHV-1 genome, which is covered in a separate Genbank entry, Accession EF682499.1. These two sequences were combined to create a reference sequence that our lab used to compare the virulent and avirulent sequencing results.

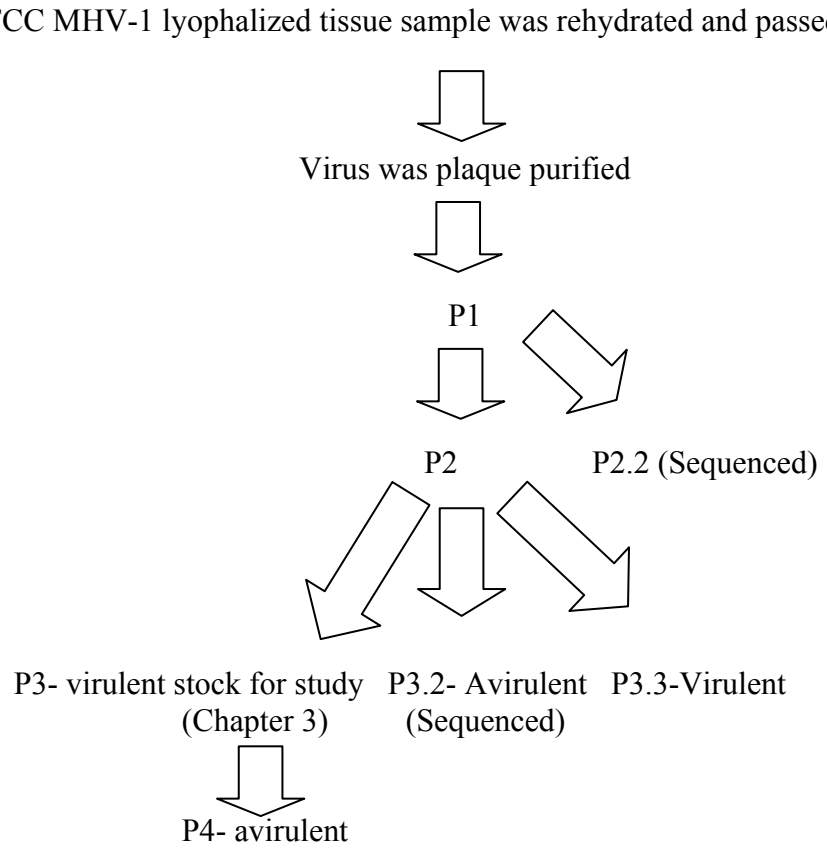

Figure 16. Flow chart showing the generation of MHV-1 passages. The lab purchased MHV-1 from the ATCC collection and received a sample as a lyophilized tissue sample. The sample was hydrated and passaged into DBT cells. The resulting virus was plaque purified and passed to generate P1. P1 was expanded into the original P2 and P3. The original P2 virus was later given to the Weiss and Levy lab groups and was used as our original stock in mouse studies. When we exhausted our P3 we generated a P4, which was avirulent. We went back to a P2 and generated P3.2, which was also avirulent. We went back to P1 and generated a P2.2 stock that was pneumovirulent.

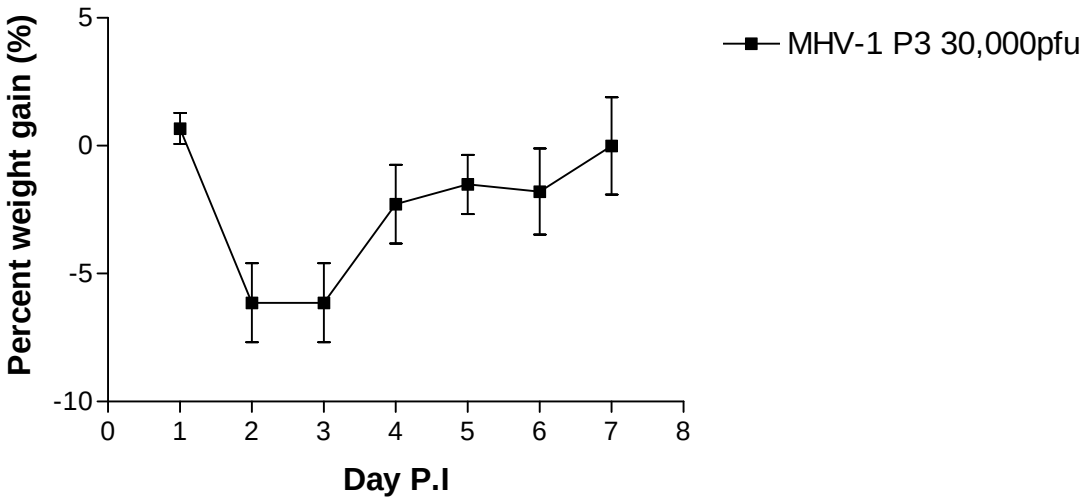

Figure 17. Percent weight gain in mice infected with P3.3 virus used in whole genome sequencing. Female A/J mice, 6 weeks old, were infected with 30,000pfu MHV-1 P3. Mice lost no more than 8% of their starting weight and there was no mortality or loss of lung function.

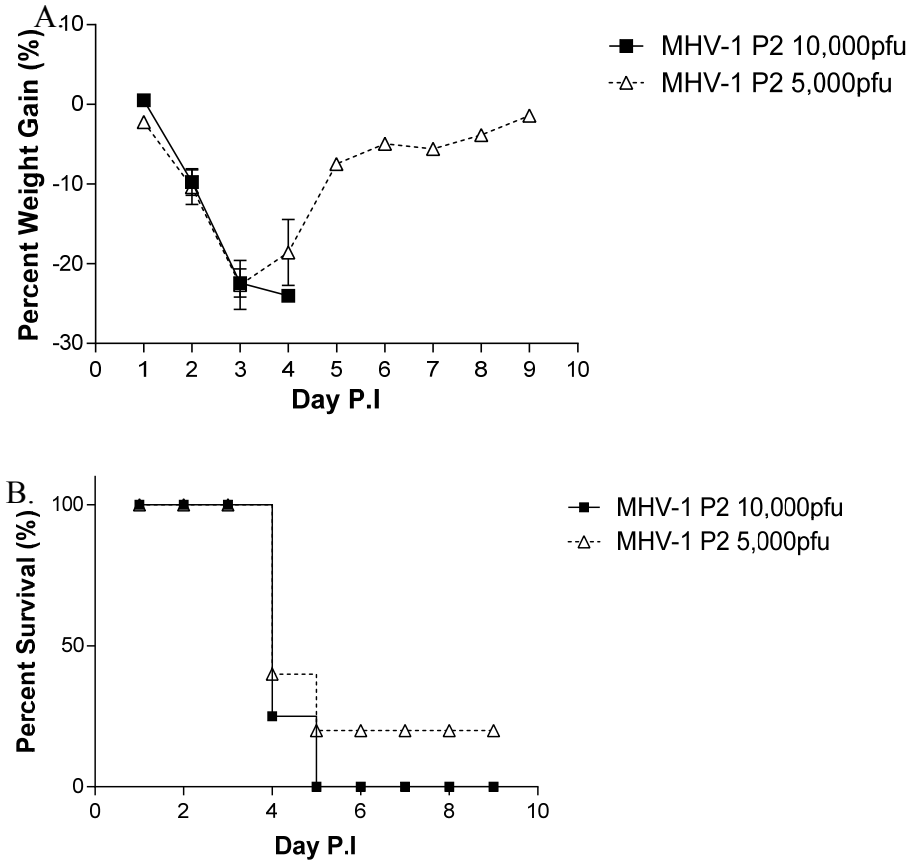

Figure 18. Percent weight gain and Percent survival of mice infected with MHV-1 P2.2 used in whole genome sequencing. A. Percent weight gain in Female A/J mice, 6 weeks old, infected with MHV-1 P2. The increase in weight after day 4 is primarily due to the one mouse that survived the challenge. (see Panel B) B. Percent survival of female A/J mice, 6 weeks old, infected with MHV-1 P2. Mice infected with 5,000 or 10,000pfu of MHV-1 P2. Because we expected P2 to be virulent we chose to use a lower infectious dose. Mice infected with 10,000pfu lost weight rapidly and all mice were dead by day 5. Mice infected with 5,000pfu also lost weight, and had 80% mortality.

Avirulent Virus Whole Genome Sequencing

The avirulent P3 virus containing cell culture supernant was purified by density gradient centrifugation as described in Materials and Methods and RNA was extracted and used to generate cDNA. We used random primers that our lab had used previously in whole genome sequencing (167). To avoid gaps and to ensure adequate coverage of the 5'end we also used specific MHV-1 primers (see Materials and Methods) because in our previous experience with whole genome sequencing there were gaps that had to be filled by amplifying specific regions by RT-PCR followed by additional Sanger sequencing reactions.

We used the CLC Genomics Workbench (version 6.5.1) to align the shotgun sequences of the avirulent virus to the MHV-1 reference sequence that was generated using the MHV-1 genome reported in NCBI (FJ647223.1) combined with the 5' leader sequence that our lab reported to NCBI (EF682499.1). We note that the NCBI MHV-1 genome (FJ647223.1) is, we believe, the sequence of an avirulent virus. TIGR sequenced a virus given to them by the Weiss lab, a virus passage we now know to be avirulent.

Our sequencing run of the avirulent virus yielded 4988704 individual reads and 66% of them aligned to our reference sequence. Figure 20 shows the sequence coverage map that was generated with the avirulent sequence when aligned to the reference sequence, showing no gaps in coverage.

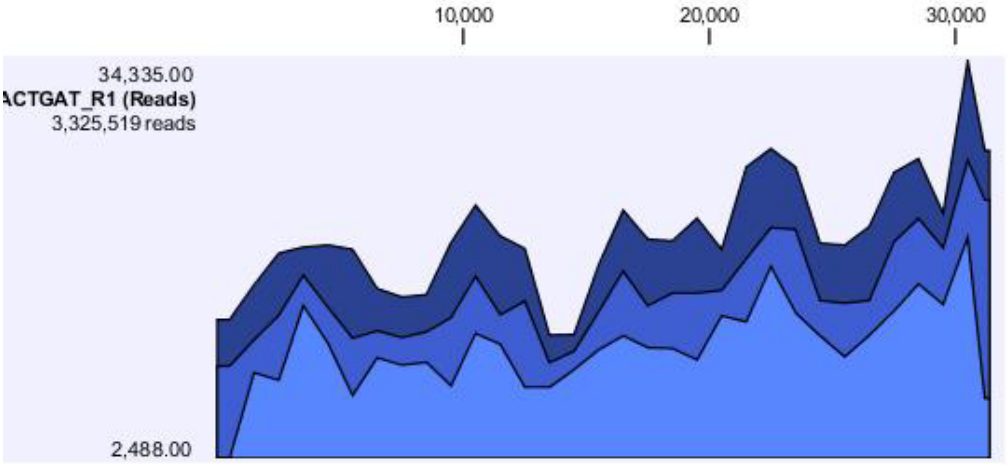

Figure 19. Coverage of MHV-1 genome, NCBI database, by shotgun sequencing the genome of an Avirulent MHV-1 P3 virus passage. The three curves show the maximum (dark blue), mean (blue) and minimum (light blue) read coverage value observed in a given region of the genome.

Table 7. List of avirulent virus genome variants at 2%

Base position*	Variant	Frequency	Gene location
59	Insertion AATCT	2.51	5’ UTR
59	AATCT deletion	4.48	5’UTR
11587	C->T	2.26	nsp6
15323	Insertion G	2.55	nsp12
17040	C->A	12.39	nsp13
17442	TT->AG	4.01	nsp13
19435	T->C	2.19	nsp14
23343	T->C	2.04	HE
23816	A->G	7.5	HE
24337	G->A	4.32	Spike
28479	G->A	2.4	Ns4
29048	A->T	2.4	Membrane

*Genome position is based on the combination of MHV-1 genome (FJ647223.1), which is 25 nucleotides short of the true 5’ terminus, and the 5’UTR containing sequence (EF682499.1) which extends to the true 5’ end of the genome. To calculate the base position in the MHV-1 genome (FJ647223.1) subtract 25 from the listed base position.

Because alignment of the avirulent shotgun sequences with the MHV-1 genome showed no deviations of the consensus sequence from the MHV-1 reference sequence we used the CLC genomics workbench to look for variants in the sequence population. We ran thresholds for variant populations at 10% and then at 5% in the hopes of finding multiple variant populations. At 5% we found two subpopulations, one in HE and one in nsp13. The variant in HE was present at 7.5% in the avirulent population and was present at a lower percent in the virulent virus (2.32%, see section below). The second variant was in nsp13 and was present at 12.39% in the avirulent population, but was present at a higher percent in the virulent population (19.1%, see section below). Because the error rate of the Illumina Hi-Seq is published at 1.18% we decided to lower our threshold and look for population variants at 2%.

When we aligned the avirulent reads to the reference and tested the population for variance at 2% we found that the avirulent population contained 12 variants (Table 7). Of these variants only three prove to be unique to the avirulent passage and all were less than 5% in frequency. One variant was in the S protein, one was in HE downstream of the stop codons, and the final variant was present in ORF1a. We decided not to look for population variants less than 2% because we did not want to risk finding populations that were effect by sequencing errors.

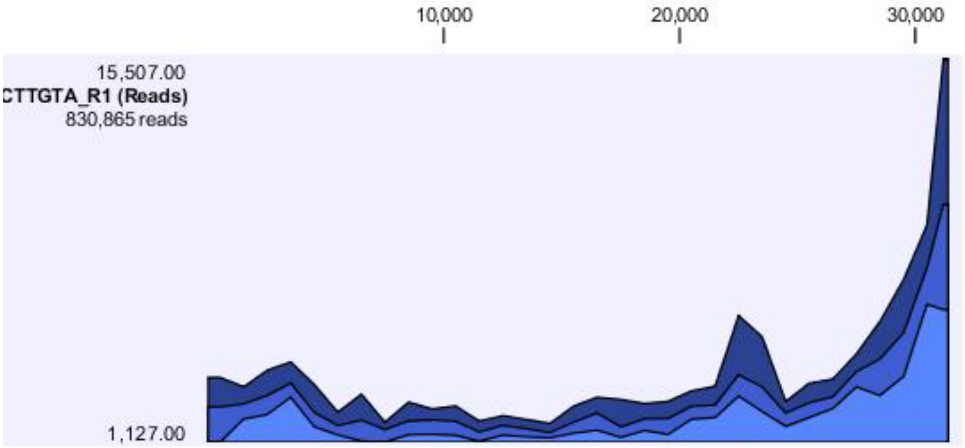

Figure 20. Coverage of MHV-1 genome, NCBI database, by shotgun sequencing the genome of a virulent MHV-1 P2 virus passage. The three curves show the maximum (dark blue), mean (blue) and minimum (light blue) read coverage value observed in a given region of the genome.

Table 8. List of virulent virus genome variants at 2%

Genome position*	Variant	Frequency	Gene location
8	A->G	7.69	5'UTR
12	A->T	3.57	5' UTR
14	Insertion A	2.38	5' UTR
59	Insertion AATCT	2.82	5' UTR
59	AATCT deletion	3.76	5' UTR
73	T->C	2.00	5' UTR
1097	A->G	2.85	nsp2
3883	T->A	2.12	nsp3
15323	Insertion G	2.63	nsp12
17040	C->A	19.10	nsp13
17442	TT->AG	2.84	nsp13
19435	T->C	2.2	nsp14
22695	T->C	2.01	HE
22701	G->T	2.52	HE
23758	G->A	2.74	HE
23816	A->G	2.32	HE
28479	G->A	10.89	Ns4
29048	A->T	3.7	Membrane

* Genome position is based on the combination of MHV-1 genome (FJ647223.1), which is 25 nucleotides short of the true 5' terminus, and the 5'UTR containing sequence (EF682499.1) which extends to the true 5' end of the genome. To calculate the base position in the MHV-1 genome (FJ647223.1) subtract 25 from the listed base position.

Virulent Virus Whole Genome Sequencing

We generated a new passage 2 (P2.2) stock of MHV-1 in a quantity sufficient for both mouse experiments and for whole genome sequencing (Figure 16). We tested this virus in 6 week old A/J female mice and found it to be more virulent that our original virulent MHV-1 P3 (Figure 19B). We did not calculate an actual LD50 for this virus. 80% of the mice that were infected with 5,000pfu died, so we can conclude that the actual LD50 of this virulent P2 is less than 5,000 pfu, which is an amount lower than that of our P3 virulent virus. This is also interesting because this P2 virulent virus is more like the MHV-1GAL virus from Dr. Levy's lab in its LD50. This may support the idea that passaging of the virus resulted in loss of a subspecies that helps generate a pathogenic virus phenotype.

Virulent P2 virus was purified and cDNA prepared in the same way as for the avirulent virus. Both random and specific primers were used to generate cDNA for sequencing. The yield of cDNA template available for sequencing was similar to that obtained from the avirulent P3 virus. The sequencing run resulted in a total of 15,197,732 reads, which was more than double the number of reads we got for the avirulent sequencing run. However, only 5.5% of the reads from the virulent sequencing results mapped to our reference sequence, though coverage still extended over the entire genome, with greater than 10x coverage being achieved (Figure 21). The decrease in reads that map to the MHV-1 reference sequence is likely due to the presence of a substantial amount of ribosomes entrapped with membrane fragments copurifying with

this virus preparation. There was also a large quantity of mycoplasma DNA segments present in the sample.

We aligned the virulent virus reads with the reference sequence, described above. Using CLC Genomics Workbench we found that again there were no difference in the consensus sequence between the virulent MHV-1 P2 and the MHV-1 reference sequence. We also tested this sequence for population variants using a 10% and 5% threshold. We found one sequence subpopulation with a point mutation in ns4 and one sequence change from the reference sequence in nsp13, both were present at a higher frequency in the virulent virus than the avirulent virus.

When we aligned the virulent virus reads to the reference and tested the population for variance at 2% we found that the virulent passage had 18 variants, 9 that were conserved between the avirulent and virulent viruses (Table 8). Of the 9 variants conserved between the two passages only one differed by more than 5% (5.18%) between the virulent and avirulent viruses, where the rest had frequency differences of less than 5%. Of the 9 variants that were unique to the virulent passage four were in the 5' UTR between bases 8 and 73 of the complete genome, mapping to sequences contained inthe 5' Leader (EF682499.1). These mutations might affect the structure of the 5'UTR region and may affect replication, as our lab has demonstrated that 5' UTR structures can play an important role in betacoronavirus replication (67, 168). However, our initial analysis shows that of these variants only the variant at base position 12 might have a significant effect on RNA folding, and that effect would likely be to destabilize

Table 9. Common variants and population percentages between P3 Avirulent and P2 virulent virus sequences above 10%

MHV-1 passage	Mutation*/ % of population	Gene location	Potential effects
P3(Avirulent)	C17040A/12.39%	Nsp13	A237D, affects conserved A, but not a known structure (63)
	G28479A /2.4%	Ns4	A133T, affects predicted helix structure at c-terminus
P2(Virulent)	C17040A/19.1%	Nsp13	A237D, affects conserved A, but not a known structure (63)
	G28479A/10.89%	Ns4	A133T, affects predicted helix structure at c-terminus

*Variant base position is based on the MHV-1 reference sequence: a combination of MHV-1 genome (FJ647223.1), which is 25 nucleotides short of the true 5' terminus, and the 5'UTR containing sequence (EF682499.1) which extends to the true 5' end of the genome. To calculate the base position in the MHV-1 genome (FJ647223.1) subtract 25 from the listed base position.

the stem of SL1. The remaining three are unlikely to have any major effect on RNA folding and downstream virus replication due to effects on the 5'UTR structures. There were three unique variants that mapped to the HE gene, two of which would affect the truncated HE protein, should that protein be produced. It should be noted that for MHV-1 the subgenomic mRNA that encodes the HE is present at undetectable levels, if at all (83, 170). The third variant occurs after the six stop codons and so is unlikely to have an effect on any protein or structure.

Differences in Population Variants between Virulent and Avirulent Viruses

Comparing the population variants, both the avirulent and the virulent viruses have a conserved subpopulation present in the 5'UTR (ACTCT deletion and insertions), in nsp13 (17040), in HE (23816), in ns4 (28479), and in M (29048). Only the nsp13 and ns4 varaints have values higher than 5%, so we will concentrate on those two (Table 9). The avirulent virus has fewer unique variants, three, whereas the virulent virus has more variants that are unique, nine. Both viruses have a subpopulation of mutations in nsp13 compared to the reference sequence in NCBI. It should be emphasized that we do not know if the virus sequenced by TIGR was virulent or avirulent but is was derived from the original virulent P2 stock that we provided to the Weiss lab. The percent of C17015A sequence reads is 12% in the avirulent virus and is 19% in the virulent population, suggesting that the population containing this mutation may play a role in pathogenesis. The C17015A mutation is a coding mutation that produces an A237D change in the nsp13 protein sequence and is predicted to affect a helical structure in the protein. The helix containing the mutation is not part of a known enzymatically active

site or a structural domain with known biochemical function, it is located in the spacer region between the zinc binding domain and the active sites present at the carboxyl end of the protein (63). The avirulent virus has an A23791G mutation that is present in 7.5% of the population that causes a noncoding mutation in the HE gene. The mutation occurs after the three stop genes that cause HE to be a pseudogene in MHV-1 so the role of this mutation, if any, is unknown. Most interestingly is the G28454A mutation that occurs in ns4 in the virulent strain. This mutation is results in an A133T amino acid change that shortens a predicted helical structure at the c-terminus of the ns4 protein.

We screened for these variations by subcloning reverse-transcribed and PCR amplified fragments and then using traditional Sanger sequencing to screen the subclones. We were unable to find the ns4 mutation in a P3.2.1 or a P4.2.1, indicating that this sequence variant is likely not maintained over passages in cell culture (Table A 2). We have also, to date, been unable to find the nsp13 variant in a P3.2.1 or a P4.2.1 (Table A 1). We also extracted viral RNA from a mouse lung, post infection day 3, and subcloned the nsp13 varaint region, and have also, to date, been unable to find the nsp13 variant in the screened population. Admittedly, subcloning is a less sensitive way to isolate variants and identify variant populations compared to Hi-Throughput sequencing methods used to sequence the whole genome.

DISCUSSION

Because there was no dominant polymorphism present in the virulent or avirulent genome sequence we used a 10% and 5% threshold we examined the whole genome sequencing data for population variants. We saw that there were nine common variant

populations between the virulent and avirulent sequences when compared to the reference sequence. We found that the avirulent virus had only three unique variant populations, whereas the virulent virus had nine unique variant populations compared to the MHV-1 reference genome. Of those variant populations the two that stood out the most because of their high frequency were the variant population in nsp13 and ns4. The nsp13 is a difference in subpopulation percentage of a coding mutation, which is a helicase with multiple enzymatic domains. While this mutation does affect a helical domain, it does not appear to be in a known functional domain so the effect on pathogenicity is unknown. However, in mouse adapted SARS-CoV there is a nsp13 mutation that is present in both lethal strains (22). It is a C16177T mutation that causes an A5305V alteration in the amino acid sequence. However, this mutation is at the amino terminus of nsp13, whereas our mutation is near the center of the protein and is predicted to interrupt and shorten a central helical domain. The A5305V mutation in MA15 does not alter the helical structure at the amino terminus of nsp13.

The mutation in the ns4 region occurs in almost 11% of the population in the virulent strain and is present at 2.4% in the avirulent strain. This is interesting because ns4 has been shown to be dispensable in replication (171). No function has been assigned to ns4 at this time. It would be novel to show that ns4 plays a role in pathogenesis.

The study evaluating the quasispecies population of SARS-CoV ORF 3a show variations of ~5-70% in patient populations with two quasispecies (142). Since clinical outcomes were not reported we cannot hypothesize a correlation between quasispecies

and disease in humans. Our studies indicate that there is a threshold, for certain genes, which are present in a virus which causes severe lung disease versus only mild weight loss.

The role of the nsp13 and ns4 sequence variants are not presently clear. They cannot be located when we reverse-transcribe and subclone cDNA. It is possible that these sequence variants need to be present in the infecting population at a certain level, that if these mutations are dominant in the population they generate a virus that has a very high LD50 and does not generate lung pathology. We also cannot be sure if these mutations occur in the same viruses or are unique mutations in two separate subpopulations, meaning we do not know how many quasispecies are involved in the virulent virus: two or three.

The presence of quasispecies in MHV-1 and the rapid tissue culture adaptation and attenuation of virulence also means that targeted recombination is not a reliable option for genetic manipulation and study of the MHV-1 model of SARS. We have shown above (chapter 3) that LD50 MHV-1 can be dramatically increased by 3 passages. The nature of the targeted recombination protocol involves multiple blind passages and repetitive passages in cell culture. This, apparently, causes a loss of quasispecies either due to loss of diversity or bottle necking during plaque purification. Because of this there will need to be a mechanism in order to be able to maintain the necessary mutations or mitigate the loss of quasispecies in cell culture.

In order to generate and study these mutations we will need to use a complete reverse genetic system. The complete reverse genetic system requires fewer passages in

cell culture to generate enough virus to use in animal studies. Also virus can easily be regenerated if more is needed without more passages in cell culture.

CHAPTER V

CURRENT PROJECTS AND FUTURE DIRECTIONS

INTRODUCTION

Originally coronaviruses were found to cause self-limiting respiratory infections and were thought to be species restricted (98, 160, 187). However, in 2002 a novel coronavirus outbreak in China quickly became the first pandemic of the new millennium and changed how scientists thought about coronaviruses and the disease causing potential of these viruses (37, 116, 150, 159, 180). Though the pandemic ended in 2003, there is still a necessity for study of coronaviruses that cause serious human respiratory illness. The recent emergence of Middle Eastern Respiratory Syndrome coronavirus (MERS-CoV) shows the continued need for the study of coronavirus disease in humans (5, 26, 62, 97). Currently the animal models that have been used to study SARS-CoV, with varying fidelity to the human disease, include primates, Syrian hamsters, cats, ferrets, rats and transgenic mice (9, 11, 13, 22, 45, 82, 99, 101, 117, 125, 127). These animal models use SARS or SARS-adapted coronaviruses for study of the disease.

The genome of coronaviruses is organized into an ORF1ab region encoding a polyprotein which is processed into proteins required for RNA replication and transcription, and downstream of this a series of virus-species specific genes mixed in with genes that code for structural proteins. All coronaviruses encode the spike protein (S), envelope protein (E), membrane protein (M), and nucleocapsid protein (N), in that

order, at the 3' end of the genome and this is followed by an untranslated region that is functionally important (111, 160). MHV-1 and the pathogenic human betacoronaviruses, CoV-HKU1 and HCoV-OC43 contain a hemagglutinin esterase gene (HE) but SARS-CoV and other SARS-like-CoV do not. Coronaviruses also contain strain specific non-structural genes, so-called accessory genes, that are interspersed with the genes encoding the structural proteins, and these genes often encode proteins that modulate or evade host antiviral responses. These non-structural genes are not critical for replication in cell culture (160, 171). MHV-1 contains genes encoding a viral cyclic phosphodiesterase (ns2 (130)), an interferon antagonist (ns5a (74)), as well as ns4, a gene that currently has no assigned function (171).

SARS-CoV is a member of the betacoronavirus genus, as is MHV, but it is a member of betacoronavirus subgroup 2, (72, 139), whereas MHV is a member of subgroup 1. MHV-1 causes a respiratory disease clinically similar to SARS-CoV in six week old A/J mice (3). Although MHV-1 and SARS-CoV, both belong to the betacoronavirus genus, they have significant sequence differences, and in particular their non-structural genes are unrelated and located in different positions betweem the genes encoding the structural proteins. MHV-1 also offers a safer and less expensive option to study SARS-Co disease since MHV-1 can be used under BL2 conditions and is not a health hazard to the individuals working with the virus.

While SARS-CoV is considered as a single entity, there are several studies that indicate that SARS-associated coronaviruses also maintain a quasispecies, and the events leading up to and during the pandemic were not solely due to the host range changes that

can be attributed to the spike protein (64, 141). During the epidemic different quasispecies strains were being generated and had potential effects on patient health and survival (144). Studies have demonstrated the presence of multiple quasispecies of SARS-CoV in an individual patient (142, 166). Our lab has demonstrated a potential role for quasispecies in the MHV-1 lung infection (Chapter 4). We found that infection with a virus that had a limited population variance in nsp13 and ns4 resulted in a mild infection that only cause limited weight loss. Whereas infection with a virus who had a higher percentage of variants in nsp13 and ns4 had a higher mortality with a lung disease that resembled the SARS-CoV like disease reported by De Alburquerque et al (3).

Research in our lab has shown that MHV-1 is capable of losing virulence in as few as three passages. Two issues have led us to develop a complete reverse genetic system: 1) the limitation of targeted recombination to manipulations of the 3' one third of the MHV genome, leaving the nsp13 mutation inaccessible; 2) the larger number of tissue culture passages required in preparing the acceptor fMHV-1, and then selecting a recombinant virus, allowing more opportunity for cell culture adaptations to arise. Thus, we have constructed a Complete Reverse Genetic System for MHV-1. Several Complete Reverse Genetic Systems have already been generated for coronaviruses; they include, but are not limited to, SARS-CoV (175), MERS-CoV (134), Infectious Bronchitis Virus coronavirus (173), MHV-A59 (176), and MHV-JHM (Susan Weiss, personal communication). We set out, originally, to make our Complete Reverse Genetic System compatible with the systems already in place for MHV-A59 and MHV-JHM to facilitate the generation of chimeras between these strains. However, because of

attributes of the MHV-1 genome we had to use alternative methods to generate our system.

CURRENT PROJECTS

Generation of an Infectious cDNA Clone

Early attempts to generate complete reverse genetic systems for coronaviruses ended in frustration due to regions of cDNA clones that were unstable in plasmid vectors propagated in *E. coli* (174). Ultimately this led to three separate strategies to create reverse genetic systems: an in vitro cDNA assembly system, a system employing bacterial artificial chromosomes, and a system that assembled a complete cDNA and propagated it using a recombinant vaccinia virus vector. We have elected to utilize the in vitro cDNA assembly approach, based on the relative ease of later introducing mutations utilizing this system and our labs experience in utilizing this type of system to study MHV-A59 replication.

In the generation of the first coronavirus complete reverse genetic system a minimum of 6 plasmids were needed to house the genome (174). This is because certain regions of the genome in ORF1a, specifically the B plasmid region, needed to be broken up into separate plasmids in order to avoid bacterial toxicity issues related to the sequence. We employed a similar design. However, our experiences with the sizable G plasmid lead us to utilize a SbfI site present in F to generate two F fragments, F1 and F2 (Figure 22). This allowed us to generate smaller cDNA fragments that were less likely to contain mutations and plasmids that were easier to manipulate.

The MHV-A59 CRGS used a type IIS restriction enzyme, Esp3I or its isoschizomer BsmBI, which was added to the ends of the MHV-A59 sequence during RT-PCR to cut out the cDNA fragment from its plasmid vector. Type IIS enzymes cut away from their recognition site and produced staggered ends, thus digestion liberates cDNAs that only contain MHV genome sequences with staggered ends suitable for ligation; the liberated fragments do not carry the recognition sequence for the enzyme. The sequence of the MHV-1 genome contained 5 BsmBI sites, making it more convenient for us to choose a different type IIS enzyme, BspQI, which is only occurs twice within the MHV-1 genome. Because of this we were not able to make our system perfectly compatible with the two MHV complete reverse genetic systems available, which utilize BsmBI sites.

Table 10 shows the genes that are included in each fragment. The boundaries used are not set to individual genes, due to toxicity issues as well as optimal primer and restriction site locations.

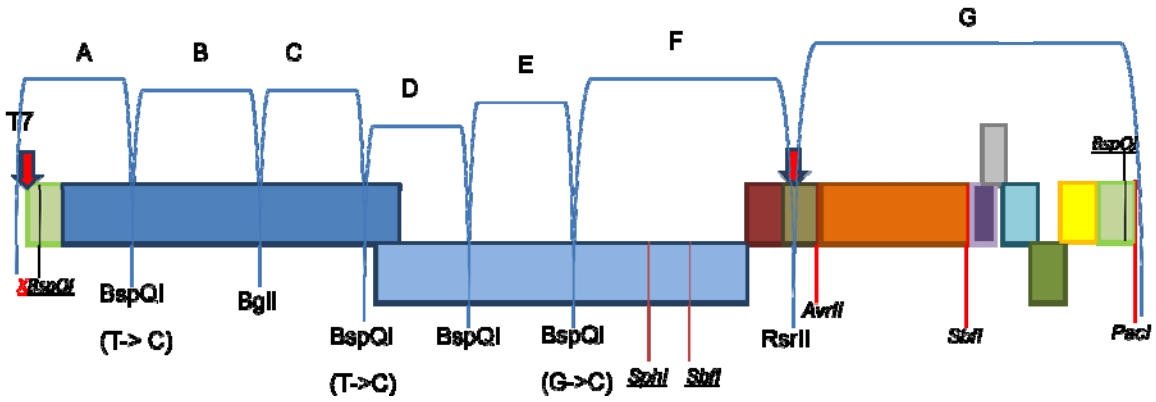

Figure 21. Outline of the MHV-1 Complete Reverse Genetic System with the restriction enzymes flanking each fragment and any mutations made in the restriction site. Mutations were made in the restriction sites in order to make the MHV-1 system more compatible with other MHV complete reverse genetic systems. However, the use of BspQI will require additional steps to make the systems genuinely compatible. MHV-1 native restriction sites are italicized and underlined, restriction sites that were engineered in by our lab are italicized, and restriction sites that are used in the reverse genetic system are plain lettering. The BspQI site in the 5'UTR (*XBspqI*) was removed by site directed mutagenesis.

Table 10. MHV-1 Complete Reverse Genetic System Plasmid Boundaries

MHV-1 genome position	Plasmid	Genes Included
1 to 4869	A	nsp1, nsp2, nsp3
48644 to 9587	B	nsp3, nsp4
9585 to 11460	C	nsp4, nsp5, nsp6
11456 to 12910	D	nsp6, nsp7, nsp8, nsp9
12907 to 15703	E	nsp9, nsp10, nsp11
15700-22688	F	nsp11, nsp12, nsp13, nsp14, nsp15, nsp16, ns2,HE
22685 to End	G	HE, S, ns4, ns5a, E, M, N

We maintained the genetic boarders that are present in the MHV-A59 system (Table 3). We also made point mutations so that, in the future, if we wanted to swap entire fragments with the MHV-A59 system with modifications to the restriction enzyme site to use a Type IIS enzyme that had an equal number of overhanging nucleotides as BsmBI. We did not use BsmBI because there were too many native sites that would have had to be mutated, so we used BspQI. However, BspQI has a three nucleotide overhang rather than the four nucleotide overhang created with BsmBI so the two enzymes would not create compatible ends. In the future though, as long as the overhang length was four nucleotides so as to be compatible with BsmBI, unique Type IIS enzyme sites could be engineered onto the ends of the MHV-1 fragments to make them compatible with the MHV-A59 and MHV-JHM systems.

One challenge with the MHV-1 complete reverse genetic system is that the virus used to generate the sequence found in NCBI and used to verify our system is derived from a stock in the Weiss lab that does not cause disease in the A/J mouse model of SARS-CoV. To this end we will have to generate mutations based on our whole genome sequencing data and compare infection studies with recovered virus to determine what sequence generates a virulent virus that can be used as a control.

FUTURE DIRECTIONS

Evaluation of the nsp13 and ns4 Mutations Found in Virulent MHV-1 P2.2

Our analysis of the genomes of virulent and avirulent passages identified two mutations that are candidates to affect pathogenicity of MHV-1 in the mouse lung. We will generate three recombinant viruses that differ from the consensus sequence in

GenBank: nsp13C/A, ns4G/A, and nsp13/ns4. Because we cannot determine from the genomic sequencing data if the mutations occur individually or in the same virus we will have to study the effects of the mutations separately and in combination.

We believe that the MHV-1 genome submission in GenBank is that of an avirulent virus, which was derived from the P3 Weiss MHV-1 which has been tested in mice and has shown to not cause penumopathogenesis. It is also worth noting that neither sequence variant is maintained in cell culture over a single passage. It is possible that the nsp13 and ns4 mutations presence at a higher frequency in the virulent virus are what contribute to the pneumopaothgenesis of the virulent passage, and this is something we plan to test with the complete reverse genetic system. Because the nsp13 mutation is not well maintained even over one passage in cell culture, dropping from 19.1% to 12.39% we will need to test the variant's role in infection, as well as it's stability in cell culture. This can be done by monitoring the mutation's population in our recombinant virus. Our lab has completed another whole genome sequencing analysis with recombinant MHV-A59 P1 and P5 and demonstrated that a single mutation can be maintained, and at 100% frequency, over multiple passages in cell culture (167). So the failure of MHV-1 to maintain these mutations is not supportive of the mutations causing a gain of function in cell culture. Though, if these mutations are adversely effecting viral replication it is possible that these viruses are what cause the massive immune response that lead to the pnuemopathogensis that occurs once the virus is cleared.

Evaulation of the Role of ns2 in an MHV-1 Lung Infection

In MHV ns2 has been shown to be a viral cyclic phosphodiesterase (130). Studies done in MHV-JHM show that ns2 has no effect on neuropathogenesis, however ns2 has been shown to be very attenuating in the MHV-A59 hepatitis model (130, 183). It is unknown as to its role in pathogenesis in the lung, thus we want to examine the role of ns2 in the lung. Using site-directed mutagenesis we generated a single (H46A) and double mutations (H46A, H126R) of the ns2 active site histidines, as described previously (130). While the single mutation was proven to be adequate to eliminate function and reduce pathogenicity in MHV-A59 infection we wanted to ensure this was similar with MHV-1 infection in the lungs.

DISCUSSION

There is still concern that the infectious cDNA method of generating recombinant MHV-1 will not be successful in generating a pneumopathogenic virus. Our data that shows that MHV-1 cannot be stably maintained as a virulent virus in cell culture over multiple passages show that there is more involved in MHV-1 pneumopathogenesis than is obvious. While our data seem to show that there may be mutations that can be introduced to create a virulent virus, it is also possible that it is the presence of a specific quantity of virus subspecies that generates a pneumopathogenic infection. In their paper discussing how quasispecies diversity determines pathogenesis Vignuzzi et al do not identify specific mutations that are consistent between a neuroinvasive/neurovirulent polio virus and one that is restricted in tissue tropism (156). Instead they propose that it is the number of mutations per genome (1.91 vs 0.31,

neuropathogenic vs restricted virus) that aid in neuroinvasiveness and pathogenesis, not specific mutations. However, their method of quantifying quasispecies relied on picking 24 virus isolates that were amplified, and the viral RNA was extracted and purified for RT-PCR and direct sequencing. This method will only identify dominant mutations that are present in a population, so it is possible that the actual quasispecies variability is much larger than what is presented in the paper. While this method is effective for polio virus, it is not quite a viable method for coronaviruses, given the difference in genome size that would need to be sequenced.

The ability to generate a population that is sufficient in number and type of subspecies may not be possible with the infectious cDNA method. This method cannot control sequence diversity to a fine degree if we do not know what specific elements need to be incorporated to generate a pneumopathogenic virus infection. So while the experiments mentioned above might be helpful in determining if specific mutations play a role in quasispecies diversity in an MHV-1 infection, they will not be productive if the requirement for pneumopathogenicity is a quasispecies quantity, not specific mutations that must be present at certain population percentages. In that case determining the role of ns2 in pneumovirulence would be impossible if one cannot generate a pneumovirulent virus.

CHAPTER VI

CONCLUSION

Since the emergence of SARS-CoV in 2003 there has been renewed interest in human coronavirus disease. The SARS-CoV is classified as BSL3 select agent; experiments with SARS-CoV are potentially dangerous to staff and are expensive for the researcher. SARS-CoV disease also has limited reproduction in animal models, or requires an adapted virus to generate a SARS-CoV like clinical disease (78, 82, 92, 100). It has been demonstrated that MHV-1 produces a disease in 6 week old female A/J mice that is clinically similar to SARS-CoV infection in elderly humans (3). In order to further study the potential of a MHV-1 model of SARS-CoV we first developed a targeted recombination system to generate recombinant MHV-1 viruses with mutations at the 3' end of the genome. This system was similar to the system designed by Kuo et al, utilizing a recombinant MHV-A59 virus (fMHV) expressing the ectodomain of the spike protein from Feline Infectious Peritonitis Virus to identify recombination events between the recombinant fMHV and Donor RNA that coded for the native MHV-A59 spike (75). We created fMHV-1 as the acceptor virus using in vitro transcribed Donor RNA that contained MHV-1 sequences that extended from HE codon 28 to the 3' end of the genome. The Donor RNA was transfected into feline cells that were infected with fMHV-1 and the infected/transfected cells were overlaid onto murine DBT cells. Over three days the mixed cell culture was observed for signs of infection, including syncytia and cell death. Recombinant viruses that resulted from the targeted recombination

protocol were expanded once in murine cells, plaque purified, expanded in DBTs, and sequenced to confirm the presence of MHV-1.

This system was used to successfully generate multiple recombinant viruses, many that were not significantly different from MHV-1 in *in vitro* analyses. There were some recombinant viruses that were generated that appeared to have a growth deficiency compared to MHV-1, however because all recombinants had multiple independent isolates we always had at least one recombinant isolate that was not significantly different than MHV-1 in cell culture. Upon infection of A/J mice with any the recombinant viruses generated, none demonstrated a pathogenicity that was similar to MHV-1. All viruses tested had a higher LD50 than MHV-1. The LD50 of our recombinant viruses was too high to calculate the actual value because of the amount of virus that would be required to do successful infections was so great that we were not confident we could generate stocks with a high enough titer to do successful infections. The recombinant viruses only caused a minor illness as evidenced by limited weight loss, compared to controls, and animals also showed less lung damage, compared the controls, as evaluated by the oxygen saturation levels using the Mouse Ox Pulse Oximeter.

During the analysis of our recombinant viruses we noticed that our lab stock of MHV-1 dramatically lost pathogenicity in A/J mice with passage in cell culture. After multiple dose and animal studies we resolved that the loss of pathogenicity in our MHV-1 stock was due to some type of cell culture adaptation. In order to evaluate the cause of the loss of virulence we did Next-Generation sequencing on an avirulent and a virulent

passage of MHV-1 (P3 and P2, respectively). We did not find any dominant mutations that deviated from the MHV-1 sequence as it appears in NCBI (FJ647223.1, noting that this sequence is missing bases at the 5' end that can be found in EF682499). Upon analysis of these sequences looking for variant populations we found that each passage, virulent and avirulent, had a population variant in common as well as an independent population variant that was unique to each, when compared to the NCBI reference sequence. Both populations contained a C17015A mutation that created an A237D mutation in the nsp13 gene. The avirulent population had this mutation in ~12% of the population and the virulent population had this mutation in ~19% of the population. This mutation appears to effect a helical structure, but does not affect a known active site contained in nsp13 (63). However, the spacer region in an equivalent protein in arterivirus, ns10, has been characterized and researchers have shown that mutations in this region tend to be detrimental to the function of the protein in terms of generation of discontinuous mRNA synthesis either resulting in non-viable virus or temperature sensitive mutants (29). Why the virulent virus would select for a potentially detrimental mutation is uncertain, though the higher percentage of viruses with a fully functional nsp13 may be contributing to virulence. Or it is possible that the mutation is generating temperature sensitive mutations that are beneficial to the viral population in the respiratory tract. The avirulent virus also contained the A23791G silent mutation in a region of the HE gene that is after the stop codons that render HE a psuedogene in MHV-1. The role of this mutation is unknown since it is non-coding and also in a pesudogene. The virulent virus passage has a C28454G mutation that is present in ns4

that creates an A133T mutation. This coding mutation interrupts a helical structure that is present at the carboxy end of the protein. However, the role and function of ns4 is not well characterized in MHV-1, so this mutation is of particular interest for future study. When we looked for these sequence variations by subcloning and Sanger sequencing we were unable to find these specific variants.

Ultimately the rapid generation of non-pathogenic MHV-1 in cell culture implies that the targeted recombination system will never be successfully adapted to the MHV-1 model of SARS-CoV disease. The nature of the targeted recombination system involves multiple passages in cell culture, more passages than were used to generate the stock MHV-1. Because of this our lab's efforts focused more on our generation of a reverse genetic system that we could utilize that would require less time being passaged in cell culture.

We have established a potential role for quasispecies in the MHV-1 virulence in lungs. The population variances between virulent and avirulent passages demonstrate that there is a need for a certain percentage of nsp13 mutants in a virulent virus. There is also a potential role for ns4 mutants in the generation of a virulent and pneumopathogenic MHV-1 infection. The exact role of these variants cannot be known because we do not know the sequence of a pneumovirulent MHV-1. We have established that the sequence present in NCBI is not sufficient to cause pneumopathogenic in five to seven week old female A/J mice. The question that remains is if pneumovirulence is a factor of specific variants or the presence of quasispecies. The finding of a potential role for quasispecies in the MHV-1 infection of

the lung is consistent with the finding of quasispecies of SARS-CoV in human patients and, potentially, gives support to the hypothesis that quasispecies can have an effect on pathogenicity and overall clinical severity of a SARS-CoV infection (144, 153, 166).

The generation of infectious cDNA from multiple cDNA fragments has been used successfully for many other coronaviruses (5–9, personal communication with Weiss lab). We generated our cDNA fragments by size and location similarly to the MHV-A59 system (176). We used type IIS restriction enzyme sites flanking most of the fragments, where unique native sites were not found, to liberate cDNA containing only MHV-1 sequence, similarly to what was done by Yount, et al. Single base mutations were introduced at some of the overhangs in order to facilitate the potential that later the fragments could be used interchangeably with other MHV reverse genetic systems, with a few other modifications. We elected not to to use the BsmBI site that is used in the MHV-A59 system for two reasons: first there is a BsmBI site in a region of the 3' UTR that is termed "the octomer" (47). This site is highly conserved between many members of the coronavirus family, and had been shown to effect virus growth in cell culture, thus we were reluctant to mutate it in the G fragment. Second, there are multiple other BsmBI sites in other fragments that would have required mutations to eliminate, and after the failures with the recombinant viruses that were generated with the targeted recombination system we wanted to introduce as few artificial mutations as possible. We chose to use the BspQI site, which did have a native site in the 5' UTR that we believed could be manipulated with little concern as it had no known associated structural function (18, 67).

The original cDNA fragments were generated to match the MHV-1 genome in NCBI. However, with our data that indicates that the NCBI sequence is not sufficient to create lung disease in A/J mice we are also generating viruses that contain the mutations in nsp13 and ns4 found in the virulent passage. We hope to test these mutations individually and in concert to determine which virus is able to generate lethal severe MHV-1 induced pneumonitis. We also plan to identify the role, if any, of ns2 in the lungs. Previous research has shown that ns2, a viral cyclic phosphodiesterase, has been shown to play an important role in pathogenesis of MHV-A59 in the liver, but is not important in the infection and pathogenesis of MHV-JHM in the brain (130, 183). Personal communication with the Weiss lab indicates that the infection and replication of MHV-A59 in alveolar macrophages (a site of MHV-1 infection) does not rely on a functioning ns2 protein. Its importance to viral replication in other cells found in the lung is unknown.

The use of reverse genetic systems is an invaluable tool in the study of virus gene function *in vitro* and *in vivo*. We have demonstrated that not all reverse genetic systems are viable options for the evaluation of gene functions due to the nature of the protocol. The targeted recombination system has proven to be a tool that is not usable in the evaluation of MHV-1 as a model for SARS-CoV because during the generation of the recombinant virus there is a loss of virulence through multiple passage in cell culture. Targeted recombination can be used to evaluate gene function *in vitro*, but will not be successful in *in vivo* animal experiments because virulent viruses are difficult to generate with this system. To that end MHV-1 recombinant viruses will have to be

generated using a system that does not require extended passage time in cell culture. The infectious cDNA clone generated from cDNA fragments is one option, though there are other methods that can be used to generate viable virus with limited passage in cell culture (146, 173).

REFERENCES

1. **Abdul-Rasool S., and B. C. Fielding**. 2010. Understanding human coronavirus HCoV-NL63. Open Virol. J. **4**:76–84.

2. **Afanasyeva M., Y. Wang, Z. Kaya, S. Park, M. J. Zilliox, B. H. Schofield, S. L. Hill, and N. R. Rose**. 2001. Experimental autoimmune myocarditis in A/J mice is an interleukin-4-dependent disease with a Th2 phenotype. Am. J. Pathol. **159**:193–203.

3. **Albuquerque N. de, E. Baig, J. Zhang, W. He, A. Rowe, M. Habal, M. Liu, I. Shalev, G. P. Downey, R. Gorczynski, J. Butany, J. Leibowitz, S. R. Weiss, I. D. Mcgilvray, J. Phillips, E. N. Fish, and G. A. Levy**. 2006. Murine hepatitis virus strain 1 produces a clinically relevant model of severe acute respiratory syndrome in A/J mice. J. Virol. **80**:10382–10394.

4. **Almazán F., M. L. Dediego, C. Galán, D. Escors, E. Alvarez, J. Ortego, I. Sola, S. Zuñiga, S. Alonso, J. L. Moreno, A. Nogales, C. Capiscol, and L. Enjuanes**. 2006. Construction of a severe acute respiratory syndrome coronavirus infectious cDNA clone and a replicon to study coronavirus RNA synthesis. J. Virol. **80**:10900–6.

5. **Assiri A., A. McGeer, T. M. Perl, C. S. Price, A. a. Al Rabeeah, D. a. T. Cummings, Z. N. Alabdullatif, M. Assad, A. Almulhim, H. Makhdoom, H. Madani, R. Alhakeem, J. a. Al-Tawfiq, M. Cotten, S. J. Watson, P. Kellam, A. I. Zumla, and Z. a. Memish**. 2013. Hospital outbreak of middle east respiratory syndrome coronavirus. N. Engl. J. Med. **369**:407-16.

6. **Baas T., A. Roberts, T. H. Teal, L. Vogel, J. Chen, T. M. Tumpey, M. G. Katze, and K. Subbarao**. 2008. Genomic analysis reveals age-dependent innate immune responses to severe acute respiratory syndrome coronavirus. J. Virol. **82**:9465–76.

7. **Becker M. M., R. L. Graham, E. F. Donaldson, B. Rockx, A. C. Sims, T. Sheahan, R. J. Pickles, D. Corti, R. E. Johnston, R. S. Baric, and M. R. Denison**. 2008. Synthetic recombinant bat SARS-like coronavirus is infectious in cultured cells and in mice. PNAS. **105**:19944-49.

8. **Bender S. J., and S. R. Weiss**. 2010. Pathogenesis of murine coronavirus in the central nervous system. J. Neuroimmune Pharmacol.

9. **Brand J. M. a van den, B. L. Haagmans, L. Leijten, D. van Riel, B. E. E. Martina, a D. M. E. Osterhaus, and T. Kuiken**. 2008. Pathology of experimental SARS coronavirus infection in cats and ferrets. Vet. Pathol. **45**:551–62.

10. **Brierley I., P. Digard, and S. C. Inglis**. 1989. Characterization of an efficient coronavirs ribosomal frameshifting signal: requirement for an RNA pseudoknot. Cell **57**:537–547.

11. **Bukreyev A., E. W. Lamirande, U. J. Buchholz, L. N. Vogel, W. R. Elkins, M. St Claire, B. R. Murphy, K. Subbarao, and P. L. Collins**. 2004. Mucosal immunisation of african green monkeys (Cercopithecus aethiops) with an attenuated parainfluenza virus expressing the SARS coronavirus spike protein for the prevention of SARS. Lancet **363**:2122–7.

12. **Burrell L. M., C. I. Johnston, C. Tikellis, and M. E. Cooper**. 2004. ACE2, a new regulator of the renin-angiotensin system. Trends Endocrinol. Metab. **15**:166–9.

13. **Cameron M. J., A. a Kelvin, A. J. Leon, C. M. Cameron, L. Ran, L. Xu, Y.-K. Chu, A. Danesh, Y. Fang, Q. Li, A. Anderson, R. C. Couch, S. G. Paquette, N. G. Fomukong, O. Kistner, M. Lauchart, T. Rowe, K. S. Harrod, C. B. Jonsson, and D. J. Kelvin**. 2012. Lack of innate interferon responses during SARS coronavirus infection in a vaccination and reinfection ferret model. PLoS One **7**:e45842.

14. **CDC**. 2003. Udpate: outbreak of severe acute respiratory syndrome- worldwide. Morbitity Mortal. Wkly. Rep. **52**:241–8.

15. **Chan K.-H., J. Fuk-Woo Chan, H. Tse, H. Chen, C. Choi-Yi Lau, J.-P. Cai, A. Ka-Lun Tsang, X. Xiao, K. Kai-Wang To, S. Kar-Pui Lau, P. Chiu-Yat Woo, B.-J. Zheng, M. Wang, and K.-Y. Yuen**. 2013. Cross-reactive antibodies in convalescent SARS patients' sera against the emerging novel human coronavirus EMC (2012) by both immunofluorescent and neutralizing antibody tests. J. Infect. Elsevier Ltd 1–11.

16. **Chen H. I., S. J. Kao, D. Wang, R. P. Lee, and C. F. Su**. 2003. Acute respiratory distress syndrome. J. Biomed. Sci. **10**:588–592.

17. **Chen J., Y. F. Lau, E. W. Lamirande, C. D. Paddock, J. H. Bartlett, S. R. Zaki, and K. Subbarao**. 2010. Cellular immune responses to severe acute respiratory syndrome coronavirus (SARS-CoV) infection in senescent BALB/c mice: CD4+ T cells are important in control of SARS-CoV infection. J. Virol. **84**:1289–301.

18. **Chen S.-C., and R. C. L. Olsthoorn**. 2010. Group-specific structural features of the 5'-proximal sequences of coronavirus genomic RNAs. Virology. **401**:29–41.

19. **Cheng V. C. C., S. K. P. Lau, P. C. Y. Woo, and K. Y. Yuen**. 2007. Severe acute respiratory syndrome coronavirus as an agent of emerging and reemerging infection. Clin. Microbiol. Rev. **20**:660–94.

20. **Chuck C.-P., L.-T. Chong, C. Chen, H.-F. Chow, D. C.-C. Wan, and K.-B. Wong**. 2010. Profiling of substrate specificity of SARS-CoV 3CL. PLoS One **5**:1–7.

21. **Clementz M. a, Z. Chen, B. S. Banach, Y. Wang, L. Sun, K. Ratia, Y. M. Baez-Santos, J. Wang, J. Takayama, A. K. Ghosh, K. Li, A. D. Mesecar, and S. C. Baker**. 2010. Deubiquitinating and interferon antagonism activities of coronavirus papain-like proteases. J. Virol. **84**:4619–29.

22. **Day C. W., R. Baric, S. X. Cai, M. Frieman, Y. Kumaki, J. D. Morrey, D. F. Smee, and D. L. Barnard**. 2009. A new mouse-adapted strain of SARS-CoV as a lethal model for evaluating antiviral agents in vitro and in vivo. Virology. **395**:210–22.

23. **DeAlbuquerque N., E. Baig, M. Xuezhong, I. Shalev, M. J. Phillips, M. Habal, J. Leibowitz, I. McGilvray, J. Butany, E. Fish, and G. Levy**. 2006. Murine hepatitis virus strain 1 as a model for severe acute respiratory distress syndrome (SARS). Adv. Exp. Med. Biol. **581**:373–8.

24. **Dediego M. L., L. Pewe, E. Alvarez, M. T. Rejas, S. Perlman, and L. Enjuanes**. 2008. Pathogenicity of severe acute respiratory coronavirus deletion mutants in hACE-2 transgenic mice. Virology. **376**:379–89.

25. **Deming D. J., R. L. Graham, M. R. Denison, and R. S. Baric**. 2007. Processing of open reading frame 1a replicase proteins nsp7 to nsp10 in murine hepatitis virus strain A59 replication. J. Virol. **81**:10280–91.

26. **Devitt E.** 2013. Lack of small animal models hinders MERS coronavirus research. Nat. Med. **19**:952.

27. **Dı C., J. Va, F. C. De Adjounian, M. F. R. Ferrari, L. Yuan, X. Silver, R. Torres, and M. K. Raizada**. 2006. ACE2 gene transfer attenuates hypertension-linked pathophysiological changes in the SHR **2**:12–19.

28. **Diez E., S.-H. Lee, S. Gauthier, Z. Yaraghi, M. Tremblay, S. Vidal, and P. Gros**. 2003. Birc1e is the gene within the Lgn1 locus associated with resistance to Legionella pneumophila. Nat. Genet. **33**:55–60.

29. **Dinten L. C. Van, H. Van Tol, E. Alexander, and E. J. Snijder**. 2000. The predicted metal-binding region of the arterivirus helicase protein is involved in subgenomic mRNA synthesis , genome replication , and virion biogenesis. J. Virol. **74**: 5213-23.

30. **Donnelly C. a, A. C. Ghani, G. M. Leung, A. J. Hedley, C. Fraser, S. Riley, L. J. Abu-Raddad, L.-M. Ho, T.-Q. Thach, P. Chau, K.-P. Chan, T.-H. Lam, L.-Y. Tse, T. Tsang, S.-H. Liu, J. H. B. Kong, E. M. C. Lau, N. M. Ferguson, and R. M.**

Anderson. 2003. Epidemiological determinants of spread of causal agent of severe acute respiratory syndrome in Hong Kong. Lancet **361**:1761–6.

31. **Drosten C., S. Günther, W. Preiser, S. van der Werf, H.-R. Brodt, S. Becker, H. Rabenau, M. Panning, L. Kolesnikova, R. a M. Fouchier, A. Berger, A.-M. Burguière, J. Cinatl, M. Eickmann, N. Escriou, K. Grywna, S. Kramme, J.-C. Manuguerra, S. Müller, V. Rickerts, M. Stürmer, S. Vieth, H.-D. Klenk, A. D. M. E. Osterhaus, H. Schmitz, and H. W. Doerr**. 2003. Identification of a novel coronavirus in patients with severe acute respiratory syndrome. N. Engl. J. Med. **348**:1967–76.

32. **Eckerle L. D., M. M. Becker, R. a Halpin, K. Li, E. Venter, X. Lu, S. Scherbakova, R. L. Graham, R. S. Baric, T. B. Stockwell, D. J. Spiro, and M. R. Denison**. 2010. Infidelity of SARS-CoV Nsp14-exonuclease mutant virus replication is revealed by complete genome sequencing. PLoS Pathog. **6**:e1000896.

33. **Eifart P., K. Ludwig, C. Böttcher, C. a M. de Haan, P. J. M. Rottier, T. Korte, and A. Herrmann**. 2007. Role of endocytosis and low pH in murine hepatitis virus strain A59 cell entry. J. Virol. **81**:10758–68.

34. **Enjuanes L., F. Almazán, I. Sola, and S. Zuñiga**. 2006. Biochemical aspects of coronavirus replication and virus-host interaction. Annu. Rev. Microbiol. **60**:211–30.

35. **Eriksson K. K., L. Cervantes-Barragán, B. Ludewig, and V. Thiel**. 2008. Mouse hepatitis virus liver pathology is dependent on ADP-ribose-1''-phosphatase, a viral function conserved in the alpha-like supergroup. J. Virol. **82**:12325–34.

36. **Farcas G. a, S. M. Poutanen, T. Mazzulli, B. M. Willey, J. Butany, S. L. Asa, P. Faure, P. Akhavan, D. E. Low, and K. C. Kain**. 2005. Fatal severe acute respiratory syndrome is associated with multiorgan involvement by coronavirus. J. Infect. Dis. **191**:193–7.

37. **Feng Y., and G. F. Gao**. 2007. Towards our understanding of SARS-CoV, an emerging and devastating but quickly conquered virus. Comp. Immunol. Microbiol. Infect. Dis. **30**:309–27.

38. **Fischer F., C. F. Stegen, C. A. Koetzner, and P. S. Masters**. 1997. Analysis of a recombinant mouse hepatitis virus expressing a foreign gene reveals a novel aspect of coronavirus transcription. J. Virol. **71**:5148–60.

39. **Frieman M. B., J. Chen, T. E. Morrison, A. Whitmore, W. Funkhouser, J. M. Ward, E. W. Lamirande, A. Roberts, M. Heise, K. Subbarao, and R. S. Baric**. 2010. SARS-CoV pathogenesis is regulated by a STAT1 dependent but a type I, II and III interferon receptor independent mechanism. PLoS Pathog. **6**:e1000849.

40. **Frieman M., and R. Baric**. 2008. Mechanisms of severe acute respiratory syndrome pathogenesis and innate immunomodulation. Microbiol. Mol. Biol. Rev. **72**:672–85, Table of Contents.

41. **Frieman M., M. Heise, and R. Baric**. 2008. SARS coronavirus and innate immunity. Virus Res. **133**:101–112.

42. **Frieman M., B. Yount, M. Heise, S. a Kopecky-Bromberg, P. Palese, and R. S. Baric**. 2007. Severe acute respiratory syndrome coronavirus ORF6 antagonizes STAT1 function by sequestering nuclear import factors on the rough endoplasmic reticulum/Golgi membrane. J. Virol. **81**:9812–24.

43. **Gadlage M. J., J. S. Sparks, D. C. Beachboard, R. G. Cox, J. D. Doyle, C. C. Stobart, and M. R. Denison**. 2010. Murine hepatitis virus nonstructural protein 4 regulates virus-induced membrane modifications and replication complex function. J. Virol. **84**:280–90.

44. **Gallagher T. M., and M. J. Buchmeier**. 2001. Coronavirus spike proteins in viral entry and pathogenesis. Virology. **279**:371–4.

45. **Glass W. G., K. Subbarao, B. Murphy, and P. M. Murphy**. 2004. Mechanisms of host defense following severe acute respiratory syndrome-coronavirus (SARS-CoV) pulmonary infection of mice. J. Immunol. **173**:4030–9.

46. **Goebel S. J., B. Hsue, T. F. Dombrowski, and P. S. Masters**. 2004. Characterization of the RNA components of a putative molecular switch in the 3' untranslated region of the murine coronavirus genome. J. Virol. **78**:669–682.

47. **Goebel S. J., T. B. Miller, C. J. Bennett, K. a Bernard, and P. S. Masters**. 2007. A hypervariable region within the 3' cis-acting element of the murine coronavirus genome is nonessential for RNA synthesis but affects pathogenesis. J. Virol. **81**:1274–87.

48. **Graham R. L., J. S. Sparks, L. D. Eckerle, A. C. Sims, and M. R. Denison**. 2008. SARS coronavirus replicase proteins in pathogenesis. Virus Res. **133**:88–100.

49. **Greenough T. C., A. Carville, J. Coderre, M. Somasundaran, J. L. Sullivan, K. Luzuriaga, and K. Mansfield**. 2005. Pneumonitis and multi-organ system disease in common marmosets (Callithrix jacchus) infected with the severe acute respiratory syndrome-associated coronavirus. Am. J. Pathol. American Society for Investigative Pathology **167**:455–63.

50. **Gu J., E. Gong, B. Zhang, J. Zheng, Z. Gao, Y. Zhong, W. Zou, J. Zhan, S. Wang, Z. Xie, H. Zhuang, B. Wu, H. Zhong, H. Shao, W. Fang, D. Gao, F. Pei, X.**

Li, Z. He, D. Xu, X. Shi, V. M. Anderson, and A. S.-Y. Leong. 2005. Multiple organ infection and the pathogenesis of SARS. J. Exp. Med. **202**:415–24.

51. **Haagmans B. L., A. C. Andeweg, and A. D. M. E. Osterhaus**. 2009. The application of genomics to emerging zoonotic viral diseases. PLoS Pathog. **5**:e1000557.

52. **Haagmans B. L., T. Kuiken, B. E. Martina, R. a M. Fouchier, G. F. Rimmelzwaan, G. van Amerongen, D. van Riel, T. de Jong, S. Itamura, K.-H. Chan, M. Tashiro, and A. D. M. E. Osterhaus**. 2004. Pegylated interferon-alpha protects type 1 pneumocytes against SARS coronavirus infection in macaques. Nat. Med. **10**:290–3.

53. **Haan C. a M. de, P. S. Masters, X. Shen, S. Weiss, and P. J. M. Rottier**. 2002. The group-specific murine coronavirus genes are not essential, but their deletion, by reverse genetics, is attenuating in the natural host. Virology. **296**:177–89.

54. **Hogan R. J., G. Gao, T. Rowe, D. Flieder, J. Paragas, G. P. Kobinger, N. A. Wivel, R. G. Crystal, J. Boyer, T. G. Voss, J. M. Wilson, P. Bell, and H. Feldmann**. 2004. Resolution of primary severe acute respiratory syndrome-associated coronavirus infection requires Stat1. J. Virol. **78**: 11416-21.

55. **Hui D. S. C., M. C. H. Chan, a K. Wu, and P. C. Ng**. 2004. Severe acute respiratory syndrome (SARS): epidemiology and clinical features. Postgrad. Med. J. **80**:373–81.

56. **Hurst K. R., R. Ye, S. J. Goebel, P. Jayaraman, and P. S. Masters**. 2010. An Interaction between the nucleocapsid protein and a component of the replicase-transcriptase complex is crucial for the infectivity of coronavirus genomic RNA. J. Virol. **84**:10276–10288.

57. **Hussain S., S. Perlman, and T. M. Gallagher**. 2008. Severe acute respiratory syndrome coronavirus protein 6 accelerates murine hepatitis virus infections by more than one mechanism. J. Virol. **82**:7212–22.

58. **Iacono K. T. T., L. Kazi, and S. R. R. Weiss**. 2006. Both spike and background genes contribute to murine coronavirus neurovirulence. J. Virol. Am Soc Microbiol **80**:6834.

59. **Ichihara M., T. Hara, M. Takagi, L. C. Cho, D. M. Gorman, and A. Miyajima**. 1995. Impaired interleukin-3 (IL-3) response of the A / J mouse is caused by a branch point deletion in the **14**:939–950.

60. **Imai Y., K. Kuba, T. Ohto-Nakanishi, and J. M. Penninger**. 2010. Angiotensin-converting enzyme 2 (ACE2) in disease pathogenesis. Circ. J. **74**:405–410.

61. **Imai Y., K. Kuba, S. Rao, Y. Huan, F. Guo, B. Guan, P. Yang, R. Sarao, T. Wada, H. Leong-poi, M. A. Crackower, A. Fukamizu, C. Hui, L. Hein, S. Uhlig, A. S. Slutsky, C. Jiang, and J. M. Penninger**. 2005. Angiotensin-converting enzyme 2 protects from severe acute lung failure. Nature **436**.

62. **Ithete N. L., S. Stoffberg, V. M. Corman, V. M. Cottontail, L. R. Richards, M. C. Schoeman, C. Drosten, J. F. Drexler, and W. Preiser**. 2013. Close relative of human middle East respiratory syndrome coronavirus in bat, South Africa. Emerg. Infect. Dis. **19**:1697–9.

63. **Ivanov K. A., V. Thiel, J. C. Dobbe, Y. Van Der Meer, E. J. Snijder, and J. Ziebuhr**. 2004. Multiple enzymatic activities associated with severe acute respiratory syndrome coronavirus helicase **78**:5619–5632.

64. **Janies D., F. Habib, B. Alexandrov, A. Hill, and D. Pol**. 2008. Evolution of genomes, host shifts and the genographic spread of SARS-CoV and related coronaviruses. Cladistics **24**:111–130.

65. **Jiang Y., J. Xu, C. Zhou, Z. Wu, S. Zhong, J. Liu, W. Luo, T. Chen, Q. Qin, and P. Deng**. 2005. Characterization of cytokine/chemokine profiles of severe acute respiratory syndrome. Am. J. Respir. Crit. Care Med. **171**:850–7.

66. **Kamitani W., C. Huang, K. Marayanan, K. G. Lokugamage, and S. Makino**. 2009. A two-pronged strategy to supress host protein synthesis by SARS coronavirus Nsp1 protein. Nat. Struct. Mol. Biol. **16**:1134–1141.

67. **Kang H., M. Feng, M. E. Schroeder, D. P. Giedroc, and J. L. Leibowitz**. 2006. Putative cis-acting stem-loops in the 5' untranslated region of the severe acute respiratory syndrome coronavirus can substitute for their mouse hepatitis virus counterparts. J. Virol. **80**:10600–14.

68. **Kanjanahaluethai A., Z. Chen, D. Jukneliene, and S. C. Baker**. 2007. Membrane topology of murine coronavirus replicase nonstructural protein 3. Virology. **361**:391–401.

69. **Keck J. G., L. H. Soe, S. Makino, S. A. Stohlman, and M. M. Lai**. 1988. RNA recombination of murine coronaviruses: recombination between fusion-positive mouse hepatitis virus A59 and fusion-negative mouse hepatitis virus 2. J. Virol. **62**:1989–1998.

70. **Khanolkar A., R. B. Fulton, L. L. Epping, N.-L. Pham, D. Tifrea, S. M. Varga, and J. T. Harty**. 2010. T cell epitope specificity and pathogenesis of mouse hepatitis virus-1-induced disease in susceptible and resistant hosts. J. Immunol.

71. **Khanolkar A., S. M. Hartwig, B. a Haag, D. K. Meyerholz, L. L. Epping, J. S. Haring, S. M. Varga, and J. T. Harty**. 2009. Protective and pathologic roles of the immune response to mouse hepatitis virus type 1: implications for severe acute respiratory syndrome. J. Virol. **83**:9258–72.

72. **Kim O. J., D. H. Lee, and C. H. Lee**. 2006. Close relationship between SARS-coronavirus and group 2 coronavirus. J. Microbiol. **44**:83–91.

73. **Koetzner C. a, M. M. Parker, C. S. Ricard, L. S. Sturman, and P. S. Masters**. 1992. Repair and mutagenesis of the genome of a deletion mutant of the coronavirus mouse hepatitis virus by targeted RNA recombination. J. Virol. **66**:1841–8.

74. **Koetzner C. a, L. Kuo, S. J. Goebel, A. B. Dean, M. M. Parker, and P. S. Masters**. 2010. Accessory protein 5a is a major antagonist of the antiviral action of interferon against murine coronavirus. J. Virol. **84**:8262–8274.

75. **Kuo L., G.-J. J. Godeke, M. J. B. Raamsman, P. S. Masters, and P. J. Rottier**. 2000. Retargeting of coronavirus by substitution of the spike glycoprotein ectodomain: crossing the host cell species barrier. J. Virol. **74**:1393–1406.

76. **Kuri T., K. K. Eriksson, A. Putics, R. Züst, E. J. Snijder, A. D. Davidson, S. G. Siddell, V. Thiel, J. Ziebuhr, and F. Weber**. 2011. The ADP-ribose-1''-monophosphatase domains of severe acute respiratory syndrome coronavirus and human coronavirus 229E mediate resistance to antiviral interferon responses. J. Gen. Virol. **92**:1899–905.

77. **Lai C. J., B. T. Zhao, H. Hori, and M. Bray**. 1991. Infectious RNA transcribed from stably cloned full-length cDNA of dengue type 4 virus. Proc. Natl. Acad. Sci. U. S. A. **88**:5139–43.

78. **Lamirande E. W., M. L. DeDiego, A. Roberts, J. P. Jackson, E. Alvarez, T. Sheahan, W.-J. Shieh, S. R. Zaki, R. Baric, L. Enjuanes, and K. Subbarao**. 2008. A live attenuated severe acute respiratory syndrome coronavirus is immunogenic and efficacious in golden Syrian hamsters. J. Virol. **82**:7721–4.

79. **Lau E. H. Y., C. A. Hsiung, B. J. Cowling, C.-H. Chen, L.-M. Ho, T. Tsang, C.-W. Chang, C. a Donnelly, and G. M. Leung**. 2010. A comparative epidemiologic analysis of SARS in Hong Kong, Beijing and Taiwan. BMC Infect. Dis. **10**:50.

80. **Lau S. K. P., K. S. M. Li, Y. Huang, C.-T. Shek, H. Tse, M. Wang, G. K. Y. Choi, H. Xu, C. S. F. Lam, R. Guo, K.-H. Chan, B.-J. Zheng, P. C. Y. Woo, and K.-Y. Yuen**. 2010. Ecoepidemiology and complete genome comparison of different strains of severe acute respiratory syndrome-related Rhinolophus bat coronavirus in China

reveal bats as a reservoir for acute, self-limiting infection that allows recombination events. J. Virol. **84**:2808–19.

81. **Law A. H. Y., D. C. W. Lee, B. K. W. Cheung, H. C. H. Yim, and A. S. Y. Lau**. 2007. Role for nonstructural protein 1 of severe acute respiratory syndrome coronavirus in chemokine dysregulation. J. Virol. **81**:416–22.

82. **Lawler J. V, T. P. Endy, L. E. Hensley, A. Garrison, E. a Fritz, M. Lesar, R. S. Baric, D. a Kulesh, D. a Norwood, L. P. Wasieloski, M. P. Ulrich, T. R. Slezak, E. Vitalis, J. W. Huggins, P. B. Jahrling, and J. Paragas**. 2006. Cynomolgus macaque as an animal model for severe acute respiratory syndrome. PLoS Med. **3**:e149.

83. **Leibowitz J. L., R. Srinivasa, S. T. Williamson, M. M. Chua, M. Liu, S. Wu, H. Kang, X.-Z. Ma, J. Zhang, I. Shalev, R. Smith, M. J. Phillips, G. a Levy, and S. R. Weiss**. 2010. Genetic determinants of mouse hepatitis virus strain 1 pneumovirulence. J. Virol. **84**:9278–91.

84. **Leparc-goffart I., S. T. Hingley, M. M. Chua, J. Phillips, E. Lavi, and S. R. Weiss**. 1998. Targeted recombination within the spike gene of murine coronavirus mouse hepatitis virus-A59: Q159 is a determinant of hepatotropism. J. Virol **72**:9628–9636.

85. **Li F.** 2008. Structural analysis of major species barriers between humans and palm civets for severe acute respiratory syndrome coronavirus infections. J. Virol. **82**:6984–91.

86. **Li F., W. Li, M. Farzan, and S. C. Harrison**. 2005. Structure of SARS coronavirus spike receptor-binding domain complexed with receptor. Science **309**:1864–8.

87. **Li W., M. J. Moore, N. Vasilieva, J. Sui, S. K. Wong, M. A. Berne, M. Somasundaran, J. L. Sullivan, K. Luzuriaga, T. C. Greenough, H. Choe, and M. Farzan**. 2003. Antiotensin-converting enzyme 2 is a functional receptor for the SARS coronavirus. Nature **426**:450–454.

88. **Lin H.-X., Y. Feng, X. Tu, X. Zhao, C.-H. Hsieh, L. Griffin, M. Junop, and C. Zhang**. 2011. Characterization of the spike protein of human coronavirus NL63 in receptor binding and pseudotype virus entry. Virus Res. Elsevier B.V. 1–11.

89. **Makino S., J. G. Keck, S. a Stohlman, and M. M. Lai**. 1986. High-frequency RNA recombination of murine coronaviruses. J. Virol. **57**:729–37.

90. **Marra M. a, S. J. M. Jones, C. R. Astell, R. a Holt, A. Brooks-Wilson, Y. S. N. Butterfield, J. Khattra, J. K. Asano, S. a Barber, S. Y. Chan, A. Cloutier, S. M. Coughlin, D. Freeman, N. Girn, O. L. Griffith, S. R. Leach, M. Mayo, H.**

McDonald, S. B. Montgomery, P. K. Pandoh, A. S. Petrescu, a G. Robertson, J. E. Schein, A. Siddiqui, D. E. Smailus, J. M. Stott, G. S. Yang, F. Plummer, A. Andonov, H. Artsob, N. Bastien, K. Bernard, T. F. Booth, D. Bowness, M. Czub, M. Drebot, L. Fernando, R. Flick, M. Garbutt, M. Gray, A. Grolla, S. Jones, H. Feldmann, A. Meyers, A. Kabani, Y. Li, S. Normand, U. Stroher, G. a Tipples, S. Tyler, R. Vogrig, D. Ward, B. Watson, R. C. Brunham, M. Krajden, M. Petric, D. M. Skowronski, C. Upton, and R. L. Roper. 2003. The genome sequence of the SARS-associated coronavirus. Science **300**:1399–404.

91. **Marshall R. P., P. Gohlke, R. C. Chambers, D. C. Howell, S. E. Bottoms, T. Unger, R. J. McAnulty, and G. J. Laurent**. 2004. Angiotensin II and the fibroproliferative response to acute lung injury. Am. J. Physiol. Lung Cell. Mol. Physiol. **286**:L156–64.

92. **Martina B. E. E., B. L. Haagmans, T. Kuiken, R. a M. Fouchier, G. F. Rimmelzwaan, G. Van Amerongen, J. S. M. Peiris, W. Lim, and A. D. M. E. Osterhaus**. 2003. SARS virus infection of cats and ferrets. Nature **425**:915.

93. **Masters P. S., C. a Koetzner, C. a Kerr, and Y. Heo**. 1994. Optimization of targeted RNA recombination and mapping of a novel nucleocapsid gene mutation in the coronavirus mouse hepatitis virus. J. Virol. **68**:328–37.

94. **McBride C. E., and C. E. Machamer**. 2010. A single tyrosine in the severe acute respiratory syndrome coronavirus membrane protein cytoplasmic tail is important for efficient interaction with spike protein. J. Virol. **84**:1891–901.

95. **McCray P. B., L. Pewe, C. Wohlford-Lenane, M. Hickey, L. Manzel, L. Shi, J. Netland, H. P. Jia, C. Halabi, C. D. Sigmund, D. K. Meyerholz, P. Kirby, D. C. Look, and S. Perlman**. 2007. Lethal infection of K18-hACE2 mice infected with severe acute respiratory syndrome coronavirus. J. Virol. **81**:813–21.

96. **Meer Y. van der, E. J. Snijder, J. C. Dobbe, S. Schleich, M. R. Denison, W. J. Spaan, and J. K. Locker**. 1999. Localization of mouse hepatitis virus nonstructural proteins and RNA synthesis indicates a role for late endosomes in viral replication. J. Virol. **73**:7641–57.

97. **Memish Z. a., A. I. Zumla, R. F. Al-Hakeem, A. a. Al-Rabeeah, and G. M. Stephens**. 2013. Family cluster of middle east respiratory syndrome coronavirus infections. N. Engl. J. Med. 130529140042003.

98. **Mesel-Lemoine M., J. Millet, P.-O. Vidalain, H. Law, A. Vabret, V. Lorin, N. Escriou, M. L. Albert, B. Nal, and F. Tangy**. 2012. A human coronavirus responsible for the common cold massively kills dendritic cells but not monocytes. J. Virol. **86**:7577–87.

99. **Nagata N., N. Iwata-Yoshikawa, and F. Taguchi**. 2010. Studies of severe acute respiratory syndrome coronavirus pathology in human cases and animal models. Vet. Pathol. **47**:881–92.

100. **Nagata N., N. Iwata, H. Hasegawa, S. Fukushi, A. Harashima, Y. Sato, M. Saijo, F. Taguchi, S. Morikawa, and T. Sata**. 2008. Mouse-passaged severe acute respiratory syndrome-associated coronavirus leads to lethal pulmonary edema and diffuse alveolar damage in adult but not young mice. Am. J. Pathol. American Society for Investigative Pathology **172**:1625–37.

101. **Nagata N., N. Iwata, H. Hasegawa, S. Fukushi, M. Yokoyama, A. Harashima, Y. Sato, M. Saijo, S. Morikawa, and T. Sata**. 2007. Participation of both host and virus factors in induction of severe acute respiratory syndrome (SARS) in F344 rats infected with SARS coronavirus. J. Virol. **81**:1848–57.

102. **Navas S., and S. R. Weiss**. 2003. Murine coronavirus-induced hepatitis: JHM genetic background eliminates A59 spike-determined hepatotropism. J. Virol **77**:4972–4978.

103. **Navas-Martin S., M. Brom, M.-M. Chua, R. Watson, Z. Qiu, and S. R. Weiss**. 2007. Replicase genes of murine coronavirus strains A59 and JHM are interchangeable: differences in pathogenesis map to the 3' one-third of the genome. J. Virol. **81**:1022–6.

104. **Neuman B. W., J. S. Joseph, K. S. Saikatendu, P. Serrano, A. Chatterjee, M. a Johnson, L. Liao, J. P. Klaus, J. R. Yates, K. Wüthrich, R. C. Stevens, M. J. Buchmeier, and P. Kuhn**. 2008. Proteomics analysis unravels the functional repertoire of coronavirus nonstructural protein 3. J. Virol. **82**:5279–94.

105. **Nicholls J., X.-P. Dong, G. Jiang, and M. Peiris**. 2003. SARS: clinical virology and pathogenesis. Respirology **8 Suppl**:S6–8.

106. **Nicholls J. M., L. L. M. Poon, K. C. Lee, W. F. Ng, S. T. Lai, C. Y. Leung, C. M. Chu, P. K. Hui, K. L. Mak, W. Lim, K. W. Yan, K. H. Chan, N. C. Tsang, Y. Guan, K. Y. Yuen, and J. S. M. Peiris**. 2003. Lung pathology of fatal severe acute respiratory syndrome. Lancet **361**:1773–8.

107. **O'Malley J., L. E. Matesic, M. C. Zink, J. D. Strandberg, M. L. Mooney, a De Maio, and R. H. Reeves**. 1998. Comparison of acute endotoxin-induced lesions in A/J and C57BL/6J mice. J. Hered. **89**:525–30.

108. **Ortín J., and F. Parra**. 2006. Structure and function of RNA replication. Annu. Rev. Microbiol. **60**:305–26.

109. **Peret T., D. Ph, S. Emery, S. Tong, C. Urbani, J. A. Comer, W. Lim, P. E. Rollin, S. F. Dowell, A. Ling, C. D. Humphrey, B. Fields, J. Derisi, J. Yang, N. Cox, J. M. Hughes, J. W. Leduc, W. J. Bellini, L. J. Anderson, and W. Group**. 2003. A novel coronavirus associated with severe acute respiratory syndrome. N. Engl. J. Med. **348**:1953–1966.

110. **Perlman S., and A. a Dandekar**. 2005. Immunopathogenesis of coronavirus infections: implications for SARS. Nat. Rev. Immunol. **5**:917–27.

111. **Perlman S., and J. Netland**. 2009. Coronaviruses post-SARS: update on replication and pathogenesis. Nat. Rev. Microbiol. **7**:439–50.

112. **Peti W., M. A. Johnson, T. Herrmann, B. W. Neuman, M. J. Buchmeier, M. Nelson, J. Joseph, and R. Page**. 2005. Structural genomics of the severe acute respiratory syndrome coronavirus : nuclear magnetic resonance structure of the protein Structural Genomics of the Severe Acute Respiratory Syndrome Coronavirus : Nuclear Magnetic Resonance Structure of the Protein nsP7. J. Virol. **79**: 12905-13.

113. **Pewe L., H. Zhou, J. Netland, C. Tangudu, H. Olivares, L. Shi, D. Look, T. Gallagher, and S. Perlman**. 2005. A severe acute respiratory protein enhances virulence of an attenuated murine coronavirus. J. Virol. **79**: 11335-42.

114. **Pfefferle S., V. Krähling, V. Ditt, K. Grywna, E. Mühlberger, and C. Drosten**. 2009. Reverse genetic characterization of the natural genomic deletion in SARS-Coronavirus strain Frankfurt-1 open reading frame 7b reveals an attenuating function of the 7b protein in-vitro and in-vivo. Virol. J. **6**:131.

115. **Plant E. P., R. Rakauskaite, D. R. Taylor, and J. D. Dinman**. 2010. Achieving a golden mean: mechanisms by which coronaviruses ensure synthesis of the correct stoichiometric ratios of viral proteins. J. Virol. **84**:4330–40.

116. **Poon L. L. M., K. H. Chan, O. K. Wong, T. K. W. Cheung, I. Ng, B. Zheng, W. H. Seto, K. Y. Yuen, Y. Guan, and J. S. M. Peiris**. 2004. Detection of SARS coronavirus in patients with severe acute respiratory syndrome by conventional and real-time quantitative reverse transcription-PCR assays. Clin. Chem. **50**:67–72.

117. **Poon L. L. M., C. S. W. Leung, K. H. Chan, K. Y. Yuen, Y. Guan, and J. S. M. Peiris**. 2005. Recurrent mutations associated with isolation and passage of SARS coronavirus in cells from non-human primates. J. Med. Virol. **76**:435–40.

118. **Pyrc K., A. C. Sims, R. Dijkman, M. Jebbink, C. Long, D. Deming, E. Donaldson, A. Vabret, R. Baric, L. van der Hoek, and R. Pickles**. 2010. Culturing the unculturable: human coronavirus HKU1 infects, replicates, and produces progeny virions in human ciliated airway epithelial cell cultures. J. Virol. **84**:11255–63.

119. **Raaben M., M. J. a Groot Koerkamp, P. J. M. Rottier, and C. a M. de Haan**. 2009. Type I interferon receptor-independent and -dependent host transcriptional responses to mouse hepatitis coronavirus infection in vivo. BMC Genomics **10**:350.

120. **Raaben M., H.-J. Prins, A. C. Martens, P. J. M. Rottier, and C. a M. De Haan**. 2009. Non-invasive imaging of mouse hepatitis coronavirus infection reveals determinants of viral replication and spread in vivo. Cell. Microbiol. **11**:825–841.

121. **Rest J. S., and D. P. Mindell**. 2003. SARS associated coronavirus has a recombinant polymerase and coronaviruses have a history of host-shifting. Infect. Genet. Evol. **3**:219–225.

122. **Reusken C. B. E. M., P. H. C. Lina, A. Pielaat, A. de Vries, C. Dam-Deisz, J. Adema, J. F. Drexler, C. Drosten, and E. a Kooi**. 2010. Circulation of group 2 coronaviruses in a bat species common to urban areas in Western Europe. Vector Borne Zoonotic Dis. **10**:785–91.

123. **Roberts A., D. Deming, C. D. Paddock, A. Cheng, B. Yount, L. Vogel, B. D. Herman, T. Sheahan, M. Heise, G. L. Genrich, S. R. Zaki, R. Baric, and K. Subbarao**. 2007. A mouse-adapted SARS-coronavirus causes disease and mortality in BALB/c mice. PLoS Pathog. **3**:e5.

124. **Roberts A., C. Paddock, L. Vogel, E. Butler, S. Zaki, and K. Subbarao**. 2005. Aged BALB / c mice as a model for increased severity of severe acute respiratory syndrome in elderly humans. J. Virol. **79**:5833–38.

125. **Roberts A., and K. Subbarao**. 2006. Animal models for SARS. Adv. Exp. Med. Biol. **581**:463–71.

126. **Roberts A., W. D. Thomas, J. Guarner, E. W. Lamirande, G. J. Babcock, T. C. Greenough, L. Vogel, N. Hayes, J. L. Sullivan, S. Zaki, K. Subbarao, and D. M. Ambrosino**. 2006. Therapy with a severe acute respiratory syndrome-associated coronavirus-neutralizing human monoclonal antibody reduces disease severity and viral burden in golden Syrian hamsters. J. Infect. Dis. **193**:685–92.

127. **Roberts A., L. Vogel, J. Guarner, N. Hayes, B. Murphy, S. Zaki, and K. Subbarao**. 2005. Severe acute respiratory syndrome coronavirus infection of golden syrian hamsters. J. Virol. **79**:503–511.

128. **Rockx B., T. Baas, G. A. Zornetzer, B. Haagmans, T. Sheahan, M. Frieman, M. D. Dyer, T. H. Teal, S. Proll, J. van Den Brand, R. Baric, and M. G. Katze**. 2009. Early upregulation of acute respiratory distress syndrome-associated cytokines promotes lethal disease in an aged-mouse model of severe acute respiratory syndrome coronavirus infection. J. Virol. **83**:7062–7074.

129. **Roth-Cross J. K., L. Martínez-Sobrido, E. P. Scott, A. García-Sastre, and S. R. Weiss**. 2007. Inhibition of the alpha/beta interferon response by mouse hepatitis virus at multiple levels. J. Virol. **81**:7189–99.

130. **Roth-Cross J. K., H. Stokes, G. Chang, M. M. Chua, V. Thiel, S. R. Weiss, A. E. Gorbalenya, and S. G. Siddell**. 2009. Organ-specific attenuation of murine hepatitis virus strain A59 by replacement of catalytic residues in the putative viral cyclic phosphodiesterase ns2. J. Virol. **83**:3743–53.

131. **Rowe T., G. Gao, R. J. Hogan, R. G. Crystal, T. G. Voss, R. L. Grant, P. Bell, G. P. Kobinger, N. A. Wivel, and J. M. Wilson**. 2004. Macaque model for severe acute respiratory syndrome **78**:11401–11404.

132. **Sawicki S. G., and D. L. Sawicki**. 1990. Coronavirus transcription: subgenomic mouse hepatitis virus replicative intermediates function in RNA synthesis. J. Virol. **64**:1050–6.

133. **Schaecher S. R., J. Stabenow, C. Oberle, J. Schriwere, R. M. Buller, J. E. Sagartz, and A. Pekosz**. 2008. An immunosuppressed syrian golden hamster model for SARS-CoV infection. Virology. **380**:312–321.

134. **Scobey T., B. L. Yount, A. C. Sims, E. F. Donaldson, S. S. Agnihothram, V. D. Menachery, R. L. Graham, J. Swanstrom, P. F. Bove, J. D. Kim, S. Grego, S. H. Randell, and R. S. Baric**. 2013. Reverse genetics with a full-length infectious cDNA of the middle east respiratory syndrome coronavirus. Proc. Natl. Acad. Sci. U. S. A. 1–6.

135. **See H., and P. Wark**. 2008. Innate immune response to viral infection of the lungs. Paediatr. Respir. Rev. **9**:243–50.

136. **Seok J., H. S. Warren, A. G. Cuenca, M. N. Mindrinos, H. V Baker, W. Xu, D. R. Richards, G. P. McDonald-Smith, H. Gao, L. Hennessy, C. C. Finnerty, C. M. López, S. Honari, E. E. Moore, J. P. Minei, J. Cuschieri, P. E. Bankey, J. L. Johnson, J. Sperry, A. B. Nathens, T. R. Billiar, M. a West, M. G. Jeschke, M. B. Klein, R. L. Gamelli, N. S. Gibran, B. H. Brownstein, C. Miller-Graziano, S. E. Calvano, P. H. Mason, J. P. Cobb, L. G. Rahme, S. F. Lowry, R. V Maier, L. L. Moldawer, D. N. Herndon, R. W. Davis, W. Xiao, and R. G. Tompkins**. 2013. Genomic responses in mouse models poorly mimic human inflammatory diseases. Proc. Natl. Acad. Sci. U. S. A. 1–6.

137. **Sheahan T., A. Whitmore, K. Long, M. Ferris, B. Rockx, W. Funkhouser, E. Donaldson, L. Gralinski, M. Collier, M. Heise, N. Davis, R. Johnston, and R. S. Baric**. 2011. Successful vaccination strategies that protect aged mice from lethal challenge from influenza virus and heterologous severe acute respiratory syndrome coronavirus. J. Virol. **85**:217–30.

138. **Smits S. L., A. De Lang, J. M. A. Van Den Brand, L. M. Leijten, W. F. Van, M. J. C. Eijkemans, G. Van Amerongen, T. Kuiken, and A. C. Andeweg**. 2010. Exacerbated innate host response to SARS-CoV in aged non-human primates. PLoS Pathogens. **6**: e1000756.

139. **Snijder E. J., P. J. Bredenbeek, J. C. Dobbe, V. Thiel, J. Ziebuhr, L. L. M. Poon, Y. Guan, M. Rozanov, W. J. M. Spaan, and A. E. Gorbalenya**. 2003. Unique and conserved features of genome and proteome of SARS-coronavirus, an early split-off from the coronavirus group 2 lineage. J. Mol. Biol. **331**:991–1004.

140. **Spagnolo J. F., and B. G. Hogue**. 2000. Host protein interactions with the 3' end of bovine coronavirus RNA and the requirement of the poly(A) tail for coronavirus defective genome replication. J. Virol. **74**:5053–65.

141. **Stavrinides J., and D. S. Guttman**. 2004. Mosaic evolution of the severe acute respiratory syndrome coronavirus. J. Virol. **78**: 76-82.

142. **Tan T. H. P., T. Barkham, B. C. Fielding, C.-F. Chou, S. Shen, S. G. Lim, W. Hong, and Y.-J. Tan**. 2005. Genetic lesions within the 3a gene of SARS-CoV. Virol. J. **2**:51.

143. **Tanaka T., W. Kamitani, M. L. DeDiego, L. Enjuanes, and Y. Matsuura**. 2012. Severe acute respiratory syndrome coronavirus nsp1 facilitates efficient propagation in cells through a specific translational shutoff of host mRNA. J. Virol. **86**:11128–37.

144. **Tang J. W., J. L. K. Cheung, I. M. T. Chu, J. J. Y. Sung, M. Peiris, and P. K. S. Chan**. 2006. The large 386-nt deletion in SARS-associated coronavirus : evidence for quasispecies?. J. Infec. Disease. **194**:808–813.

145. **Tangudu C., H. Olivares, J. Netland, S. Perlman, and T. Gallagher**. 2007. Severe acute respiratory syndrome coronavirus protein 6 accelerates murine coronavirus infections. J. Virol. **81**:1220–9.

146. **Thiel V., J. Herold, B. Schelle, and S. G. Siddell**. 2001. Infectious RNA transcribed in vitro from a cDNA copy of the human coronavirus genome cloned in vaccinia virus. J. Gen. Virol. **82**:1273–81.

147. **Thiel V.** 2003. Mechanisms and enzymes involved in SARS coronavirus genome expression. J. Gen. Virol. **84**:2305–2315.

148. **Thiel V., and F. Weber**. 2008. Interferon and cytokine responses to SARS-coronavirus infection. Cytokine Growth Factor Rev. **19**:121–32.

149. **Thorp E. B., and T. M. Gallagher**. 2004. Requirements for CEACAMs and cholesterol during murine coronavirus cell entry. J. Virol. **78**:2682–2692.

150. **Tsang K. W., P. L. Ho, G. C. Ooi, W. K. Yee, T. Wang, M. Chan-Yeung, W. K. Lam, W. H. Seto, L. Y. Yam, T. M. Cheung, P. C. Wong, B. Lam, M. S. Ip, J. Chan, K. Y. Yuen, and K. N. Lai**. 2003. A cluster of cases of severe acute respiratory syndrome in Hong Kong. N. Engl. J. Med. **348**:1977–85.

151. **Tseng C.-T. K., C. Huang, P. Newman, N. Wang, K. Narayanan, D. M. Watts, S. Makino, M. M. Packard, S. R. Zaki, T.-S. Chan, and C. J. Peters**. 2007. Severe acute respiratory syndrome coronavirus infection of mice transgenic for the human angiotensin-converting enzyme 2 virus receptor. J. Virol. **81**:1162–73.

152. **Tu C., G. Crameri, X. Kong, J. Chen, Y. Sun, S. Liu, T. Ren, Y. Yu, B. Eaton, H. Xuan, and L.-F. Wang**. 2004. Antibodies to SARS coronavirus in civets. Emerg. Infect. Dis. **10**:2244–2248.

153. **Vega V. B., Y. Ruan, J. Liu, W. H. Lee, C. L. Wei, S. Y. Se-Thoe, K. F. Tang, T. Zhang, P. R. Kolatkar, E. E. Ooi, A. E. Ling, L. W. Stanton, P. M. Long, and E. T. Liu**. 2004. Mutational dynamics of the SARS coronavirus in cell culture and human populations isolated in 2003. BMC Infect. Dis. **4**:32.

154. **Verhoeven D., J. Teijaro, and D. L. Farber**. 2009. Pulse-oximetry accurately predicts lung pathology and the immune response during influenza infection. Virology. **390**:151–156.

155. **Versteeg G. a, P. J. Bredenbeek, S. H. E. van den Worm, and W. J. M. Spaan**. 2007. Group 2 coronaviruses prevent immediate early interferon induction by protection of viral RNA from host cell recognition. Virology. **361**:18–26.

156. **Vignuzzi M., J. K. Stone, J. J. Arnold, C. E. Cameron, and R. Andino**. 2006. Quasispecies diversity determines pathogenesis through cooperative interactions in a viral population. Nature **439**:344–8.

157. **Vooght V. De, J. a J. Vanoirbeek, K. Luyts, S. Haenen, B. Nemery, and P. H. M. Hoet**. 2010. Choice of mouse strain influences the outcome in a mouse model of chemical-induced asthma. PLoS One **5**:e12581.

158. **Wang H., P. Yang, K. Liu, F. Guo, Y. Zhang, G. Zhang, and C. Jiang**. 2008. SARS coronavirus entry into host cells through a novel clathrin- and caveolae-independent endocytic pathway. Cell Res. **18**:290–301.

159. **Wang L.-F., Z. Shi, S. Zhang, H. Field, P. Daszak, and B. T. Eaton**. 2006. Review of bats and SARS. Emerg. Infect. Dis. **12**:1834–40.

160. **Weiss S. R., and J. L. Leibowitz**. 2011. Coronavirus pathogenesis. Advances in virus research, 1st ed. Elsevier Inc.

161. **Weiss S. R., and S. Navas-martin**. 2005. Coronavirus pathogenesis and the emerging pathogen severe acute respiratory syndrome coronavirus. Microbiol. Mol. Biol. Rev. **69**:635–664.

162. **Whitman L., H. Zhou, S. Perlman, and T. E. Lane**. 2009. IFN-gamma-mediated suppression of coronavirus replication in glial-committed progenitor cells. Virology. Elsevier Inc. **384**:209–15.

163. **Wills-Karp M., and S. L. Ewart**. 1997. The genetics of allergen-induced airway hyperresponsiveness in mice. Am. J. Respir. Crit. Care Med. **156**:S89–96.

164. **Wood J. L. N., M. Leach, L. Waldman, H. Macgregor, A. R. Fooks, K. E. Jones, O. Restif, D. Dechmann, D. T. S. Hayman, K. S. Baker, A. J. Peel, A. O. Kamins, J. Fahr, Y. Ntiamoa-Baidu, R. Suu-Ire, R. F. Breiman, J. H. Epstein, H. E. Field, and A. a Cunningham**. 2012. A framework for the study of zoonotic disease emergence and its drivers: spillover of bat pathogens as a case study. Philos. Trans. R. Soc. Lond. B. Biol. Sci. **367**:2881–92.

165. **Wu D., C. Tu, C. Xin, H. Xuan, Q. Meng, Y. Liu, Y. Yu, Y. Guan, Y. Jiang, X. Yin, G. Crameri, M. Wang, C. Li, S. Liu, M. Liao, L. Feng, H. Xiang, J. Sun, J. Chen, Y. Sun, S. Gu, N. Liu, D. Fu, B. T. Eaton, L. Wang, and X. Kong**. 2005. Civets Are equally susceptible to experimental infection by two different severe acute respiratory syndrome coronavirus isolates. J. Virol. **79**:2620–2625.

166. **Xu D., Z. Zhang, and F.-S. Wang**. 2004. SARS-associated coronavirus quasispecies in individual patients. N. Engl. J. Med. **350**:1366–1367.

167. **Yang D.** 2013. The secondary structures of the 5’ untranslated region and amino-terminus of NSP1 coding sequences of mouse hepatitis virus and their functional role in \viral replication (A Dissertation). Texas A&M University.

168. **Yang D., P. Liu, D. P. Giedroc, and J. Leibowitz**. 2011. Mouse hepatitis virus stem-loop 4 functions as a apacer element required to drive subgenomic RNA synthesis. J. Virol. **65**:5605–5608.

169. **Yang J., Z. Sun, Y. Y. Y. Wang, J. Lü, D. Qü, R. Ye, J. Lv, and D. Qu**. 2010. Partial deletion in the spike endodomain of mouse hepatitis virus decreases the cytopathic effect but maintains foreign protein expression in infected cells. J. Virol. Methods **172**:1–8.

170. **Yokomori K., L. R. Banner, and M. M. Lai**. 1991. Heterogeneity of gene expression of the hemagglutinin-esterase (HE) protein of murine coronaviruses. Virology. **183**:647–57.

171. **Yokomori K., and M. M. C. Lai**. 1991. Mouse hepatitis virus S RNA sequence reveals that nonstructural proteins ns4 and ns5a are not essential for murine coronavirus replication. Virology. **65**:5605–5608.

172. **Yoshikawa T., T. E. Hill, N. Yoshikawa, V. L. Popov, C. L. Galindo, H. R. Garner, C. J. Peters, and C.-T. K. Tseng**. 2010. Dynamic innate immune responses of human bronchial epithelial cells to severe acute respiratory syndrome-associated coronavirus infection. PLoS One **5**:e8729.

173. **Youn S., J. L. Leibowitz, and E. W. Collisson**. 2005. In vitro assembled, recombinant infectious bronchitis viruses demonstrate that the 5a open reading frame is not essential for replication. Virology. **332**:206–15.

174. **Yount B., K. M. Curtis, and R. S. Baric**. 2000. Strategy for systematic assembly of large RNA and DNA genomes: transmissible gastroenteritis virus model. J. Virol. **74**:10600–10611.

175. **Yount B., K. M. Curtis, E. A. Fritz, L. E. Hensley, P. B. Jahrling, E. Prentice, M. R. Denison, T. W. Geisbert, and R. S. Baric**. 2003. Reverse genetics with a full-length infectious cDNA of severe acute respiratory syndrome coronavirus. Proc. Natl. Acad. Sci. U.SA. **100**:12995–13000.

176. **Yount B., M. R. Denison, S. R. Weiss, and R. S. Baric**. 2002. Systematic assembly of a full-length infectious cDNA of mouse hepatitis virus strain A59. J. Virol. **76**:11065–11078.

177. **Yount B., R. S. Roberts, L. Lindesmith, and R. S. Baric**. 2006. Rewiring the severe acute respiratory syndrome coronavirus (SARS-CoV) transcription circut: engineering a recombination-resistant genome. Proc. Natl. Acad. Sci. U. S. A. **103**:12546–12551.

178. **Zhang C.-Y., J.-F. Wei, and S.-H. He**. 2006. Adaptive evolution of the spike gene of SARS coronavirus: changes in positively selected sites in different epidemic groups. BMC Microbiol. **6**:88.

179. **Zhang Y., J. Li, Y. Zhan, L. Wu, X. Yu, W. Zhang, L. Ye, S. Xu, Y. Wang, J. Lou, and R. Sun**. 2004. Analysis of serum cytokines in patients with severe acute respiratory syndrome. Infect. Immun. **72**:4410–4415.

180. **Zhao G.** 2007. SARS molecular epidemiology: a Chinese fairy tale of controlling an emerging zoonotic disease in the genomics era. Philos. Trans. R. Soc. Lond. B. Biol. Sci. **362**:1063–81.

181. **Zhao J. J., and S. Perlman**. 2010. T cell responses are required for protection from clinical disease and for virus clearance in severe acute respiratory syndrome coronavirus-infected mice. J. Virol. **84**:9318–25.

182. **Zhao J., J. Zhao, N. Van Rooijen, and S. Perlman**. 2009. Evasion by stealth: inefficient immune activation underlies poor T cell response and severe disease in SARS-CoV-infected mice. PLoS Pathog. **5**:e1000636.

183. **Zhao L., B. K. Jha, A. Wu, R. Elliott, J. Ziebuhr, A. E. Gorbalenya, R. H. Silverman, and S. R. Weiss**. 2012. Antagonism of the interferon-induced OAS-RNase L pathway by murine coronavirus ns2 protein is required for virus replication and liver pathology. Cell Host Microbe. Elsevier Inc. **11**:607–16.

184. **Zhao L., K. M. Rose, R. Elliott, N. Van Rooijen, and S. R. Weiss**. 2011. Cell-type-specific type I interferon antagonism influences organ tropism of murine coronavirus. J. Virol. **85**:10058–68.

185. **Zheng D., G. Chen, B. Guo, G. Cheng, and H. Tang**. 2008. PLP2, a potent deubiquitinase from murine hepatitis virus, strongly inhibits cellular type I interferon production. Cell Res. **18**:1105–13.

186. **Zhou H., and S. Perlman**. 2007. Mouse hepatitis virus does not induce Beta interferon synthesis and does not inhibit its induction by double-stranded RNA. J. Virol. **81**:568–74.

187. **Zhou W., W. Wang, H. Wang, R. Lu, and W. Tan**. 2013. First infection by all four non-severe acute respiratory syndrome human coronaviruses takes place during childhood. BMC Infect. Dis. BMC Infectious Diseases **13**:433.

188. **Zuniga S., I. Sola, S. Alonso, and L. Enjuanes**. Sequence motifs involved in the regulation of discontinuous coronavirus subgenomic RNA synthesis. J. Virol. **78**:2004.

189. 2003. Acute respiratory syndrome in China. World Heal. Organization.

APPENDIX

Analysis of nsp13 population variant in lung and cell culture.

Viral RNA was extracted from day 3 post infection mouse lung homogenate, P3.2.1, and P4.2.1. The nsp13 region of interest was reverse transcribed and PCR amplified. The PCR product was subcloned into PGEM-T Easy. Colonies were sequenced and the variant population was analyzed. By this method we are, currently, unable to find our original C17040A variant from the whole genome sequencing. This is likely due to the fact that colony screening is less sensitive in quantifying population variants. Our screening did not detect the C17040A variant, demonstrating that this variant is not well conserved over passage in tissue culture nor in infection in the A/J mouse.

Table A 1. Passage population of nsp13 C17040A variants from different sources

Passage ID	Cell type	Variant population	Percent frequency
P2.2	Lung homogenate	0/14	0%
P3.2.1	DBT	0/17	0%
P 4.2.1	DBT	0/21	0%
P 2.2	DBT	456/2387	19.1%
P3.3	DBT	2,085/16,842	12.3%

Analysis of ns4 variant population in lung and cell culture

Viral RNA was extracted from a P3.2.1 and P4.2.1 and the ns4 region of interest was reverse transcribed and PCR amplified. The PCR product was subcloned into PGEM-T Easy. Colonies were sequenced and the variant population was analyzed. By this method we were unable to find our original G28479A variant from the whole genome sequencing. This is likely due to the fact that colony screening is less sensitive in quantifying population variants. Especially since the highest population variant of the ns4 G28479A was 10% in P2.2, and was reduced to 2% in P3.2, it was unlikely that we would find the variant by colony screening. This does confirm that the ns4 variant is not maintained in tissue culture passage.

Table A 2. Passage population of ns4 G28479A variants

Passage ID	Cell Type	Variant Population	Percent Frequency
P3.2.1	DBT	0/22	0%
P4.2.1	DBT	0/21	0%
P2.2	DBT	445/4087	10.89%
P3.3	DBT	434/18065	2.4%

Conservation of nsp13 variant in group 1 betacoronaviruses

Because the nsp13 G17040A variant causes a coding difference we decided to evaluate this amino acid change in the context of other group 1 betacoronaviruses. Using ClustalW2 we compared the nsp13 regions of the virulent MHV-1, MHV-A59, MHV-JHM, Human Coronavirus HKU1 (NC_006577.2), and Human Coronavirus OC43 (NP_937951.1). The alignment (Figure A1) shows that the nsp13 A237D amino acid change present in the virulent MHV-1 is not present in any other group 1 betacoronavirus. This amino acid change also creaks up a highly conserved region of 12 consecutive amino acids.

```
MHV-JHMnsp13        SVGACVVCSSQTSLRCGSCIRKPLLCCKCAYDHVMSTDHKYVLSVSPYVCNSPGCDVNDV 60
MHV-A59nsp13        SVGACVVCSSQTSLRCGSCIRKPLLCCKCAYDHVMSTDHKYVLSVSPYVCNSPGCDVNDV 60
MHV-1nsp13V         SVGACVVCSSQTSLRCGSCIRKPLLCCKCAYDHVMSTDHKYVLSVSPYVCNSPGCDVNDV 60
HOC43nsp13          SVGACVVCSSQTSLRCGSCIRKPLLCCKCCYDHVMATDHKYVLSVSPYVCNAPGCDVNDV 60
HCoVHKU1nsp13       SVGACVVCSSQTSLRCGSCIRKPLLCCKCCYDHVMATNHKYVLSVSPYVCNAPNCDVSDV 60
                    ****************************.*****:*:*************:*.***.**

MHV-JHMnsp13        TKLYLGGMSYYCEAHKPQYSFKLVMNGMVFGLYKQSCTGSPYIEDFNKIASCKWTEVDDY 120
MHV-A59nsp13        TKLYLGGMSYYCEDHKPQYSFKLVMNGMVFGLYKQSCTGSPYIEDFNKIASCKWTEVDDY 120
MHV-1nsp13V         TKLYLGGMSYYCEDHKPQYSFKLVMNGMVFGLYKQSCTGSPYIEDFNKIASCKWTEVDDY 120
HOC43nsp13          TKLYLGGMSYYCEDHKPQYSFKLVMNGLVFGLYKQSCTGSPYIDDFNRIASCKWTDVDDY 120
HCoVHKU1nsp13       TKLYLGGMSYYCENHKPHYSFKLVMNGMVFGLYKQSCTGSPYIDDFNKIASCKWTEVDDY 120
                    ************* ***:*********:***************:***:*******:****

MHV-JHMnsp13        VLANECTERLKLFAAETQKATEEAFKQCYASATIREIVSDRELILSWEIGKVRPPLNKNY 180
MHV-A59nsp13        VLANECTERLKLFAAETQKATEEAFKQCYASATIREIVSDRELILSWEIGKVRPPLNKNY 180
MHV-1nsp13V         VLANECTERLKLFAAETQKATEEAFKQCYASATIREIVSDRELILFWEIGKVRPPLNKNY 180
HOC43nsp13          ILANECTERLKLFAAETQKATEEAFKQSYASATIQEIVSERELILSWEIGKVKPPLNKNY 180
HCoVHKU1nsp13       VLANECIERLKLFAAETQKATEEAFKQSYASATIQEIVSDREVILCWETGKVKPPLNKNY 180
                    :***** ********************.******:****:**:** ** ***:*******

MHV-JHMnsp13        VFTGYHFTNNGKTVLGEYVFDKSELTNGVYYRATTTYKLSVGDVFILTSHAVSSLSAPTL 240
MHV-A59nsp13        VFTGYHFTNNGKTVLGEYVFDKSELTNGVYYRATTTYKLSVGDVFILTSHAVSSLSAPTL 240
MHV-1nsp13V         VFTGYHFTSNGKTVLGEYVFDKSELTNGVYYRATTTYKLSVGDVFILTSHAVSSLSDPTL 240
HOC43nsp13          VFTGYHFTKNGKTVLGEYVFDKSELTNGVYYRATTTYKLSVGDVFVLTSHSVANLSAPTL 240
HCoVHKU1nsp13       VFTGYHFTSTGKTVLGEYVFDKSELTNGVYYRATTTYKLSIGDVFVLTSHSVASLSAPTL 240
                    ********..*******************************:****:****:*:.** ***
```

Figure A 1. ClustalW2 alignement of a fragment of the nsp13 proteins of select group 1 betacoroanviruses. The highlighted region shows inidicated the A237D amino acid change in the virulent strain of MHV-1. This alignement shows that the amino acid change is in a region that is conserved in selected group 1 beatcoronaviruses.

Conservation of ns4 variant in group 1 betacoronaviruses

Because the ns4 G28479A variant causes a coding difference we decided to evaluate this amino acid change in the context of other group 1 betacoronaviruses. Using ClustalW2 we compared the ns4 regions of the virulent MHV-1, MHV-A59, MHV-JHM, Human Coronavirus HKU1 (NC_006577.2), and Human Coronavirus OC43 (NP_937951.1). This alignment (Figure A2) shows that the region at the carboxy terminus is not well conserved among group 1 betacoronaviruses. Only MHV-1 and MHV-JHM share a similar carboxy terminus end, so we cannot make comparisons about the potential role of this amino acid change based on this information.

```
MHV-1ns4V       ---------------------------------MAIIGPKTTIAAVFIGPFIVACMLGIG 27
MHV-JHMns4      ---------------------------------MALIGPKTTIAAVFIGPFLVACMLGIG 27
MHV-A59ns4      MRIDYHSLSWKDRKSKQFIAFSLLPGPVRGSHSYGRVGPKATLAAVFIGPFIVACMLGIG 60
HCoVHKU1ns4     ---------------------------------MDVWRPSYTHSLVIR---------EFG 18
HOC43ns4        ---------------------------------MDIWRPEKKYLRYIN---------GFN 18
                                                  *. .    :           :.

MHV-1ns4V       LVYLLQLQVQIFHVNDTIRVTGKPATVSYTISTPVTPSATTLDGTTYTLIRPTSSYTRVH 87
MHV-JHMns4      LVYLLQLQVQIFHVKDTIRVTGKPATVSYTTSTPVTPVATTLDGTTYTLIRPTSSYTRVY 87
MHV-A59ns4      LVYLLQLQVQIFHVKDTIRVTGKPATVSYTTSTPVTPSATTLDGTTYTLIRPTSSYTRVY 120
HCoVHKU1ns4     VTNLEDLCLKYNYCQPIVGYCIVPLNVWCRKFGKFA--------SHFTLRSHDISHS-NN 69
HOC43ns4        VSELEDACFKFNYQFPKVGYCRVPSHAWCRNQGRFC--------ATFTLYGKSKHYD-KY 69
                :  * :  .:  :    :     *  .       .         : :**      :

MHV-1ns4V       LGSPRGFDTSTFGPKTLDYTTSSKPHLNSGRPYTLRHLPKYMTPPTIWRFGM 139
MHV-JHMns4      LGSSRGFDTSTFGPKTLDYITSSKPHLNSGRPYTLRHLPKYMTPPATWRFGL 139
MHV-A59ns4      LGTPRGFDYSTFGPKTLDYVTNLNLILILVVHILLRHCP------------GI 161
HCoVHKU1ns4     FGVVTSFT--TYGNTVSEAVSRLVESASEFIVWRAEALNKYG----------- 109
HOC43ns4        FGVINGFT--AFANTVEDAVNKLVFLAVDFITWRRQELNVYG----------- 109
                :*   .*   ::. .. :  .             .
```

Figure A 2. ClustalW2 alignement of ns4 proteins of select group 1 betacoroanviruses. The ns4 proteins from each virus were aligned using ClustalW2 and show that the A133T amino acid change (highlighted region) caused by the variant population in the virulent MHV-1 is not conserved among selected group 1 betacoronaviruses.